Effect of the second mode on the optical properties of quantum-dot microcavity lasers

Thesis
for the degree of

doctor rerum naturalium (Dr. rer. nat.)

approved by the Faculty of Natural Sciences of
Otto von Guericke University Magdeburg

by M.Sc. Masoumeh Fanaei
born on 06.08.1986 in Arak, Iran

Examiner: Prof. Dr. rer. nat. habil. Jan Wiersig
Prof. Dr. rer. nat. habil. Andreas Knorr

submitted on: 24.09.2019
defended on: 22.01.2020

Declaration of honour

I hereby declare that I prepared this thesis without the impermissible help of third parties and that none other than the aids indicated have been used; all sources of information are clearly marked, including my own publications.

In particular I have not consciously:

- fabricated data or rejected undesirable results,
- misused statistical methods with the aim of drawing other conclusions than those warranted by the available data,
- plagiarized external data or publications,
- presented the results of other researchers in a distorted way.

I am aware that violations of copyright may lead to injunction and damage claims by the author and also to prosecution by the law enforcement authorities. I hereby agree that the thesis may be electronically reviewed with the aim of identifying plagiarism.

This work has not yet been submitted as a doctoral thesis in the same or a similar form in Germany, nor in any other country. It has not yet been published as a whole.

Magdeburg, 03/03/2020

M.Sc. Masoumeh Fanaei

Abstract

For several decades light-matter interaction has been an important scientific field and has led to numerous investigations and researches in various fields such as condensed matter physics, medicine and electrical engineering, and is still expected to be one of the most active areas of research over the coming years. However, there are still many open questions that necessitate further investigation. In this doctoral thesis we investigate the coherence properties of light emitted by quantum-dot microcavity lasers. To accomplish this task, we consider an open quantum-mechanical system to formulate equation of motion based on the theory of microscopic semiconductor. In this way, the cluster expansion method is employed to solve the infinite hierarchy problem. Within this theory, we can generate correlations required to calculate the quantities of interest in microcavities.

Current work is concerned with the effect of the second mode on the lasing behavior of the quantum-dot microcavity lasers where the quantum dot contains two shells, a s- and a p-shell in the valence and in the conduction band. In this regard, this thesis addresses two main parts: Two-mode, and two-state quantum-dot-microcavity lasers.

In the first half of this thesis, we investigate correlations between two cavity modes in a quantum-dot-microcavity laser where both modes are coupled to the quantum-dot s-shell transition. The significant differences in the lasing behavior of two modes indicate the gain competition between modes which is also confirmed by autocorrelation and cross-correlation functions. In this part we especially emphasize on the effects of the direct dissipative coupling on the gain competition. Numerical results for a semiconductor quantum-dot microcavity laser demonstrate an enhanced autocorrelation of both modes and also an enhanced anticorrelation with increasing the direct coupling between two modes. In order to describe and analyze these issues, we introduce dark and bright modes by applying the unitary transformation. It is seen that beyond a certain lasing threshold original modes are composed and as a result a bright mode is generated that is coupled to the quantum dots. In addition, a dark mode is created that has only indirect interaction with the quantum dots through the bright mode. It will be also shown that the population of the dark mode can justify an efficient transfer of photons between two original cavity modes.

In the second half of the thesis, we investigate two-state lasing in quantum-dot laser, through ground-state (s-shell) and excited-state (p-shell) transitions. Based on the microscopic semiconductor theory, we show that the ground-state laser is qualitatively uninfluenced by the onset of lasing in the excited-state mode due to the delay time between carrier saturation of two states. It is influenced solely by the relaxation of the carrier into the ground state which can be affected via the

Q-factor of the excited mode, however it has only quantitative effect on lasing operation of the ground-state mode.

Zusammenfassung

Einfluss des zweiten Mode auf die optischen Eigenschaften von Quantenpunkt-Mikrokavitätslasern

Die Wechselwirkung zwischen Licht und Materie ist seit mehreren Jahrzehnten ein wichtiges Wissenschaftsgebiet und hat zu zahlreichen Untersuchungen und Forschungen auf verschiedenen Gebieten wie der Physik, der kondensierten Materie, der Medizin und der Elektrotechnik geführt, und es wird erwartet, dass sie auch in den kommenden Jahren eines der aktivsten Forschungsgebiete sein wird. Es gibt jedoch noch viele offene Fragen, die eine weitere Untersuchung erfordern. In dieser Doktorarbeit untersuchen wir die Kohärenzeigenschaften von Licht, das von Quantenpunkt-Mikrokavitätslasern emittiert wird. Um diese Aufgabe zu erfüllen, betrachten wir ein offenes quantenmechanisches System, um Bewegungsgleichungen basierend auf mikroskopischen Halbleitertheorie zu formulieren. Auf diese Weise wird die Cluster-Expansionsmethode eingesetzt, um das Hierarchieproblem zu lösen. Innerhalb dieser Theorie können wir Korrelationen erzeugen, die zur Berechnung der Interessenquantitäten an Mikrokavitäten erforderlich sind.

Die aktuelle Arbeit beschäftigt sich mit dem Einfluss des zweiten Mode auf das Laserverhalten der Quantenpunkt-Mikrokavitätslaser, bei denen der Quantenpunkt zwei Schalen enthält, eine s- und eine p-Schale im Valenz und im Leitungsband. In diesem Zusammenhang befasst sich diese Arbeit mit zwei Hauptteilen: Zwei-Moden- und Zwei-Zustands-Quantenpunkt-Mikrokavitätslaser.

In der ersten Hälfte dieser Arbeit untersuchen wir Korrelationen Moden in einem Quantenpunkt-Mikrokavitätslaser, bei dem beide Moden mit dem Quantenpunkt s-Schalenübergang gekoppelt sind. Die signifikanten Unterschiede im Laserverhalten zweier Moden zeigen den Modenwettbewerb, der auch durch Autokorrelations- und Kreuzkorrelationsfunktionen bestätigt wird. In diesem Teil betonen wir besonders die Auswirkungen des direkten dissipativen Kopplung zwischen den Moden auf den Moden-Wettbewerb. Numerische Ergebnisse für einen Halbleiter-Quantenpunkt-Mikrokavitätslaser zeigen eine erhöhte Autokorrelation beider Moden und auch eine erhöhte Antikorrelation mit zunehmender direkter Kopplung zwischen zwei Moden. Um diese Probleme zu beschreiben und zu analysieren, führen wir ‚Dunkle' und ‚Helle' Moden ein, indem wir die einheitliche Transformation anwenden. Es zeigt sich, dass ab einem bestimmten Laserschwellenwert originale Moden zusammengesetzt sind und dadurch ein Helle Mode erzeugt wird, der mit den Quantenpunkten gekoppelt ist. Zusätzlich wird ein Dunkle Mode erzeugt, der nur eine indirekte Interaktion mit den Quantenpunkten über den Hellen Mode hat. Es wird auch gezeigt, dass die Population des Dunkelmode einen effizienten Photonentransfer zwischen zwei ursprünglichen Moden rechtfertigen kann.

In der zweiten Hälfte der Arbeit untersuchen wir den Zwei-Zustände Laser im Quantenpunkt-Laser, durch Übergänge zwischen Grundzustand (s-Schale) und angeregtem Zustand (p-Schale). Basierend auf der mikroskopischen Halbleitertheorie zeigen wir, dass der Grundzustand-Laser aufgrund der Verzögerungszeit zwischen der Trägersättigung zweier Zustände qualitativ unbeeinflusst vom Beginn des Lasereinsatzes in der Anregungsmode ist. Sie wird ausschließlich durch die Relaxation des Trägers in den Grundzustand beeinflusst, die über den Q-Faktor des angeregten Mode beeinflusst werden kann, hat aber nur quantitative Auswirkungen auf den Laserbetrieb der Grundzustandsmode.

List of Figures

Contents

Chapter 1

Introduction

Quantum optics is a major field of study in modern physics that deals in particular with the theory and application of interactions between light and matter. The main feature of the quantum theory of optics evolves from the nature of light as an ensemble of quantized photons. One of the first main advancements of the light theory that assumed the light emission as discrete units of energy was proposed by Max Planck in 1899 by explaining of the blackbody radiation spectrum. Later in 1905, Albert Einstein could develop the hypothesis of discrete quanta of light and the concept of photons in order to describe the photoelectric effect. This was a milestone in further development of quantum optics that was continued by Dirac [1927] and Fermi [1932] and progressed in recent decades to our current knowledge of this concept.

Recent developments in semiconductor nanotechnology enable us to study quantum optics. The 3-D confinement of light and matter in semiconductor micro- and nanostructures with the size of the de Broglie wavelength leads to the quantization of the light. Thereby state-of-the-art semiconductor devices make it possible to study the quantum optical phenomena. In this doctoral thesis we explore semiconductor quantum-dot microcavity lasers.

To understand the concept of quantum-dot lasers we need first to shortly review the laser structure and principle. Lasers are known as sources of light that usually have high output and are emitted in a narrow bandwidth. A main feature that makes lasers different from other sources of light is that laser emits light coherently [Hakan, 1986]. This concept can be traced back to 1917, when Albert Einstein published the paper "On the Quantum Theory of Radiation" [Einstein, 1917] where he proposed that light carries its energy in quantized

states, or the so-called photons. He proposed that, in addition to spontaneous absorption and emission of light, electrons are able to emit the light with a particular wavelength as they are stimulated. This is the underlying theory of Laser and Maser that can be seen in Figure 1.1. This figure shows a sketch of the three single-photon processes where the spontaneous, the stimulated and the absorption emissions are illustrated. In spontaneous emission, an electron goes down from an excited state with energy E_2 to a ground state with energy E_1 and consequently emits a photon with the energy corresponding to the difference in two energy levels. While the phase and also the direction of the emitted photon are random. Stimulated emission is a procedure in which an incoming photon of matching energy $\hbar\omega = E_2 - E_1$ interacts with the electron in the excited state before decaying to the ground state to create a new photon which emits in the same phase and direction with respect to the first one. As a result, the light intensity is coherently amplified by this process. Finally, absorption is a process where a photon is consumed to lift an electron to the excited state.

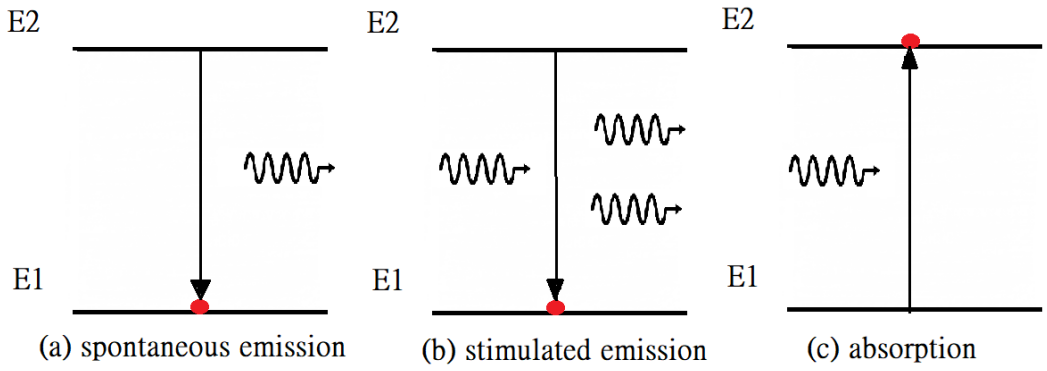

Figure 1.1: Principle of the three main photon interaction mechanisms in a two-level system: (a) spontaneous emission where an electron decays from E_2 to E_1 and then emits a photon with random phase, (b) stimulated emission where incoming photon can excite the electron and it leads to decay to E_1 by emitting a photon. A new photon emits in the same phase and direction with the first one, (c) absorption where an electron goes up to E_2 by consuming a photon.

The history of lasers goes back to 1960 when Theodore H. Maiman built the first solid-state pink ruby laser [Maiman, 1960], based on theoretical studies of Schawlow and Townes [1958]. Only one year later, Basov et al. [1961] published a paper to introduce the concept of semiconductor lasers. In 1962, Hall et al. [1962]

and Nathan et al. [1962] produced the first gallium arsenide (GaAs) semiconductor laser diodes nearly at the same time. There was, however, the drawback of a working point at moderately low temperature and of a high laser threshold. It led to next researches on heterostructures by Kroemer [1963], Alferov [1970] in order to overcome the problems of the first diodes and make laser ready to use outside the lab. These scientists were awarded the Nobel prize in the year 2000 for their outstanding achievements and for the development of semiconductor heterostructures that can be utilized in high-speed- and opto-electronics.

In the last decade, micro/nano-lasers have gained significant interest, because they are faster, more compact and power-efficient than the conventional lasers [Gourley, 1998, Samuel et al., 2009]. One of the main features that makes micro- and nano-lasers superior to conventional lasers is the Purcell effect which was discovered by Purcell [1946]. The Purcell effect is known as the enhancement of the spontaneous emission into cavity modes by its environment [Kleppner, 1981, Lodahl et al., 2004a]. This effect can be formulated by the enhancement factor [Purcell, 1946]

$$F_p = \frac{3}{4\pi^2}\left(\frac{\lambda_{free}}{n}\right)^3\left(\frac{Q}{V}\right),$$

where λ_{free}/n is the wavelength in a cavity material with refractive index n. Here, Q is the quality factor and V is mode volume of the cavity. This equation indicates that increasing the quality factor by using high-quality modes together with the reduction of mode volume lead to an enhancement of the Purcell factor and consequently to higher spontaneous emissions.

There are also other parameters that can characterize the efficiency of a laser device. One of these factors is the β-factor which is also associated with the Purcell factor. The β-factor is defined as the ratio of spontaneous emission into the laser mode to the overall spontaneous emission of the laser-gain medium. The β-factor and the Purcell factor determine the threshold behavior [Chow and Jahnke, 2013, Gies et al., 2007, Björk et al., 1994]. Nowadays used lasers with a β-factor close to unity has been reported in some recent works [Strauf et al., 2006, Thyrrestrup et al., 2010] (see Fig. 1.2). Significant intensity jump at the threshold can be used to determine the β-factor in conventional devices. However, for β-factors close to one, the intensity jump approaches zero in the input-output curve, indicating the concept of 'thresholdless' devices. In such devices the vanishing intensity jump cannot be used to determine the threshold

and a new approach should be adopted. In these thresholdless lasers, the onset of stimulated emission at threshold is identified by the considering the changes in the photon characteristics of the emitted light [Rice and Carmichael, 1994, Ulrich et al., 2007, Wiersig et al., 2009].

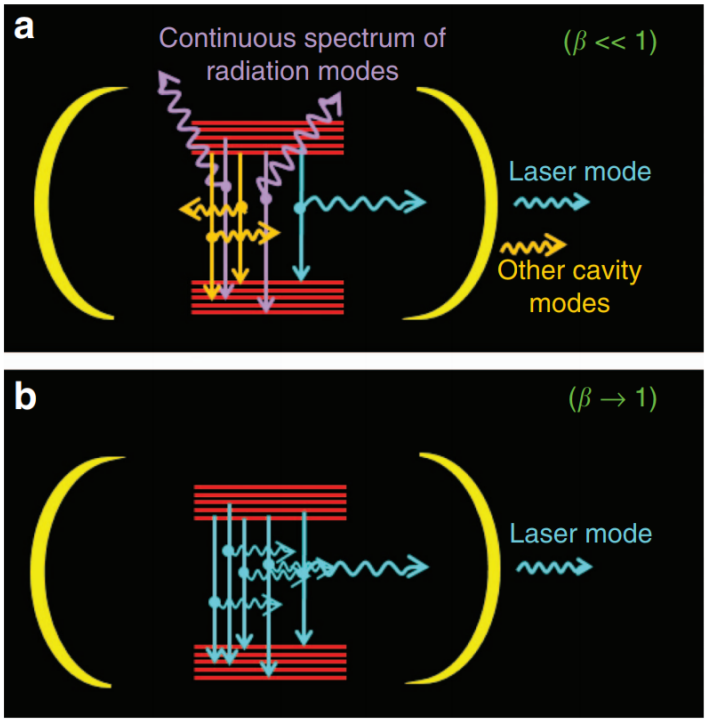

Figure 1.2: (a) A conventional resonator with small β-factor. For low β-factor values the spontaneous emission can take one of the following modes: conversion to a lasing mode, emission into other cavity modes or being emitted as a continuous spectrum of radiation waves. (b) A resonator in a laser with β-factor approaching unity. Picture from Ref. [Hayenga and Khajavikhan, 2017].

One of the crucial parts of a laser is the optical microresonator that is widely developed and improved. This improvement has led to the production of ultralow-threshold lasers or even thresholdless lasers [Strauf et al., 2006, Noda, 2006]. In general, various types of microresonators can be identified where their type of design, optimization, properties, and application depend on the specific area of study. Among the most used approaches, cavities vary from micro-pillars [Reitzenstein and Forchel, 2010, Reithmaier et al., 2004] to photonic crystals [Strauf et al., 2006], and to microdiscs [Michler et al., 2000, Vahala, 2003], as shown in Figure 1.3. The type of microresonators that are used in this thesis are

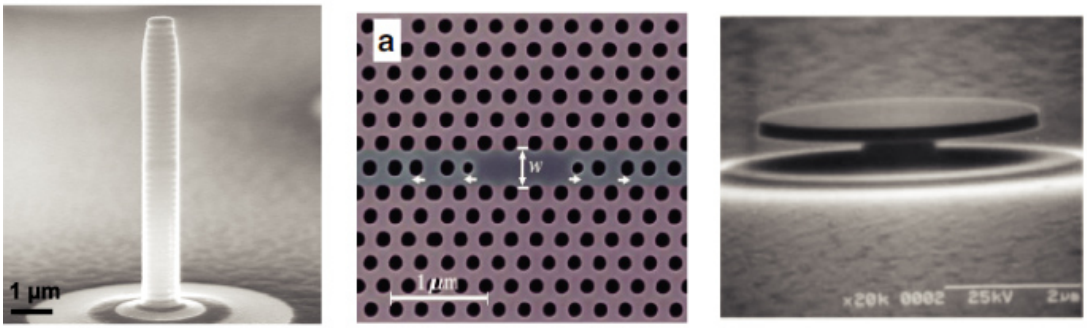

Figure 1.3: Scanning tunneling microscopy images of different types of microcavities. From left to right: a micropillar cavity [Reithmaier et al., 2004], a photonic crystal membrane cavity [Strauf et al., 2006], and a microdisc cavity [Michler et al., 2000].

micropillars.

A gain medium is a material which allows to amplify laser beams as a result of the stimulated emission. Semiconductors as a gain medium play an important role in a wide range of industrial and fundamental applications owing to their important characteristics like low threshold current, high efficiency, small emission spot size, high temperature application, continuous wave (cw) output and lower fabrication costs. The development of semiconductor lasers made a leap forward by realizing that the reduction of dimensionality in a semiconductor has tremendous effect on the density of states, and in consequence on the lasing properties. Reducing the spatial expansion to values smaller than the 'de Broglie wavelength' in one, two or even three dimensions leads to carrier confinement in structures which will be classified into three categories as quantum well, quantum wire, and quantum dots that are shown in Figure 1.4.

After the first experimental proof of two-dimensional quantum well lasers by Dingle and Henry [1976] the advantages of quantum wells as active materials were realized for laser applications. Due to the narrow active region of the quantum well laser, the quantum confinement occurs. The wavelength of the light emitted by a quantum well laser can be specified by using the width of the active region instead of the bandgap of the fabricating material. Moreover, this allows to obtain lasers with lower threshold currents. Also, replacing a two-dimensional quantum well with a zero dimensional quantum-dot laser leads to beneficial features in terms of efficiency and temperature stability as illustrated by Arakawa and Sakaki [1982].

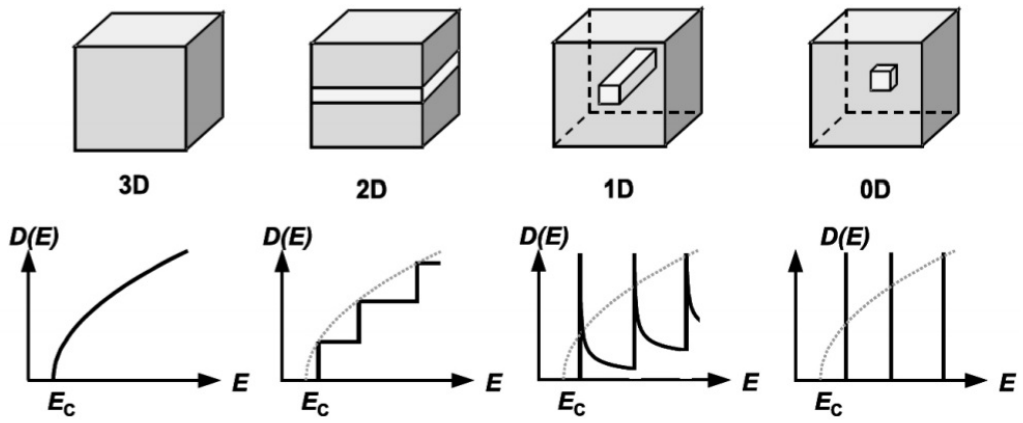

Figure 1.4: Sketch of the free density of states for a system with zero-, one-, two-, or three-dimensional extension (from right to left) [Bimberg et al., 1999]. Changes in the density of states are illustrated from a square root behavior for a three dimensional bulk material to a delta behavior in zero-dimensional quantum dots.

The specific type of semiconductor lasers that will be studied in this thesis is quantum dot microlasers. Quantum dots are very small particles or crystals of a semiconductor material in the range of several nanometers. Due to small size of quantum dot their optical and electronic properties are different from those of larger particles so that quantum dots are sometimes described as artificial atoms. This issue emphasizes that a quantum dot is a single object with bound and quantized energy levels, like atoms or molecules that naturally occur [Ashoori, 1996, Fafard et al., 1999]. However, in contrast to atoms the confining potential and the level spacing of the confined carriers can be modified by the geometry, size and also the material of the quantum dots [Murray et al., 2000].

During the last two decades quantum dots (QDs) have attracted great attention and interest in both fundamental research and practical applications [Michler, 2003, Bimberg et al., 1999]. One of the most important properties of QDs is their high gain and low temperature dependence that make QDs an ideal choice for low-threshold lasers [Asada et al., 1986, Arakawa and Sakaki, 1982, Chhantyal et al., 2018]. Nowadays, there exist dozens of different approaches in nanotechnology to fabricate semiconductor QDs out of various materials. In this work we focus on techniques that allow for embedding the QDs in a bulk semiconductor in order to form an electrical device. QDs can be fabricated by

their self-organized growth that takes place in the Stranski-Krastanow-mode [Bimberg et al., 1999, Jacobi, 2003, Legrand et al., 1998]. In this approach coherently strained self-assembled QDs are produced. Semiconductor material grows epitaxially by using a molecular beam or a metal organic gas on top of a substrate material that has a greater band gap. At the beginning of the process the new material layer expands homogeneously and its lattice constant is nearly the same as that of the substrate. This leads to a tension between these two materials. At a certain critical thickness this tension decreases as small material island appears that are the actual QDs. During this mechanism a thin and homogeneous wetting layer is formed between the QDs and the substance as shown in Figure 1.5. It took several years of research to find suitable materials and to produce QDs with optical wavelengths of a good quality so that they could be used in a cavity to form a QD microlaser. Here we consider typical self-assembled InGaAs QDs. However, the achievements that will be presented here can be extended to other material systems.

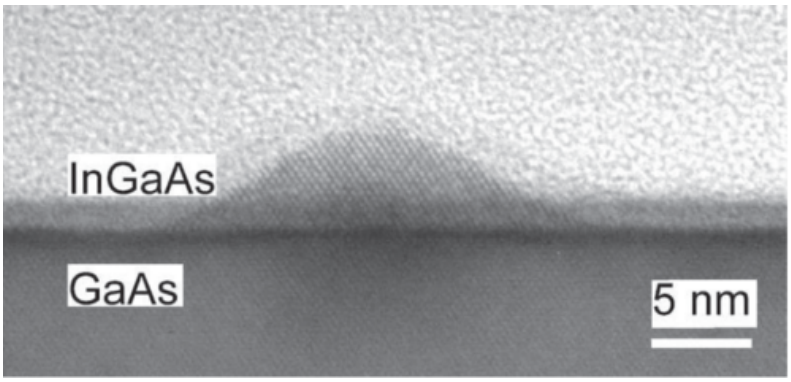

Figure 1.5: Transmission electron microscope of single QD which is coupled to the wetting layer on a GaAs substrate. The picture is taken from Ref. [Anders et al., 2002].

To describe the optical properties of QDs, we need a model that cannot be dealt with using neither a pure atom model nor a pure semiconductor model. Since the level spacing of the lowest confined states for QD is much smaller in comparison to atoms, a two-level model of atoms can not be an appropriate model to describe all optical properties of QDs. For QDs, many-particle effects have to be considered due to the other energetically higher states. Additionally, its

semiconductor nature makes a difference to an atom laser. Not only the QDs are not isolated semiconductor systems, but also the interaction with the environment must be taken into account for a practical QD model. The basic model that shows these key features and is used in this thesis is illustrated in Figure 1.6. The described QDs have a cylindrical symmetry, and therefore confined carrier states can be classified according to the angular momentum as an appropriate quantum number. In this thesis, QDs with two confined states for electrons and holes with quantum number s, p are considered[1]. For a fixed spin direction the s-state is non degenerated, while the p-state is two-fold degenerated. The pump process in experiments can either be initiated through optical pumping or through electrical pumping in the wetting layer or in the barrier or resonantly into the p-shell. For the sake of simplicity we assume that subsequent fast relaxation to the discrete electronic states of the QDs, so that we can assume that the pump process takes place directly in the QD p-shell.

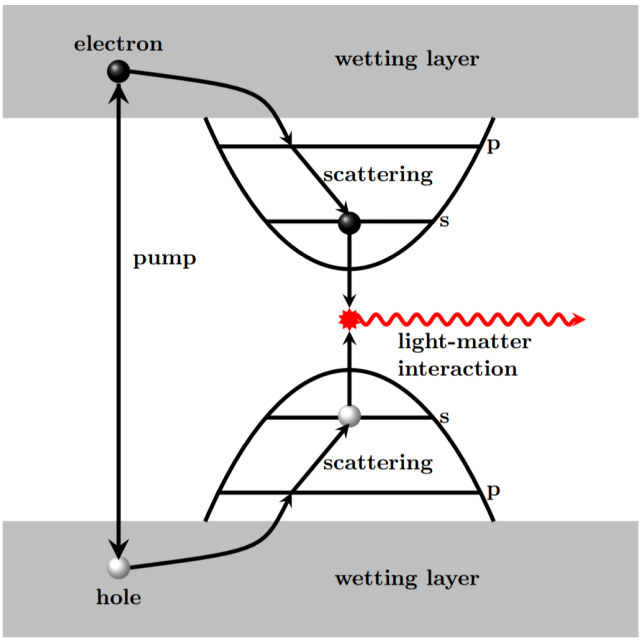

Figure 1.6: Sketch of the QD model in the electron-hole picture. In our model the quantum dot contains two shells, a s- and a p-shell. The pump process can produce electrons and holes in the quasicontinuum states of the wetting layer. For the sake of simplicity, we assume that the creation of carriers takes place directly in the p- shell. Moreover, carriers can scatter into the s- shell, where the recombination of electron-hole pair occurs.

[1] In chapter 4, we use the ground state and excited state instead of s- and p-shell, respectively.

The starting point of this thesis is the microscopic model of Gies et al. [2007] to describe the light-matter interaction in semiconductor QD microcavity lasers with some variations. In order to describe the semiconductor model precisely, we assume an open quantum system where the system interacts with an environment. Since many-body quantum-mechanical systems are too big to be solved with exact numerical methods or are too small to be studied with the well known statistical methods, we use a new generalized formalism of the cluster expansion approach [Fricke, 1996, Kira and Koch, 2008, Richter et al., 2009, Leymann et al., 2013a, 2014]. Finally, results are obtained based on the theory and provide progress for novel light sources.

Since most previous studies of microcavity lasers have mainly concentrated on the lasing characteristics based on the interaction of a single laser mode with QDs, we will focus our attention on microcavity lasers with two optical modes that have been less studied so far [Faghihi et al., 2014, Majumdar et al., 2012, Leymann et al., 2013b, Khanbekyan et al., 2015, Redlich et al., 2016]. This allows us to realize some essential features of the gain competition in lasers and to explain the resulting effective mode coupling. In the current work, we will figure out how the second mode lasing can affect the laser characteristic of QD microcavity lasers. To this end, we consider two cases: two-mode and two-state QD microcavity lasers.

In the first part of this thesis we study the competition in the two-mode microcavity lasers where both modes are coupled to the s-shell transitions. Due to the openness of the system, we can provide an explanation for competing behavior that arises from the direct dissipative coupling between optical modes [Fanaei et al., 2016]. On the other side, the statistical properties of two-state lasers will be investigated where the second mode is connected to the QD p-shell (excited-state) transitions, while only the first mode is coupled to the s-shell (ground-state) transitions. The competition behavior of two-state microcavity laser is an interesting research topic of many recent publications [Markus et al., 2003, Gioannini, 2012, Röhm et al., 2015a,b].

Thesis Outline

First, the general and innovative theoretical concepts of this work are presented in the next chapter followed by the application of the theory to two types of

semiconductor QD lasers: two-mode and two-state lasers.

This thesis is organized as follows:

Chapter 2 reviews briefly the general aspects of an open quantum many-particle system and describes the derivation of the Hamiltonian. Next, we will explain the microscopic semiconductor theory of Gies et al. [2007] to describe the light-matter interactions in semiconductor QDs nanostructures. Since QDs are embedded in a dense semiconductor environment, we need to consider the influence of the environment on the system. This will be described by adding Lindblad terms to the von-Neumann equation [Lindblad, 1976] in section 2.1. Moreover, we will review briefly the cluster expansion method to terminate the hierarchy of equation of motion for a system that was developed by Leymann et al. [2013a, 2014].

In chapter 3 we investigate the statistical properties of two competing modes in a QD-microcavity laser. We assume that two modes are connected to the s-shell transition. The two modes display completely different behavior, revealing the gain competition. The impact of mode coupling in two different cases will be also considered. In the first case, we will recapitulate the statistical properties of the emitted light assuming that there is no direct dissipative coupling between two modes and only the coupling of two optical modes via the common gain medium is presented [Leymann et al., 2013b]. In the second case, the two modes are directly coupled to each other and we investigate the additional direct mode coupling due to the dissipative character of the laser resonator. In order to analyze the mode-coupling effects, we will apply a unitary transformation from the original modes to a new set of modes, namely bright and dark modes in section 3.5. The bright mode is coupled to the QD, while the dark mode interacts only indirectly with QDs through the bright mode. As a result, the population of dark mode can be a good signature of a transfer of photons between the two original cavity modes.

Chapter 4 is concerned with the impact of the excited-state mode on the ground-state lasing. Two modes behave independently as typical laser but with different lasing threshold. It indicates that there is no gain competition between modes which is also confirmed by the constant behavior of cross-correlation function. The gain competition cannot be observed in laser characteristics because of a delay time between carrier saturation of two states which will be predicted based on our microscopic semiconductor model.

Chapter 5 provides a summary of the main achievements of this study and gives an overview of the impact of presented results as well as possible future studies.

Chapter 2

Theory of light-matter interactions in semiconductors

To theoretically describe the light-matter interactions in semiconductor nanostructures a semiconductor model will be formulated and presented in this chapter. This microscopic semiconductor theory can be used to assess the required correlations that determine the emission statistics from a system involving QDs located in a semiconductor environment. In the following, we provide this theoretical framework of light-matter interactions in QDs in two main parts:

First, a short overview of the general description of an open quantum-mechanical many-body system using the density operator and the von Neumann-Lindblad equation will be given in section 2.1. We use the Lindblad formalism to describe the openness of the system and in this regard, the Hilbert space is divided into a system and an environment. Due to difficulty of deriving master equations for a system and for an environment, a common technique is to limit the dynamical calculations to the system.

Second, in order to formulate the microscopic QD theory, we need to find a Hamiltonian that is suitable for the intended situation. Thus, with respect to the microscopic semiconductor theory the Hamiltonian of semiconductor QD lasers will be derived and presented in section 2.2. Then we discuss in detail how to derive the equation of motion (EoM) for time evolution of a system at time t in section 2.3.

It is worth noting that our microscopic semiconductor theory uses a truncated system of equations for correlation functions to limit the infinite hierarchy. The

truncation scheme depends strongly on the considered system and here various methods will be pointed out and discussed [Leymann et al., 2013a, 2014, Fricke, 1996, Hoyer et al., 2004].

2.1 Open quantum-mechanical systems

In reality, a quantum system cannot be modeled as being thoroughly isolated from its environments. This openness of the system leads to some dissipation. In order to describe an open quantum system we use the quantum-mechanical Markovian master equation in Lindblad form to assess the the time evolution of the density operator (for more details, see Refs. [Breuer and Petruccione, 2002, Carmichael, 1999]).

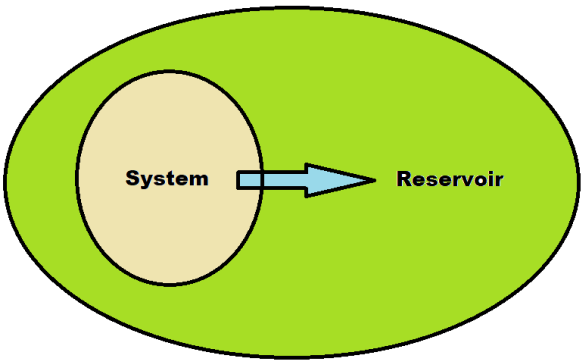

Figure 2.1: Schematic of an open quantum system illustrated in an interacting system-reservoir picture.

The main assumption here is that we can split the whole system into a subsystem S and a reservoir R as illustrated in Figure 2.1. Under this assumption, the Hamiltonian of the whole system can be described as a combination of three items

$$\hat{H} = \hat{H}_S + \hat{H}_R + \hat{H}_{SR}, \quad [1] \tag{2.1}$$

where $\hat{H}_S$ is the subsystem Hamiltonian that we are mainly interested in, and

[1] The hat $\hat{}$ symbol is only used in this chapter to distinguish quantum-mechanical operators from classical quantities.

$\hat{H}_R$ describes the reservoir. $\hat{H}_R$ is not the main focus of study but it enters the calculations only by its general properties like temperature and density of states. A third term $\hat{H}_{SR}$ describes the interaction of these two subsystems,

$$\hat{H}_{SR} = \hbar \sum \hat{L}_i \hat{\Gamma}_i. \tag{2.2}$$

In Eq. (2.2), the Lindblad operators $\hat{L}_i$ act on the Hilbert space of the system S and the operators $\hat{\Gamma}_i$ act on the Hilbert space of the reservoir R. We apply the von-Neumann equation for the full density operator $\hat{\rho}$ to outline the dynamics of the system,

$$\frac{d}{dt}\hat{\rho} = \frac{i}{\hbar}[\hat{\rho}, \hat{H}]. \tag{2.3}$$

The density operator of the system $\hat{\rho}_S$ can be calculated by taking the partial trace over the reservoir

$$\hat{\rho}_S = tr_R\{\hat{\rho}(t)\} = tr_R\{\hat{U}(t)\hat{\rho}(0)\hat{U}^\dagger(t)\}, \tag{2.4}$$

where $\hat{U}(t)$ is the unitary time evolution operator. By applying the Markov approximation we assume that the relaxation time of the reservoir R is much smaller than the relaxation time of subsystem S that is generally valid for wetting layer compared to the QDs. As a result, the reservoir correlations vanish immediately,

$$\langle \hat{\Gamma}_i(t)\hat{\Gamma}_j(t')\rangle_R \propto \delta(t - t'). \tag{2.5}$$

Moreover, to obtain a simple dynamical equation we apply the Born approximation meaning that the subsystem S has no significant effect on the reservoir R and the reservoir can affect the system only with its general parameters that are time-independent like temperature, T. For instance, by using the temperature T as reservoir parameter the whole density operator can be given by

$$\hat{\rho}(t) \approx \hat{\rho}_S(t)\hat{\rho}_R(T). \tag{2.6}$$

These approximations leads to the von Neumann-Lindblad equation (vNL) for a system with reduced density operator $\hat{\rho}_S$ (for more details refer to Ref. [Breuer and Petruccione, 2002]).

$$\frac{d}{dt}\hat{\rho}_S = \frac{i}{\hbar}[\hat{\rho}_S, \hat{H}_S] + \sum_{\nu,\nu'} \gamma_{\nu\nu'}(2\hat{L}_{\nu'}\hat{\rho}_S\hat{L}_\nu^\dagger - \hat{L}_\nu^\dagger\hat{L}_{\nu'}\hat{\rho}_S - \hat{\rho}_S\hat{L}_\nu^\dagger\hat{L}_{\nu'}). \tag{2.7}$$

The first term on the right-hand side describes the unitary dynamics of S that is equal to Eq. (2.3). The interaction with the reservoir via the Lindblad term is reflected in the second term of the right hand side, where $\gamma_{\nu\nu'}$ implies the rates that depend on the reservoir parameters.

In addition, the von Neumann-Lindblad equation can be applied to a specific system operator, $\langle\hat{A}\rangle = tr_S(\hat{A}\hat{\rho}_S)$ to obtain the EoM for an expectation value (EV),

$$\begin{aligned}\frac{d}{dt}\langle\hat{A}\rangle &= \frac{i}{\hbar}\langle[\hat{H}_S,\hat{A}]\rangle + \sum_{\nu,\nu'}\lambda_{\nu\nu'}\langle 2\hat{L}_\nu^\dagger\hat{A}\hat{L}_{\nu'} - \hat{L}_\nu^\dagger\hat{L}_{\nu'}\hat{A} - \hat{A}\hat{L}_\nu^\dagger\hat{L}_{\nu'}\rangle \\ &= \frac{i}{\hbar}\langle[\hat{H}_S,\hat{A}]\rangle + \sum_i\langle C_i(\hat{A})\rangle \\ &= \langle\mathcal{L}(\hat{A})\rangle.\end{aligned} \tag{2.8}$$

This equation is called the generalized Ehrenfest equation of motion that is derivable in the Schrödinger picture and is different from the generalized Heisenberg EoM. The Lindblad processes are labeled by the operator functions $C_i(\hat{A})$ and here $\mathcal{L}$ stands for the Lindblad superoperator[2] that is used as short form for symbolic calculation in next chapters. For the sake of simplicity, we omit also the index S in the rest of this thesis.

2.2 System and Hamiltonian

Electromagnetic field emission features of a QD microcavity laser can be investigated via a microscopic semiconductor theory. By considering the many-body effects of the carriers, the developed microscopic semiconductor theory can compute correlations required to determine the emission statistics of QD microcavities. To be more specific, we consider QDs with only two confined QD shells for both electrons and holes in the valence and in the conduction band (as can be seen in Fig. 1.6). Moreover, we assume that the carrier generation process (pumping) takes place in the p-shell that suits well to an experimental case.

As a first step to formulate a microscopic QD theory we have to acquire a Hamiltonian that fulfills the temporal evolution of the whole system. For a QD

[2]Superoperator is an object that acts on an operator and then results in a new operator.

microcavity laser the Hamiltonian can be given as a summation of four terms

$$\hat{H} = \hat{H}_{Ph} + \hat{H}^0_{Carr} + \hat{H}_{Coul} + \hat{H}_D. \tag{2.9}$$

The first part $\hat{H}_{Ph}$ is the electromagnetic field in the cavity, the second term, $\hat{H}^0_{Carr}$, describes the carriers that are confined in the QDs, the third term, $\hat{H}_{Coul}$, represents the Coulomb interaction of the carriers and the fourth term, $\hat{H}_D$, is the light-matter interaction. In the following sections, we will derive each of these Hamiltonians in detail.

2.2.1 Quantization of the electromagnetic field

The basic concept of quantization is to assume that electromagnetic fields are comprised of discrete energy packets, or the so-called photons. The Hamiltonian $\hat{H}_{Ph}$ expresses the quantized electromagnetic energy. We can apply the formalism of the second quantization by employing Maxwell equations [Haug and Koch, 2009]. In order to make the vector potential $\mathbf{A}(\mathbf{r}, t)$ transversal, we use the Coulomb gauge, $\nabla.\mathbf{A}(\mathbf{r}, t) = 0$. The wave equation for the vector potential in a cavity reads

$$\nabla^2\mathbf{A}(\mathbf{r}, t) = \frac{n^2(\mathbf{r})}{c^2}\partial_{tt}\mathbf{A}(\mathbf{r}, t). \tag{2.10}$$

Here, $n(\mathbf{r})$ is the refractive index that is related to the material of the resonator. The vector potential $\mathbf{A}(\mathbf{r}, t)$ is expanded into modes $\mathbf{u}_\xi(\mathbf{r})$

$$\mathbf{A} = \sum_\xi c_\xi(t)\mathbf{u}_\xi(\mathbf{r}) + c^*_\xi(t)\mathbf{u}^*_\xi(\mathbf{r}), \tag{2.11}$$

where $c_\xi(t) = c_\xi(0)e^{-i\omega_\xi t}$ with ξ labeling the modes. It is worth mentioning that the shape of the cavity and the refractive index $n(\mathbf{r})$ have effects on the form of $\mathbf{u}_\xi(\mathbf{r})$. We apply the canonical quantization where $c_\xi = A_\xi\hat{b}_\xi$ with the factor $A_\xi = \sqrt{\frac{\hbar}{2\epsilon_0\omega_\xi vol_\xi}}$, the mode volume vol_ξ and the permittivity ϵ_0. The electromagnetic field operator can be expressed in terms of bosonic annihilation $\hat{b}_\xi$ and creation operators $\hat{b}^\dagger_\xi$. The operators $\hat{b}_\xi$ and $\hat{b}^\dagger_\xi$ fulfill the standard bosonic commutation relations:

$$\begin{aligned} &[\hat{b}_\xi, \hat{b}^\dagger_{\xi'}] = \delta_{\xi,\xi'}, \\ &[\hat{b}_\xi, \hat{b}_{\xi'}] = 0 = [\hat{b}^\dagger_\xi, \hat{b}^\dagger_{\xi'}]. \end{aligned} \tag{2.12}$$

This leads to the the quantized vector potential being formulated as:

$$\mathbf{A} = \sum_{\xi} \hat{b}_{\xi} \mathbf{u}_{\xi}(\mathbf{r}) + \hat{b}_{\xi}^{\dagger} \mathbf{u}_{\xi}^{*}(\mathbf{r}), \tag{2.13}$$

and finally the expression for the quantized field energy can be written as[3]

$$\hat{H}_{Ph} = \sum_{\xi} \hbar\omega_{\xi} \left(\hat{b}_{\xi}^{\dagger} \hat{b}_{\xi} + \frac{1}{2} \right). \tag{2.14}$$

2.2.2 Single-particle states

The step required prior to formulate the many-body approach is the choice of the single-particle basis of the non-interacting system. Calculation of single-particle states depends strongly on the experimental conditions and the material size and characteristics. Here we focus on III-V compound semiconductors like InGaAs QDs on a GaAs substrate. For this type of material accurate but sophisticated approaches like tight-binding models [Schulz and Czycholl, 2005, Singleton, 2001, Sheng et al., 2005, Baer et al., 2005] can be used. An example of the application of this model to InN/GaN QDs can be found in the work of Baer et al. [2005]. It has been also shown that phenomenological theories like the 8-band k.p. wave functions provide good estimations for InGaAs/GaAs QDs [Schliwa and Winkelnkemper]. In this thesis, we employ the envelope-function approximation [Haug and Koch, 2009, Bimberg et al., 1999] that is simpler and provides an acceptable accuracy for our purpose.

In the envelope function ansatz, the wave function $\psi_{\nu}^{\lambda}(\mathbf{r})$ is assumed to be the product of the periodic Bloch function at the band edge $u_{k\approx 0}(\mathbf{r})$, describing the volume material, times the envelope function that represents the additional confinement of the QD $\phi_{\nu}^{\lambda}(\mathbf{r})$,

$$\psi_{\nu}^{\lambda}(\mathbf{r}) = u_{k\approx 0}^{\lambda}(\mathbf{r}) \phi_{\nu}^{\lambda}(\mathbf{r}). \tag{2.15}$$

Here, λ is the corresponding band index and ν indicates the quantum numbers specifying the confined state. The effective single-particle Schrödinger equation

[3] In this work we shift the zero energy so that the $+\frac{1}{2}$ does not appear in the Hamiltonian of quantized field energy.

can be used to evaluate the envelope function

$$\left(-\frac{\hbar^2}{2m^\lambda}\Delta + V(\mathbf{r})\right)\phi_\nu^\lambda(\mathbf{r}) = \epsilon_\nu^\lambda \phi_\nu^\lambda(\mathbf{r}), \tag{2.16}$$

where m^λ is the effective mass and $V(\mathbf{r})$ denotes an approximate confinement potential which depends on the shape of the QDs. For typical lens-shaped QDs (like the one depicted in Figure 1.5), the potential can be approximated by a two dimensional harmonic potential [Wojs et al., 1996, Bimberg et al., 1999] with the strong confinement in growth direction z and a harmonic oscillator potential in the x-y-plane

$$V(\mathbf{r}) = \frac{m^\lambda \omega^2}{2}(x^2+y^2) + V_0\left(\theta(z-L/2) + \theta(-z-L/2)\right), \tag{2.17}$$

where V_0 and L denote the confinement energy and the extension, respectively. Now the field operators can be constructed with the single-particle states as

$$\hat{\Psi}(\mathbf{r},t) = \sum_{\lambda,\nu} \hat{a}_{\lambda,\nu}(t)\psi_\nu^\lambda(\mathbf{r}), \tag{2.18}$$

with the fermionic annihilation (creation) operators $\hat{a}_{\lambda,\nu}(t)(\hat{a}^\dagger_{\lambda,\nu}(t))$ that fulfill the standard anti-commutation relations for any indices k and k' [Schwabl, 2008, Mahan, 2000]

$$\begin{aligned} [\hat{a}_k, \hat{a}^\dagger_{k'}]_+ &= \delta_{k,k'}, \\ [\hat{a}_k, \hat{a}_{k'}]_+ &= 0 = [\hat{a}^\dagger_k, \hat{a}^\dagger_{k'}]_+. \end{aligned} \tag{2.19}$$

The number of states ν and levels are determined by the depth of the confinement potential. One simple approach that is widely used is the two-level description [Del Valle et al., 2009, Richter et al., 2009, Lodahl et al., 2004b]. However, in this work we use a four-level QD model which is much closer to realistic cases. This QD model has two confined states for electrons and holes [Gies et al., 2011] and therefore is able to provide a more accurate picture of our system. The angular momentum is a robust quantum number and in this chapter the states are called s- and p-shell.

2.2.3 The many-body Hamiltonian

The many-body Hamiltonian can be now constructed based on the concept of the single-particle field operators. The many-particle Hamiltonian includes several terms:
First, Hamiltonian of the free carriers is given by

$$\hat{H}^0_{Carr} = \int d^3\mathbf{r}\hat{\Psi}^\dagger(\mathbf{r},t)\left(-\frac{\hbar^2}{2m}\Delta + V(\mathbf{r})\right)\Psi(\mathbf{r},t), \tag{2.20}$$

which is a diagonal sum of creation and annihilation operators $\hat{n} = \hat{a}^\dagger_{\lambda,\nu}\hat{a}_{\lambda,\nu}$ with the single-particle energies ϵ^λ_ν

$$\hat{H}^0_{carr} = \sum \epsilon^\lambda_\nu \hat{a}^\dagger_{\lambda,\nu}\hat{a}_{\lambda,\nu}. \tag{2.21}$$

Second, the Coulomb Hamiltonian is constructed in a similar way with the Coulomb matrix element

$$V^{\lambda\lambda'}_{\nu\alpha\nu'\alpha'} = \int d^3\mathbf{r}\int d^3\mathbf{r}'\psi^{\lambda*}_\nu(\mathbf{r})\psi^{\lambda'*}_\alpha(\mathbf{r}')V(\mathbf{r}-\mathbf{r}')\psi^{\lambda'}_{\nu'}(\mathbf{r}')\psi^\lambda_{\alpha'}(\mathbf{r}), \tag{2.22}$$

with the Coulomb potential $V(\mathbf{r}) = e^2/(4\pi\epsilon_0\epsilon|\mathbf{r}|)$, the electron charge e and the dielectric function $\epsilon_0\epsilon$. The complete Coulomb Hamiltonian in second quantization can be also expressed by creation and annihilation operators:

$$\hat{H}_{coul} = \sum V^{\lambda\lambda'}_{\nu\alpha\nu'\alpha'}\hat{a}^\dagger_{\lambda,\nu}\hat{a}^\dagger_{\lambda,\alpha}\hat{a}_{\lambda',\nu'}\hat{a}_{\lambda,\alpha'}. \tag{2.23}$$

Third, the light-matter interaction can be expressed in dipole approximation [Wiersig, 2007, Garrison and Chiao, 2014]. It is typically valid for a system with the wavelength of the mode being much bigger than the size of the QD. As a result, the mode function of the electromagnetic field remains almost constant over position and therefore $\mathbf{u}_\xi(\mathbf{r}) \approx \mathbf{u}_\xi(\mathbf{r}_0)$, where $\mathbf{r}_0$ is the location of QD. The dipole Hamiltonian can be written as

$$\hat{H}_D = \int d^3\mathbf{r}\hat{\Psi}^\dagger(\mathbf{r})(-e\vec{E}_T(\mathbf{r}_0))\hat{\Psi}(\mathbf{r},t). \tag{2.24}$$

The strength of the light-matter coupling is calculated by dipole matrix elements,

$$g_{\xi\alpha\nu}^{\lambda\lambda'} = \sqrt{\frac{\hbar\omega_\xi}{2\epsilon\epsilon_0 vol_\xi}} \int d^3r \psi_\alpha^{\lambda *}(\mathbf{r}) e\mathbf{r}\mathbf{u}_\xi(\mathbf{r}_0)\psi_\nu^{\lambda'}(\mathbf{r}). \tag{2.25}$$

In the above equation the prefactor is called the vacuum amplitude which contains the normalizing mode volume vol_ξ of mode ξ. Hence, the dipole Hamiltonian can be given by

$$\hat{H}_D = \sum_{\xi,\alpha,\nu,\nu',\alpha',\lambda,\lambda'} g_{\xi\alpha\nu}^{\lambda\lambda'} \hat{a}_{\lambda,\alpha}^\dagger \hat{a}_{\lambda',\nu}(\hat{b}_\xi^\dagger + \hat{b}_\xi) + H.c., \tag{2.26}$$

in terms of bosonic and fermionic creation and annihilation operators. It describes the emission and the absorption of a photon in mode ξ due to the transition of a carrier from band λ' in state ν to band λ in state α as well as the conjugate process. For the sake of simplicity, we use the equal envelope approximation for valence- and conduction-bands [Baer et al., 2006]. The dipole matrix elements read $g_{\xi\alpha\nu}^{\lambda\lambda'} = \mathbf{u}_\xi(\mathbf{r}_0)\mathbf{d}_{\lambda\lambda'}\delta_{\alpha\nu}$ with the inter-band matrix elements $\mathbf{d}_{\lambda\lambda'}$. Furthermore, the Rotating Wave Approximation is employed to neglect fast oscillating terms in a dipole for situations of weak coupling near the resonance [Meystre and Sargent, 1999, Wu and Yang, 2007].

By applying these approximations, we can rewrite the many-body Hamiltonian in terms of the fermionic operators $\hat{c}_j$ ($\hat{c}_j^\dagger$) and $\hat{v}_j$ ($\hat{v}_j^\dagger$). $\hat{c}_j$ ($\hat{c}_j^\dagger$) annihilates (creates) a conduction-band carrier in the state $|j\rangle_c$. Also, $\hat{v}_j$ ($\hat{v}_j^\dagger$) annihilates (creates) a valence-band carrier in the state $|j\rangle_v$. With this notion, the single-particle Hamiltonian can be written as

$$\hat{H}_{Carr}^0 = \sum_j \varepsilon_j^c \hat{c}_j^\dagger \hat{c}_j + \sum_j \varepsilon_j^v \hat{v}_j^\dagger \hat{v}_j, \tag{2.27}$$

where $\varepsilon_j^{c,v}$ are the energies for conduction and valence band carriers. The two-particle Coulomb Hamiltonian reads

$$\hat{H}_{Coul} = \frac{1}{2}\sum_{k'jj'k} (V_{k'jj'k}^{cc} \hat{c}_{k'}^\dagger \hat{c}_j^\dagger \hat{c}_{j'} \hat{c}_k + V_{k'jj'k}^{vv} \hat{v}_{k'}^\dagger \hat{v}_j^\dagger \hat{v}_{j'} \hat{v}_k) + \sum_{k'jj'k} V_{k'jj'k}^{cv} \hat{c}_{k'}^\dagger \hat{v}_j^\dagger \hat{v}_{j'} \hat{c}_k, \tag{2.28}$$

and the dipole Hamiltonian is given by

$$\hat{H}_D = -i\sum_{\xi,j} (g_{\xi j} \hat{c}_j^\dagger \hat{v}_j \hat{b}_\xi - g_{\xi j}^* \hat{v}_j^\dagger \hat{c}_j \hat{b}_\xi^\dagger). \tag{2.29}$$

Here all Hamiltonians have been written for the case of two shells with s- and

p-shell, $j, j', k, k' \in s, p$, and mode ξ.

2.3 Equation of motion

The dynamics of an open quantum mechanical system can be described by the von Neumann–Lindblad (vNL) model for the case of reduced density operator ($\hbar = 1$)

$$\frac{d}{dt}\rho = -i[H, \rho] + L\rho, \tag{2.30}$$

where the Hamiltonian H generates the internal coherent dynamics and the Lindblad superoperator L denotes the dissipative coupling to the environment. Because of the size of the system, the explicit solution of $\rho(t)$ is not straightforward and knowledge of some expectation values would be enough. We describe the system by considering the time evolution of expectation values formulated by a generalized Ehrenfest EoM in Eq. (2.8) for observable quantities. This approach however encounters an infinite hierarchy of equations for various expectation values of photon and carrier operators due to the interaction of the Hamiltonian and the scattering terms in the Lindblad terms. A common way to solve this problem and to make the numerical integration feasible is to truncate the hierarchies at a certain level. The accuracy of the truncation result depends mainly on the used technique and type of investigated system. In general, we can divide these techniques into two main types: One scheme is to use correlation functions (CFs) in the cluster expansion [Fricke, 1996, Hoyer et al., 2004], where the equations of motion for expectation values are substituted by equations of motion for correlation functions. Higher-order correlation functions are assumed to have a negligible contribution and are therefore neglected [Wiersig et al., 2009, Kapetanakis and Perakis, 2008, Kira et al., 1998, Hoyer et al., 2003]. The second approach is to apply the expectation values (EVs) in the cluster expansion and to truncate the hierarchy in the same way [Gartner, 2011, Richter et al., 2009, Witthaut et al., 2011, Carmele et al., 2010]. The formulation in CFs is algebraically more complex but is shown to be numerically more efficient for large systems. On the other hand, EV model reduces considerably the algebraic complexity and generates a linear and transparent system of EoM, but is mainly appropriate for small systems. In this doctoral thesis, we use the formulation in CFs to describe the statistical properties of the photon emission events in QD microcavity lasers. In

the following section, we give a brief overview of this model; more details can be found in Refs. [Leymann et al., 2013a, 2014, Leymann, 2016, Foerster, 2017], where a new formulation, expectation value based cluster expansion (EVCE), has been also introduced to ease a switch between an EV and CF formulation.

2.3.1 Definition of correlation functions

In this section, we first address the main concept of correlation functions. Basic definitions of correlation functions and more details in this regards can be found in Ref. [Fricke, 1996]. Next, we study various approximations that are used to neglect EVs and CFs.

The starting point is the principle that each EV $\langle b_1 b_2 ... b_k \rangle$ of operators b_i[4] can be presented by summation over the products of CFs. For mathematical formulation, we need to define a set of indices $I = 1, 2, ..., k$ as well as a product of operators $b^I = b_1 b_2 ... b_k$. The factorization operator $\mathbf{F}$ is also introduced that only alters the representation of the EV (similar to a passive transformation of a vector) without affecting the value of complex number $\langle b^I \rangle$. Therefore, CFs $\delta(b^J)$ can be defined as

$$\mathbf{F}\langle b^I \rangle = \delta(b^I) + \delta(b^J)_F = \sum_{P \in P_I} \prod_{J \in P} \delta(b^J), \tag{2.31}$$

where $\delta(b^J)_F$ represents the sum of products of all probable factorizations of the operator EV $\langle b^I \rangle$ into CFs that contains only a smaller number of operators than the cardinality of I ,$\#(I)$. Moreover, P is a partition of the set I implying a set group of disjoint nonempty subsets J of I with $\cup_{J \in P} J = I$. P_I is the set of all partitions of I.

For example, for the first three orders of expectation values we can decompose an expectation value according to Eq. (2.31):

$$\begin{aligned} \mathbf{F}\langle b_1 \rangle &= \delta(b_1), \\ \mathbf{F}\langle b_1 b_2 \rangle &= \delta(b_1 b_2) + \delta(b_1)\delta(b_2), \\ \mathbf{F}\langle b_1 b_2 b_3 \rangle &= \delta(b_1 b_2 b_3) + \delta(b_1 b_2)\delta(b_3) \\ &\quad + \delta(b_1 b_3)\delta(b_2) + \delta(b_2 b_3)\delta(b_1) + \delta(b_1)\delta(b_2)\delta(b_3). \end{aligned} \tag{2.32}$$

[4] In this part we consider bosonic operators to retain the general ideas more explicit. We can also introduce an identical explanation of CFs for fermionic operators f_i.

Also the inverse operation $\mathbf{F}^{-1}\mathbf{F} = \mathbf{1}$ can be written as

$$\mathbf{F}^{-1}\delta(b^I) = \langle b^I \rangle - \mathbf{F}^{-1}\delta(b^I)_F = \sum_{P\in P_I} c_P \prod_{J\in P} \delta\langle b^J \rangle, \tag{2.33}$$

with $c_P = (-1)^{\#(P)-1}[\#(P)-1]!$. As can be seen in Eq. (2.33), a CF is now replaced completely by EV. The first three refactorized CFs based on the data of Eq. (2.33) read

$$\begin{aligned}
\mathbf{F}^{-1}\delta(b_1) &= \langle b_1 \rangle, \\
\mathbf{F}^{-1}\delta(b_1 b_2) &= \langle b_1 b_2 \rangle - \langle b_1 \rangle \langle b_2 \rangle, \\
\mathbf{F}^{-1}\delta(b_1 b_2 b_3) &= \langle b_1 b_2 b_3 \rangle - \langle b_1 b_2 \rangle \langle b_3 \rangle \\
&\quad - \langle b_1 b_3 \rangle \langle b_2 \rangle - \langle b_2 b_3 \rangle \langle b_1 \rangle + \langle b_1 \rangle \langle b_2 \rangle \langle b_3 \rangle.
\end{aligned} \tag{2.34}$$

We may conclude that every EV can be substituted in an explicit way by CFs. The same holds for CFs and each CF can be represented by EVs as well.

2.3.2 Approximations by lower-order quantities

Now, we explain that how the representation of a quantity in terms of a sum of products of other quantities can be applied for the approximation schemes. We use the abbreviated notation $\delta(N)$, which denotes any function of CFs $\delta(b^I)$ of order N or smaller. For example, the third line of Eqs. (2.32) can be presented in this form as

$$\mathbf{F}\langle b_1 b_2 b_3 \rangle \equiv \delta(3) + 3\delta(2)\delta(1) + \delta(1)^3. \tag{2.35}$$

The basic idea of CE is to neglect all CFs of order larger than N. For this purpose a truncation operator $\Delta_{\delta(N)}$ is introduced:

$$\Delta_{\delta(N)}\delta(N+1) = \delta(N). \tag{2.36}$$

For instance, here $\Delta_{\delta(2)}$ is applied on the third line of Eq. (2.32):

$$\Delta_{\delta(2)}(\delta(3) + 3\delta(2)\delta(1) + \delta(1)^3) = 3\delta(2)\delta(1) + \delta(1)^3 \equiv \delta(2). \tag{2.37}$$

To further illustrate this concept, Figure 2.2 shows that only CFs up to the second order must be neglected.

Moreover $\langle N \rangle$ is introduced as a short form of any function of EVs

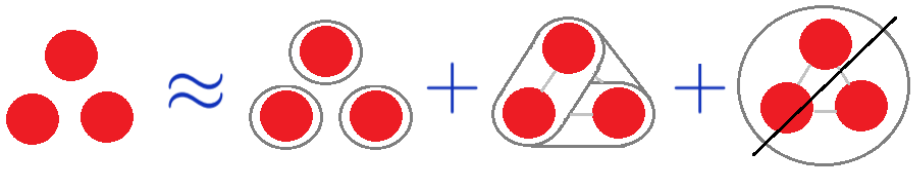

Figure 2.2: The result of applying $\Delta_{\delta(2)}\mathbf{F}$ on a third order EV according to Eq. (2.37).

corresponding N or less operators. The truncation operator $\Delta_{\langle N\rangle}$ can be given by

$$\Delta_{\langle N\rangle}\langle N+1\rangle = \langle N\rangle, \tag{2.38}$$

here, any function of order $N+1$ of $EV\langle N+1\rangle$ is reduced to a function with only terms of order N.

The truncation method is therefore based on applying the $\Delta_{\delta(N)}$ to CFs and $\Delta_{\langle N\rangle}$ to EVs thereby neglecting high-order terms. This fact that the representation of the quantities depends on the truncation method make it complicated. The factorization operator is helpful to switch between a formulation in EVs or CFs. The EV $\langle b^I\rangle$ can be formulated by applying the $\Delta_{\delta(\#I-1)}$

$$\mathbf{F}^{-1}\Delta_{\delta(\#I-1)}\mathbf{F}\langle b^I\rangle = -\sum_{P\in P_I\setminus I} c_P \prod_{J\in P}\langle b^J\rangle. \tag{2.39}$$

We give an example to illustrate the approach with transformations between EVs and CFs:

$$\begin{aligned}
\mathbf{F}^{-1}\delta_{\delta(1)}\mathbf{F}\langle b_1b_2\rangle &= \langle b_1\rangle\langle b_2\rangle,\\
\mathbf{F}^{-1}\delta_{\delta(1)}\mathbf{F}\langle b_1b_2b_3\rangle &= \langle b_1\rangle\langle b_2\rangle\langle b_3\rangle,\\
\mathbf{F}^{-1}\delta_{\delta(2)}\mathbf{F}\langle b_1b_2b_3\rangle &= \langle b_1b_2\rangle\langle b_3\rangle + \langle b_1b_3\rangle\langle b_2\rangle\\
&\quad + \langle b_2b_3\rangle\langle b_1\rangle - 2\langle b_1\rangle\langle b_2\rangle\langle b_3\rangle.
\end{aligned} \tag{2.40}$$

It is also possible to transfer between CFs and EVs to formulate CFs $\delta(b^I)$ by applying the truncation operator $\Delta_{\langle N\rangle}$ and reaching a sum of products of low-order CFs:

$$\mathbf{F}\Delta_{\langle N-1\rangle}\mathbf{F}^{-1}\delta(b^I) = -\sum_{P\in P_I\setminus I}\prod_{J\in P}\delta(b^J). \tag{2.41}$$

The selected way of approximation depends completely on the physical system

that we want to study.

2.3.3 The hierarchy problem

To describe our open quantum system, we use the generalized Ehrenfest EoM in Eq. (2.8). The EoM for expectation values of the quantities of interest lead to coupling a n-order quantity to a $(n+1)$-order quantity. This hierarchy problem can be symbolically presented as:

$$\begin{aligned} \frac{d}{dt}\langle 1\rangle &= \langle \mathcal{L}(1)\rangle = \langle 2\rangle \\ \frac{d}{dt}\langle 2\rangle &= \langle \mathcal{L}(2)\rangle = \langle 3\rangle \\ &\vdots \end{aligned} \tag{2.42}$$

Various formulations and approximation techniques are used to truncate the hierarchy of differential equations. In the following, we explain in more detail the formulation of the EoM using EVs or CFs.

The truncation technique for a finite physical system that consists of a small number of particles n is to vanish EVs with $n+1$ particles. This technique is similar to the application of the truncation operator $\Delta_{\langle N\rangle}$. This operator can be applied on the Nth line of the hierarchy in Eqs. (2.42):

$$\begin{aligned} \frac{d}{dt}\langle 1\rangle &= \langle \mathcal{L}(1)\rangle = \langle 2\rangle \\ &\vdots \\ \frac{d}{dt}\langle N\rangle &= \langle \mathcal{L}(N)\rangle \approx \Delta_{\langle N\rangle}\langle N+1\rangle = \langle N\rangle, \end{aligned} \tag{2.43}$$

This method is also schematically illustrated in Figure 2.3. The resulting linear equations describe a finite physical system including a small number of particles that occupy a confined number of states.

On the other hand, for a large system the cluster expansion method is efficient [Fricke, 1996, Hoyer et al., 2004], where the EoM is formulated in CFs and then the CFs set zero at a certain order. In order to derive the differential equation for the CF δb^I, we apply the Ehrenfest EoM to the relevant EV and then the resulting EVs switch to CFs by factorization operator $\mathbf{F}$. Finally, previously obtained derivatives of lower-order factorizations must be subtracted as shown

Figure 2.3: Schematic representation of an EV hierarchy. The EV of a certain order connects linearly to the next order that is shown by the black line. The truncation operator $\Delta_{\langle N\rangle}$ is applied by setting the $(N+1)$ EV to zero. The figure is taken from [Leymann et al., 2014]

.

below:

$$\frac{d}{dt}\delta(b^I) = \mathbf{F}\langle\mathcal{L}(b^I)\rangle - \frac{d}{dt}\delta(b^I)_F. \tag{2.44}$$

In this equation, the $\mathcal{L}$ term leads to an infinite hierarchy of CFs (like its effect on the formulation in EVs) as shown below:

$$\begin{aligned}
\frac{d}{dt}\delta(1) &= \mathbf{F}\langle\mathcal{L}(1)\rangle - \frac{d}{dt}\delta(1)_F = \delta(2)\\
\frac{d}{dt}\delta(2) &= \mathbf{F}\langle\mathcal{L}(2)\rangle - \frac{d}{dt}\delta(2)_F = \delta(3)\\
&\vdots\,\vdots\,\vdots
\end{aligned} \tag{2.45}$$

Now the truncation operator $\Delta_{\delta(N)}$ is applied to the Nth line of Eqs. (2.45) to reduce the order of CFs:

$$\begin{aligned}
\frac{d}{dt}\delta(1) &= \mathbf{F}\langle\mathcal{L}(1)\rangle - \frac{d}{dt}\delta(1)_F = \delta(2)\\
&\vdots\,\vdots\,\vdots\\
\frac{d}{dt}\delta(N) &= \mathbf{F}\langle\mathcal{L}(N)\rangle - \frac{d}{dt}\delta(N)_F\\
&\approx \Delta_{\delta(N)}\mathbf{F}\langle\mathcal{L}(N)\rangle - \frac{d}{dt}\delta(N)_F = \delta(N).
\end{aligned} \tag{2.46}$$

A schematic illustration of Eq. (2.46) is presented in Figure 2.4.

Comparing now Figures 2.3 and 2.4 one realizes that the EV-based formulation originates directly from the linear Ehrenfest EoM and the resulting EVs are also entirely linear, while the CF-based formulation is nonlinear due to the presence of time derivatives of the lower-order factorizations. Though the latter technique has higher numerical effort it can be applied to characterize dynamics of a large

Figure 2.4: Schematic representation of a CF hierarchy. The black line indicates the connection between the first-order CF to the second-order CF and the second-order to the third-order quantity and so on. The blue lines illustrate the production of lower-order CF. The $(N+1)$th CF is set to zero by using the truncation operator $\Delta_{\delta(N)}$. In contrast to Fig. 2.3, the structure of CF hierarchy is nonlinear. The figure is taken from [Leymann et al., 2014].

system. In the current doctoral thesis, in order to investigate the optical properties of QD microcavity lasers, our microscopic semiconductor model is based on the cluster expansion where an acceptable accuracy can be provided for our purpose.

In the following we will briefly touch the expectation value cluster expansion (EVCE) model that combines the both formulations retaining their advantages. This approach is originally developed by Leymann et al. [2013a, 2014], Leymann [2016], Foerster [2017]. The main idea of EVCE is to apply the truncation operator $\Delta_{\delta(N)}$ to the N-th line of Eq. (2.43) to reach a system of EV-based EoM by using $\mathbf{F}^{-1}$ that is equivalent to a CF-based system:

$$\begin{aligned} &\frac{d}{dt}\langle 1\rangle = \langle \mathcal{L}(1)\rangle = \langle 2\rangle \\ &\qquad \vdots\,\vdots\,\vdots \\ &\frac{d}{dt}\langle N\rangle = \langle \mathcal{L}(N)\rangle \approx \mathbf{F}^{-1}\Delta_{\delta(N)}\mathbf{F}\langle N+1\rangle = \langle N\rangle. \end{aligned} \tag{2.47}$$

Figure 2.5: Schematic representation of an EV hierarchy truncated by applying $\Delta_{\delta(N)}$. This hierarchy is very similar to the hierarchy illustrated in Fig. 2.4. On the other hand, its structure is equal to the EV structure that has been shown in Fig. 2.3. The figure is taken from [Leymann et al., 2014].

Because of the same truncation scheme in Eqs. (2.47) and Eqs. (2.46), their

results are equivalent. However, as can be seen in Figure 2.5, Eqs. (2.47) are almost linear and only actual approximations that are used in the EoM are nonlinear.

2.4 Statistical properties of light

Some unique properties like temporal and spatial coherence make lasers distinguished from other light sources. Statistical characteristics of light can be investigated to explore the properties of a light source. An appropriate measure to characterize the statistical properties of an electromagnetic field emission are photon-autocorrelation function measurements. Now different types of these functions will be described.

First-order photon-autocorrelation function $g^{(1)}(t,\tau)$ is the normalized amplitude-amplitude correlation to study the coherence features of light. It can be written as

$$g^{(1)}(t,\tau) = \frac{G^{(1)}(t,\tau)}{\langle \hat{b}^\dagger(t)\hat{b}(t)\rangle} = \frac{\langle \hat{b}^\dagger(t+\tau)\hat{b}(t)\rangle}{\langle \hat{b}^\dagger(t)\hat{b}(t)\rangle}, \tag{2.48}$$

where t and τ are time and delay time, respectively. The autocorrelation function can be experimentally measured by a linear optical interferometer like the Michelson interferometer, the Mach-Zehnder interferometer or the Sagnac interferometer [Mandel and Wolf, 1995].

Second-order photon-autocorrelation function $g^{(2)}(t,\tau)$ is one of the most crucial characteristic functions for an emitted light that can be experimentally measured in a Hanbury Brown–Twiss setup [Hanbury Brown and Twiss, 1956, Mandel and Wolf, 1995] which can be schematically illustrated in Figure 2.6. We can write this function as

$$g^{(2)}(t,\tau) = \frac{G^{(2)}(t,\tau)}{\langle \hat{b}^\dagger(t)\hat{b}(t)\rangle\langle \hat{b}^\dagger(t+\tau)\hat{b}(t+\tau)\rangle} = \frac{\langle \hat{b}^\dagger(t)\hat{b}^\dagger(t+\tau)\hat{b}(t+\tau)\hat{b}(t)\rangle}{\langle \hat{b}^\dagger(t)\hat{b}(t)\rangle\langle \hat{b}^\dagger(t+\tau)\hat{b}(t+\tau)\rangle}. \tag{2.49}$$

In most cases of this thesis we consider this photon autocorrelation function at a delay time equal zero. Thus, we can rewrite it as

$$g^{(2)}(0) = \frac{\langle \hat{b}^\dagger\hat{b}^\dagger\hat{b}\hat{b}\rangle}{\langle \hat{b}^\dagger\hat{b}\rangle^2}. \tag{2.50}$$

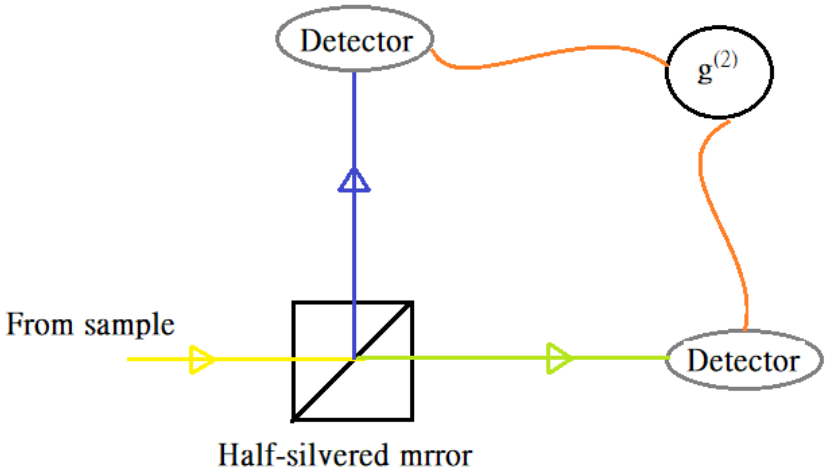

Figure 2.6: Schematic illustration of a HBT setup.

Figure 2.7 shows different values of the second-order photon-autocorrelation function at zero delay time. The emitted photons are uncorrelated as in laser light $g^{(2)}(0) = 1$, or if the photons are correlated and emitted in bunches $g^{(2)}(0) > 1$ or if the photons are anticorrelated and display an antibunching behavior $g^{(2)}(0) < 1$.

Moreover, we can define the photon-autocorrelation function of order n by extending the second-order function:

$$g^{(n)}(0) = \frac{\langle \hat{b}^{\dagger n} \hat{b}^n \rangle}{\langle \hat{b}^\dagger \hat{b} \rangle^n}. \tag{2.51}$$

Here, we can analytically calculate the values for the special cases of thermal light $g^{(n)}(0) = n!$ and coherent light $g^{(n)}(0) = 1$.

2.5 Statistical properties of microlaser emission in the single-mode case

To study the physics of QD microcavity systems, we consider the dipole interaction between charge carriers confined in QDs with the light field of discrete cavity modes. Within the well-known Jaynes-Cummings model [Cummings, 1965], the dipole interaction is described in terms of a coherent exchange of energy between

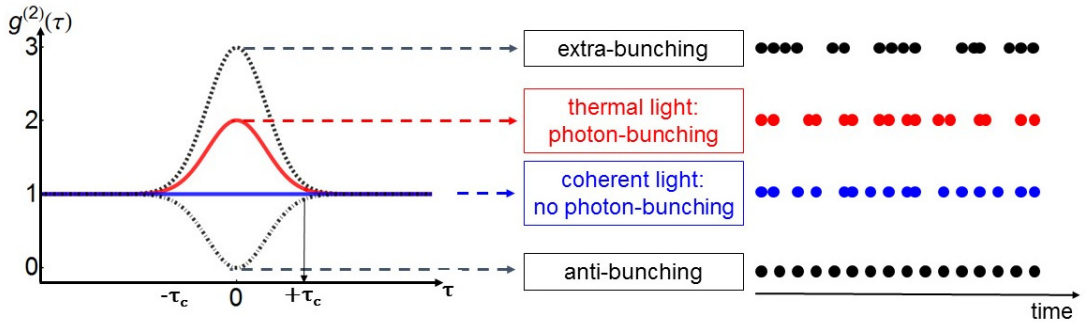

Figure 2.7: Illustration of the statical properties of emitted light through the second-order photon-autocorrelation function at zero delay time. Left: The intensity auto-correlation functions are characterized for coherent light (blue), for thermal light (red), for non-classical light (dash-dotted) and for light illustrating extra-bunching (dotted). Right: Visualization of characterization of light for various states of photon bunching [Blumenstein, 2017].

the emitters and the electromagnetic field. Comparing light-matter coupling strength and irreversible losses from both emitter and optical modes, cavity quantum electrodynamics appears in the weak and strong light-matter coupling regime [Reithmaier et al., 2004, Badolato et al., 2005, Vahala, 2003, Yoshle et al., 2004]. The weak-coupling regime plays an important role in modern microcavity laser physics. In this regime it is possible to control the β factor which expresses the fraction of spontaneous emission coupled into the lasing mode.

Furthermore, a sudden intensity jump in the input/output curve is an indicator for the onset of lasing. The threshold and the β-factor can be commonly determined by the height of the intensity jump at the lasing threshold, whereas for high β-factor lasers the intensity jump vanishes and it is difficult to determine the onset of lasing only through the input-output curves. This issue led to several researches on the second-order photon autocorrelation function to determine the onset of lasing [Strauf et al., 2006, Ulrich et al., 2007, Gies et al., 2007]. As can be seen in Figure 2.8, for small β-factors, the intensity jump coincides the sudden reduction of the second-order autocorrelation function from the Poisson value $g^{(2)}(0) = 2$ corresponding to the statistics of a thermal light to $g^{(2)}(0) = 1$ corresponding to the emission of coherent laser light. With increasing β values, the sudden decline of the autocorrelation function becomes softer. The fact that much below threshold the autocorrelation function is slightly smaller than 2 is due to the finite number of QDs [Gies et al., 2012].

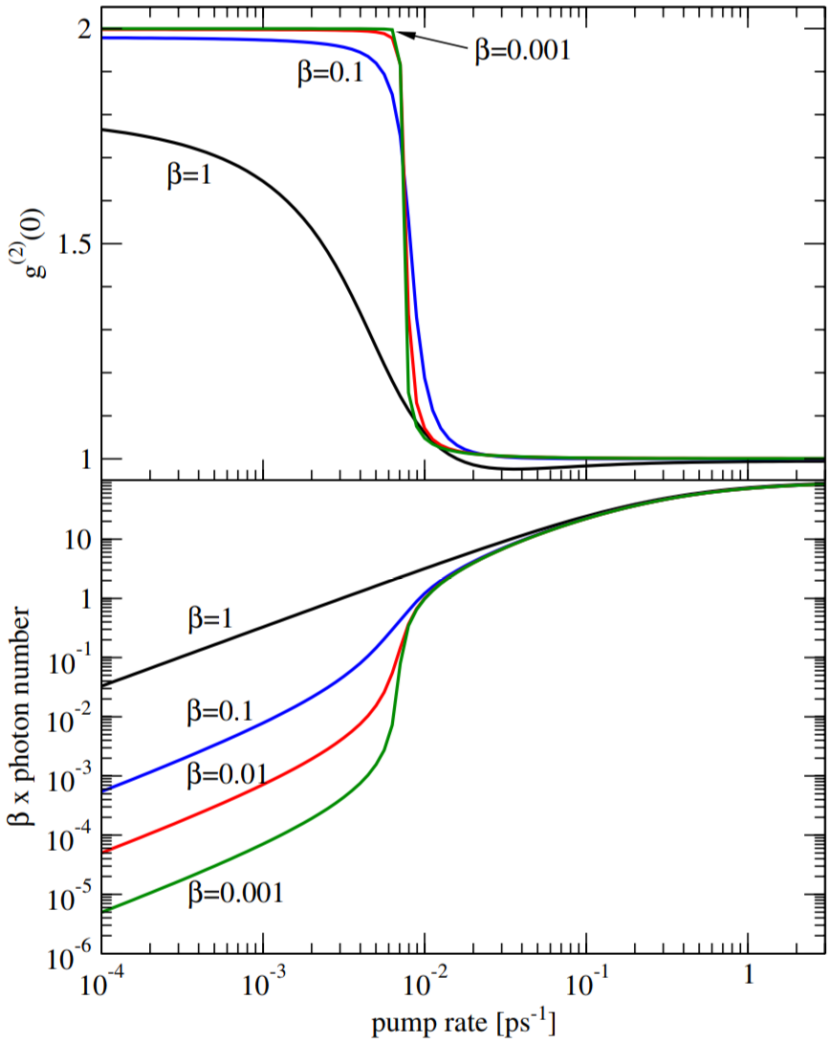

Figure 2.8: Statistical properties of emitted light in the single-mode microcavity laser. The curves in the upper panel correspond to the calculated input-output curve. In the lower panel autocorrelation function $g^{(2)}(\tau = 0)$ is shown for various values of $\beta = 0.001$, 0.01, 0.1 and 1. The picture is taken from [Gies et al., 2007].

Based on this theory explained in this chapter, we will discuss the effect of the second mode on the lasing behavior of the QD microcavity laser in the next chapters.

Chapter 3

Two-mode microcavity laser

The research on physics of microcavity lasers has been so far mainly focused on interactions between a single optical mode and the QD gain medium. However, study of microcavity lasers with two optical modes allows addressing main features of gain competition in lasers and also the resulting effective mode coupling that leads to characteristic oscillations in coherence properties [Leymann et al., 2013b, Ates et al., 2007], deterministic polarization chaos in the presence of optical feedback [Virte et al., 2013], and increased sensitivity on external perturbations in the presence of optical self-feedback [Albert et al., 2011]. Figure 3.1 displays schematically a QD coupled to a single- and two-mode cavities.

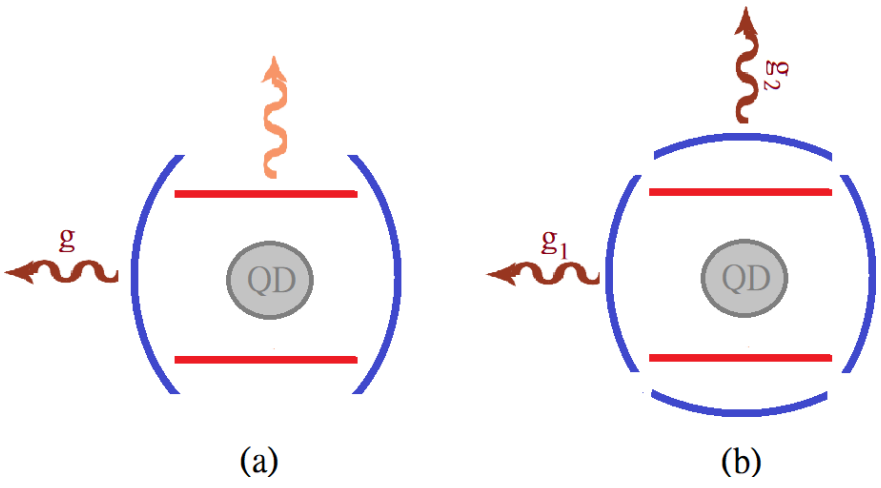

Figure 3.1: Schematic illustration of interaction between a QD and a single- or two-mode cavity. (a) QD coupled to a single mode cavity with a coupling strength g, (b) a two-mode cavity coupled to a QD with coupling strengths g_1 and g_2.

We further investigate here two-mode photon correlations in a QD microcavity laser that has been studied before by Leymann et al. [2013b], Eremeev et al. [2011], Majumdar et al. [2012], Khanbekyan et al. [2015], Schlottmann et al. [2018], Khanbekyan [2018] with a novel emphasis on the effects induced by a direct coupling of two competing modes. Here we assume that both modes are connected to the QD s-shell transition. In order to investigate the coupling of two cavity modes in a regime of recent experiments [Leymann et al., 2013b, Khanbekyan et al., 2015], we consider the behavior of an open quantum system described by the extended microscopic semiconductor theory from Ref. [Gies et al., 2007]. However, the previous works assumed that two modes were not directly coupled. In the current work, the microscopic QD theory is further developed to study the additional terms that arise from the direct dissipative coupling between optical modes. This kind of coupling terms has been introduced in Ref. [Hackenbroich et al., 2002]. The first study of the consequences of these additional terms on two interacting modes was performed by Eremeev et al. [2011] where both modes interact with the common gain medium consisting of an ensemble of two-level atoms. The atoms were randomly pumped and interacted with the two modes only one by one; while we theoretically study bimodal microcavity lasers with QDs as active gain medium where QDs are pumped continuously and interact simultaneously with the optical modes.

In the following sections, first an overview of the experimental benchmark and the underlying theory of simulations will be presented. Then, in order to describe and analyze the behavior of the mode coupling of bimodal microlasers, we consider two different cases:
In section 3.3, we review the statistical properties of the emitted light with zero off-diagonal elements of the damping matrix γ in Eq. (2.7) and compare out results to the study of Ref. [Leymann et al., 2013b]. This model indicates that two modes are not directly coupled but instead interact indirectly via the QD-gain medium as schematically shown in Figure 3.2(a). The simulation results will be presented for two modes with nearly equal Q factors, where only mode 1 is in exact resonance with the QDs and mode 2 is separated by the spectral detuning $\Delta_{12} = \omega_1 - \omega_2$. The input-output characteristic of the first mode shows typical statistical behavior of a laser mode, i.e. the intensity presents a characteristic S-shaped behavior in a double logarithmic plot, whereas the intensity of the second mode exhibits a threshold behavior and can even decrease with further

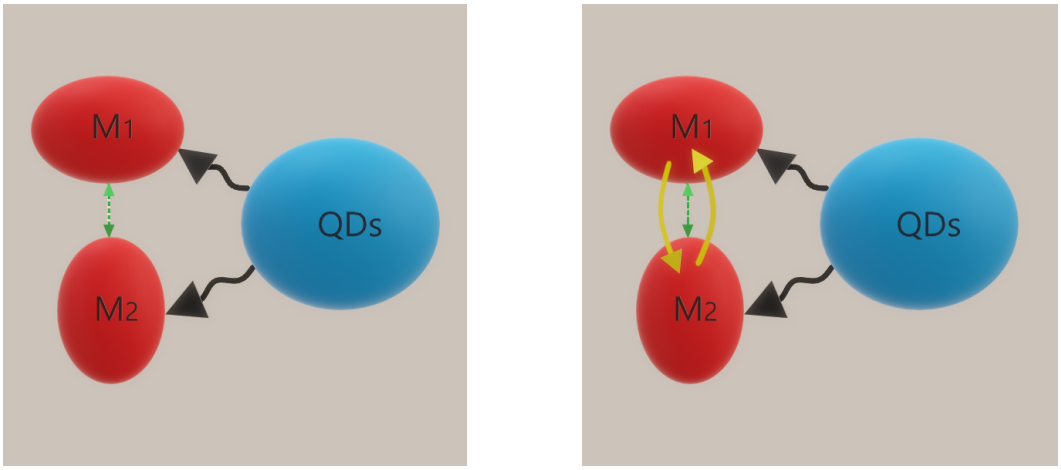

(a) (b)

Figure 3.2: Illustration of the interaction of the modes M1 and M2 (cavity modes) with QDs that induces unconventional coherent coupling between these modes (green dashed line) in (a) without direct dissipative coupling, and (b) with direct dissipative coupling (yellow lines).

enhancement of the pump rates. Measuring the autocorrelation function of mode 1 at zero delay time ($\tau = 0$) $g^{(2)}(0)$ indicates the onset of lasing above the threshold. In contrast, in mode 2, for pump rates higher than the threshold values, the autocorrelation function at zero delay time $g^{(2)}(0)$ demonstrates strong photon bunching associated with superthermal values. The gain competition is reflected in explicit differences in behaviors of two modes that can be also confirmed by photon cross-correlation measurements. Cross-correlation magnitude decreases to values smaller than unity indicating a definite anticorrelation between the cavity emission modes. The theoretical studies based on a microscopic semiconductor theory are found to be in qualitative agreement with experimental findings of the team of Prof. Reitzenstein at TU Berlin [Leymann et al., 2013b].

Later in section 3.4, we study the effects of direct dissipative mode coupling in a bimodal microcavity laser by considering a system with non-zero off-diagonal elements of the damping matrix γ in Eq. (2.7). A schematic illustration is shown in Figure 3.2(b), where direct and indirect coupling of two modes can be seen. In order to describe and analyze these specific features, the microscopic QD theory is developed by considering the off-diagonal elements of γ and the results can be regarded as modification of findings of the first case where there was no direct coupling between modes. Numerical results reveal an enhanced autocorrelation of

both modes and an enhanced anticorrelation between the modes with increasing γ_{12} and γ_{21}. A detailed analysis is given in terms of dark and bright modes. It will be shown that above the lasing threshold the original modes build up a bright mode coupled to the QDs and a dark mode, that interacts only indirectly with the QDs. We will show that a populated dark mode can enable an efficient transfer of photons between the two original cavity modes, mediating an effective coupling between them. Results of this chapter are partly published in Ref. [Fanaei et al., 2016].

3.1 Experiment

We first provide a brief review of the experimental results obtained from a two-mode micropillar laser in the group of Prof. S. Reitzenstein which have been previously presented in Ref. [Leymann et al., 2013b]. The electrically pumped micropillar lasers are based on a high-quality factor planar AlAs/GaAs microcavity structure that includes InGaAs QDs in the active layer. To increase the β-factor, various technological works like plasma-enhanced etching, high-resolution electron-beam lithography and metal deposition have been performed on electrically pumped microlasers. The emission has been then studied at low temperature (20 K) by a high-resolution microelectroluminescence (μEL) setup. To make polarization-resolved measurements of the laser mode a combination of a linear polarizer and a $\lambda/4$-wave plate is set up in front of the entrance of the monochromator. The photon autocorrelation function $g^{(2)}(\tau)$ which has been estimated by a fiber-coupled Hanbury Brown and Twiss (HBT) configuration with a temporal resolution $\tau_{\mathrm{irf}} = 40$ ps, provides information of the photon statistics of the emitted light. In order to do this, the emitted light is divided by a polarization-maintaining 50 : 50 beam splitter and connected to two monochromators having a linear polarizer at the input slit and a fiber-coupled single-photon-counting module at the output slit. Thus, polarization-resolved cross-correlation can be measured with a spectral resolution of 25 μeV.

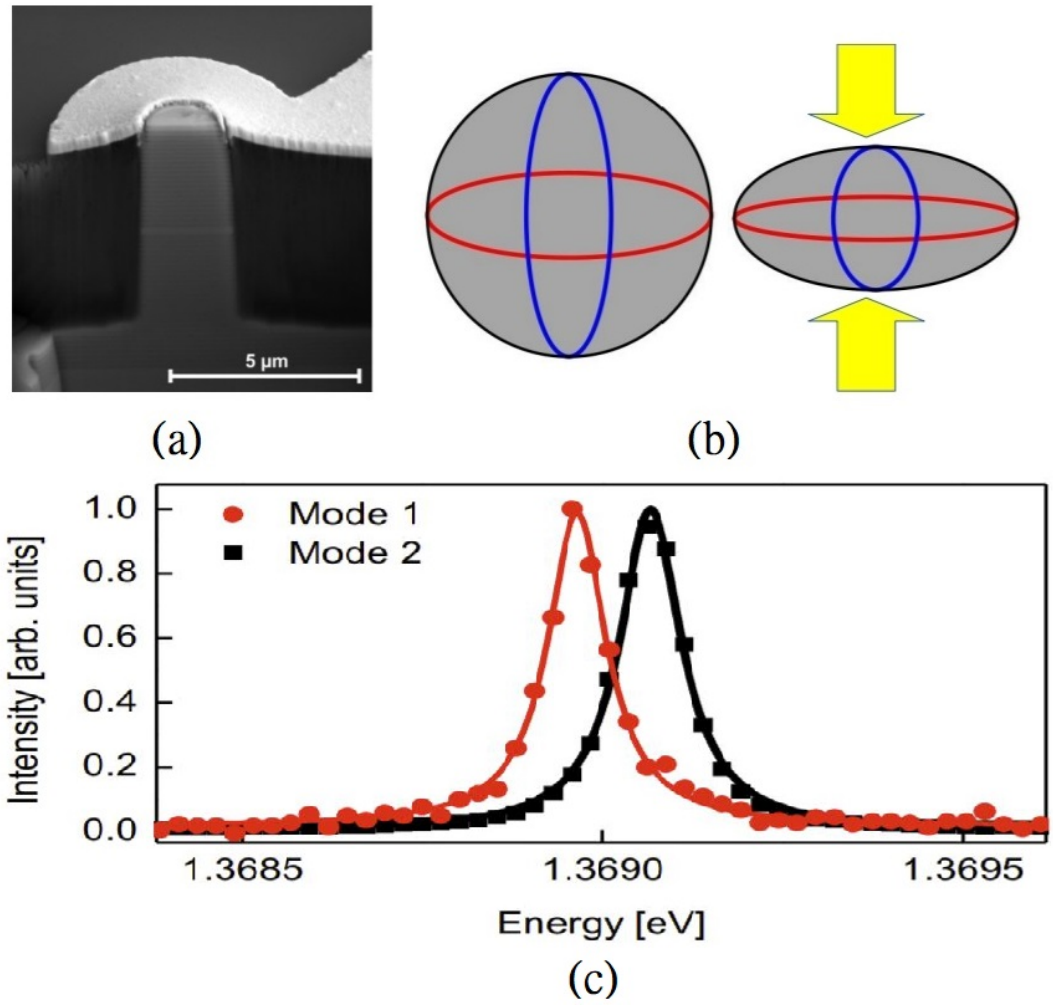

Figure 3.3: (a) Illustration of the development of two linearly polarized modes [Reitzenstein and Forchel, 2010]. (b) Slight asymmetry of the cross-section of the pillar and the ring-shaped contact leads to two distinct linearly polarized modes in a micropillar [Sebald et al., 2009]. (c) Two orthogonally polarized cavity modes with a spectral detuning of 103 μeV and nearly equal Q factors, for mode 1 ($Q = 13900$) and mode 2 ($Q = 13100$) [Leymann et al., 2013b].

The minor asymmetry of the cross-section of the pillar and the ring-shaped contact leads to distinguished linearly polarized modes [Reitzenstein et al., Sebald et al., 2009] as displayed in Figure 3.3. The two modes are separated in energy by 103 μeV and have nearly equal quality factor with $Q = 13900$ (mode 1) and $Q = 13100$ (mode 2).

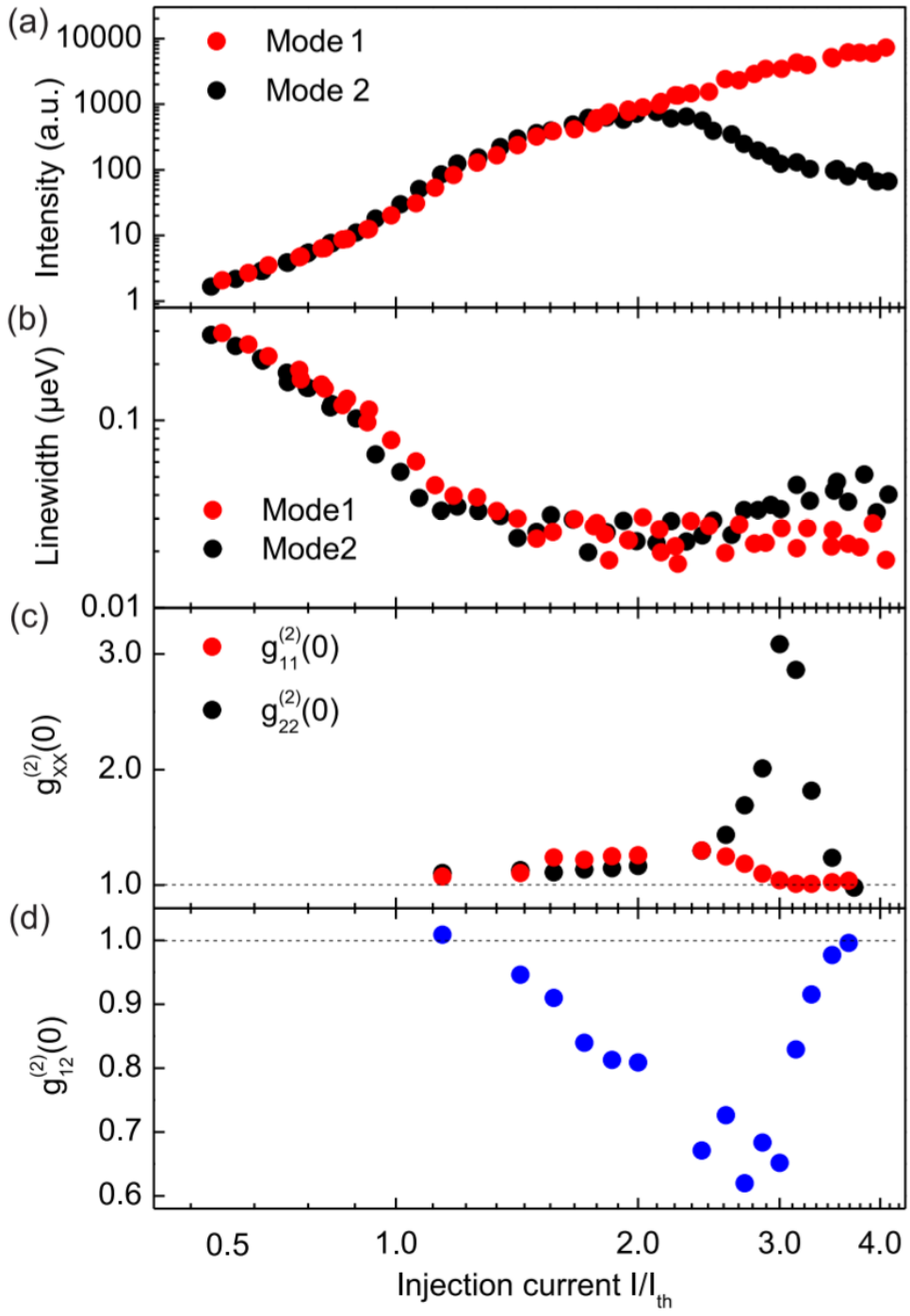

Figure 3.4: Experimental characteristics of a two-mode microcavity laser: (a) Input-output characteristic, (b) emission-mode linewidth, (c) auto-correlation functions of two modes, $g^{(2)}_{11}(0)$ as well as $g^{(2)}_{22}(0)$, and (d) cross-correlation function $g^{(2)}_{12}(0)$. The picture is taken from [Leymann et al., 2013b].

The laser characteristics of the two cavity modes are presented in Figure 3.4. The first mode demonstrates a typical S-shaped input-output curve at a threshold current of $I_{\mathrm{th}} = 5.1\ \mu A$, while the intensity of the second mode saturates at $I_{\mathrm{inj}}/I_{\mathrm{th}} = 2$ and even decreases for values of injection currents higher than $I_{\mathrm{inj}}/I_{\mathrm{th}} = 2.5$. This indicates the gain competition between mode 1 and 2 which is also confirmed by the photon autocorrelation function $g_{11}^{(2)}(0)$ and $g_{22}^{(2)}(0)$ as shown in Figure 3.4(c). Above the laser threshold $g_{11}^{(2)}(0)$ and $g_{22}^{(2)}(0)$ are quite different; for mode 1, the photon autocorrelation function drops to values close to one, corresponding to Poissonian statistics. In contrast, the photon autocorrelation function of the second mode increases and reaches values larger than 2, indicating super-thermal statistics. Finally, the cross-correlation function $g_{12}^{(2)}(0)$ in Figure 3.4(d) demonstrates a noticeable dip $g_{12,\mathrm{min}}^{(2)}(0) = 0.62$ which implies an anti-correlation between the two laser modes. It reveals that $g_{12}^{(2)}(0)$ depends on the injection current and the strongest anti-correlation can be observed in the regime of certain injection currents above the threshold ($2.7 < I/I_{th} < 3.3$).

3.2 Coherence Properties

Microcavity lasers with two optical modes provide the possibility to investigate the gain competition and the effective mode coupling. A well established approach to study the statistical properties of emission events of the two modes is to consider intensity correlations. With the intensity autocorrelation function for a cavity mode the lasing effects controlled by a single QD [Reitzenstein et al., 2008, Xie et al., 2007, Ritter et al., 2010] and dynamical antibunching [Wiersig et al., 2009] in QD-microcavity lasers can be studied. The intensity correlation function in Eq. (2.49) can be generalized to the case of two modes

$$g_{\xi\zeta}^{(2)}(\tau) = \frac{\langle b_\xi^\dagger(t) b_\zeta^\dagger(t+\tau) b_\zeta(t+\tau) b_\xi(t)\rangle}{\langle b_\xi^\dagger(t) b_\xi(t)\rangle \langle b_\zeta^\dagger(t) b_\zeta(t)\rangle}. \tag{3.1}$$

Here, b ($b^\dagger$) is the bosonic annihilation (creation) operator of the two modes which are labeled by $\xi, \zeta \in \{1, 2\}$ for time t and delay time τ. The autocorrelation functions $g_{\xi\xi}^{(2)}(\tau)$ and the cross-correlation function $g_{12}^{(2)}(\tau)$ at zero delay time τ have been successfully used to characterize the gain competition between two modes in QD-microcavity lasers [Eremeev et al., 2011, Leymann et al., 2013b,

Singh and Mandel, 1979, Khanbekyan et al., 2015, Redlich et al., 2016]. Some features of two-mode microlasers will be discussed in detail in the section 3.2.1.

3.2.1 Microscopic semiconductor theory

In order to investigate the interaction of the charge carriers confined in QDs with the light field of discrete cavity modes, we used the developed microscopic semiconductor theory from Ref. [Leymann et al., 2013b] where two modes are not directly coupled. To study additional terms that arise from the direct dissipative coupling between optical modes, this theory is extended in this work by taking the off-diagonal elements of damping matrix γ in Eq. (2.7) into account [Fanaei et al., 2016]. This theory allows to calculate correlations required to determine the emission statistics in the two-mode microcavity laser by considering the many-body effects. It can also estimate the full photon statistics of the two-mode laser and is in fact the groundwork for calculation of the coupling of two modes in terms of the gain competition.

According to the QD model in Figure 1.6 which is used throughout this thesis, only two confined QD shells for both electrons and holes are assumed. Two cavity modes are coupled to the QD s-shell transition and the carrier generation by pumping is into the p-shell transition. We assumed that all QDs are of similar size, thus all QDs have the same energy levels.

To study the statistical properties of two-mode QD-microcavity lasers the Hamiltonian which can describe the whole system follows Eq. (2.9) together with Eqs. (2.14), (2.27), (2.28) and (2.29). Using the assumption of low-temperature and low-carrier density leads to neglecting the interaction with the wetting layer carriers [Schwab et al., 2006]. Thus, the carrier Coulomb effects can be implicitly included by an effective transition energy, a modified oscillator strength for the coupling to the laser mode, and carrier scattering rates similar to Ref. [Gies et al., 2007].

The dynamics of the open quantum mechanical system is then given by the von Neumann-Lindblad equation as in Eq. (2.8). Since the EoM for intended quantities consists of higher order terms, this approach gives an infinite hierarchy. In this chapter, the truncation calculations are based on the cluster expansion approach introduced in chapter 2 in terms of correlation functions. We truncate the hierarchy on the doublet level which includes two-particle correlations. As

in most laser theories we ignore correlations corresponding to superradiant coupling between the QDs [Gies et al., 2007]. For the effects of superradiance on steady-state properties in (single-mode) QD-microcavity laser systems, we refer to Refs. [Jahnke et al., 2016, Leymann et al., 2015, Scully and Svidzinsky, 2009, Temnov and Woggon, 2005, 2009].

In the following dynamical evolution of the emission correlation functions is presented. The first step is to replace the EoM for operator expectation values by EoM for correlation functions. For instance, the EoM for expectation values of average photon number in the cavity modes $\langle b_\xi^\dagger b_\zeta\rangle$ can be replaced by the EoM for corresponding correlation functions $\delta\langle b_\xi^\dagger b_\zeta\rangle = \langle b_\xi^\dagger b_\zeta\rangle - \langle b_\xi^\dagger\rangle\langle b_\zeta\rangle$. Then the truncation of the equations for correlation functions is applied on the doublet level.

For a particular system without coherent external excitation the terms $\langle b\rangle$, $\langle b^\dagger\rangle$ and $\langle c_j^\dagger v_{j'}\rangle$ vanish. We can therefore write the amplitude correlation functions of the mode operators as

$$\begin{aligned}\frac{d}{dt}\delta\langle b_\xi^\dagger b_\zeta\rangle = &-(\gamma_{\xi\xi}+\gamma_{\zeta\zeta})\delta\langle b_\xi^\dagger b_\zeta\rangle + \sum_{\xi\neq\xi',\zeta\neq\zeta'}(\gamma_{\xi\xi'}\delta\langle b_\xi^\dagger b_{\zeta'}\rangle + \gamma_{\zeta'\zeta}\delta\langle b_{\xi'}^\dagger b_\zeta\rangle)\\ &+\sum_{j,q}(g_{\xi j}\delta\langle c_j^\dagger v_j b_\xi\rangle + g_{\xi j}\delta\langle v_j^\dagger c_j b_\zeta^\dagger\rangle),\end{aligned} \tag{3.2}$$

where γ is the damping matrix. The diagonal elements of γ are loss rates of the cavity modes which are directly related to the Q-factor of modes and nondiagonal elements indicate a direct dissipative coupling between the two optical modes. Also, $q = 1, 2, ..., N$, where N indicates the total number of QDs. The last terms on the right-hand side of Eq. (3.2) reveals that the intensity of modes depends on the photon-assisted polarization $\delta\langle c_j^\dagger v_j b_\xi\rangle$ and $\delta\langle v_j^\dagger c_j b_\zeta^\dagger\rangle$. It means that the creation of a photon in the mode ξ is coupled to the s-shell transition. It is worth to mention that amplitude correlation functions and the coupled photon-assisted polarization amplitude correlations are labeled as doublet terms in the cluster-expansion approach. The EoM for the photon-assisted polarization is given by

$$\begin{aligned}\frac{d}{dt}\delta\langle v_j^\dagger c_j b_\xi\rangle =& -i(\Delta_{\xi j}-i\gamma_{\xi\xi}-i\Gamma)\delta\langle v_j^\dagger c_j b_\xi\rangle + g_{\xi j}\delta\langle c_j^\dagger c_j\rangle(1-\delta\langle v_j^\dagger v_j\rangle)\\ &+\sum_{\xi\neq\xi'}\gamma_{\xi'\xi}\delta\langle v_j^\dagger c_j b_{\xi'}\rangle + \sum_{\zeta}[g_{\zeta j}\delta\langle b_\zeta^\dagger b_\xi\rangle(\delta\langle c_j^\dagger c_j\rangle-\delta\langle v_j^\dagger v_j\rangle)\\ &+ g_{\zeta j}\delta\langle c_j^\dagger c_j b_\zeta^\dagger b_\xi\rangle - g_{\zeta j}\delta\langle v_j^\dagger v_j b_\zeta^\dagger b_\xi\rangle].\end{aligned} \tag{3.3}$$

The ξth cavity mode is detuned from the QD transition by $\Delta_{\xi j}=\epsilon_j^c-\epsilon_j^v-\hbar\omega_\xi$ and Γ denotes the QD dephasing rate. For two-mode microlasers we can assume that only the cavity modes with indices $\xi=1,2$ are coupled to the QD s-shell transition and other modes with $\xi\neq 1,2$ are not included in the gain spectrum of the QD ensemble or have low Q-factor.

In this chapter we consider two-mode microcavity lasers assuming both cavity modes are coupled to the s-shell transition and the carriers are generated in the p-shell at a constant rate P. Therefore, the EoM of the carrier population of the electrons in the s-shell is given by

$$\begin{aligned}\frac{d}{dt}\delta\langle c_s^\dagger c_s\rangle =& -\left(\sum_\xi g_{\xi q}\delta\langle c_s^\dagger v_s b_\xi\rangle + H.c.\right) + \delta\langle c_p^\dagger c_p\rangle(1-\delta\langle c_s^\dagger c_s\rangle)\tau_c^{-1}\\ &-\delta\langle c_s^\dagger c_s\rangle(1-\delta\langle v_s^\dagger v_s\rangle)\tau_{nl}^{-1},\end{aligned} \tag{3.4}$$

where τ_{nl} describes the spontaneous emission into nonlasing modes which is related to a β factor by

$$\beta=\frac{\tau_l^{-1}}{\tau_{sp}^{-1}}=\frac{\tau_l^{-1}}{\tau_l^{-1}+\tau_{nl}^{-1}}. \tag{3.5}$$

Equation (3.4) can be considered as the sum of three terms corresponding to the interaction between QDs and the cavity modes in the first term, to the relaxation of carriers from the p- to the s- shell with a relaxation time scale τ_c in the second term and to the loss of excitation into the nonlasing modes in the last term.

Similar to Eq. (3.4), the EoM for the carrier population of the electrons in the p-shell can be written as

$$\begin{aligned}\frac{d}{dt}\delta\langle c_p^\dagger c_p\rangle =& P(\delta\langle v_p^\dagger v_p\rangle-\delta\langle c_p^\dagger c_p\rangle) - \delta\langle c_p^\dagger c_p\rangle(1-\delta\langle c_s^\dagger c_s\rangle)\tau_c^{-1}\\ &-\delta\langle c_p^\dagger c_p\rangle(1-\delta\langle v_p^\dagger v_p\rangle)\tau_{sp}^{-1},\end{aligned} \tag{3.6}$$

where the spontaneous recombination of p-shell carriers is described by the last term on the right-hand side. The other corresponding equations for valence band carriers are given in Appendix A.

In order to determine the statistical properties of the light emission, one approach is to use the intensity correlation function which requires the quadruplet order of the cluster expansion. The EoM for cavity-mode intensity correlations is given by

$$\begin{aligned}\frac{d}{dt}\delta\langle b_\xi^\dagger b_{\xi'}^\dagger b_\zeta b_{\zeta'}\rangle =& -(\gamma_{\xi\xi}+\gamma_{\xi'\xi'}+\gamma_{\zeta\zeta}+\gamma_{\zeta'\zeta'})\delta\langle b_\xi^\dagger b_{\xi'}^\dagger b_\zeta b_{\zeta'}\rangle \\ &+\sum_{\xi\neq\xi'',\xi'\neq\xi'''}\sum_{\zeta\neq\zeta'',\zeta'\neq\zeta'''}(\gamma_{\xi\xi''}\delta\langle b_\xi^\dagger b_{\xi'''}^\dagger b_{\zeta''}b_{\zeta'''}\rangle+\gamma_{\xi'\xi'''}\delta\langle b_{\xi''}^\dagger b_{\xi'}^\dagger b_{\zeta''}b_{\zeta'''}\rangle \\ &+\gamma_{\zeta''\zeta}\delta\langle b_{\xi''}^\dagger b_{\xi'''}^\dagger b_\zeta b_{\zeta'''}\rangle+\gamma_{\zeta'''\zeta'}\delta\langle b_{\xi''}^\dagger b_{\xi'}^\dagger b_{\zeta''}b_{\zeta'''}\rangle)+\sum_{j,q}(g_{\xi j}\delta\langle c_j^\dagger v_j b_{\xi'}^\dagger b_\zeta b_{\zeta'}\rangle \\ &+g_{\xi' j}\delta\langle c_j^\dagger v_j b_\xi^\dagger b_\zeta b_{\zeta'}\rangle+g_{\zeta j}\delta\langle v_j^\dagger c_j b_\xi^\dagger b_{\xi'}b_{\zeta'}\rangle+g_{\zeta j}\delta\langle v_j^\dagger c_j b_\xi^\dagger b_{\xi'}b_\zeta\rangle).\end{aligned} \tag{3.7}$$

The EoM that consists of correlations between the photon-assisted polarization and the photon number is shown in the Appendix A. In what follows, the developed theory will be used for two cases of with and without direct dissipative coupling.

3.3 Laser characteristics without direct coupling

In this section, we recapitulate the statistical properties of the emitted light [Leymann et al., 2013b] assuming that there is no direct coupling between two modes ($\gamma_{12}=\gamma_{21}=0$) and the indirect coupling is induced by the interaction with the common gain medium. To connect the theory to the experimental data [Leymann et al., 2013b], we assume N identical QDs with an effective inhomogeneous line broadening Γ that has an overlap with two modes with the loss rates γ_{11} and γ_{22}. The two modes are separated by the spectral detuning $\Delta_{12}=\omega_1-\omega_2$ where cavity mode 1 is in perfect resonance with the QD s-shell transition ($\Delta_{1s}=0$) as can be seen in Figure 3.5. Moreover we simulate the bimodal microcavity laser with a realistic set of parameters $\beta=0.2$, number of QDs $N=40$, $\gamma_{11}=0.03\ ps^{-1}$, $\gamma_{22}=0.0318\ ps^{-1}$, QD dephasing $\Gamma=2.06\ ps^{-1}$, spontaneous emission time $\tau_{sp}=50\ ps$ and time for relaxation of carriers from p- to s-shell in conduction and valence band $\tau_c=10\ ps$ and $\tau_\nu=5\ ps$, respectively.

Also the light-matter coupling strengths are expressed as [Gies et al., 2007]

$$g_i = \sqrt{\frac{\gamma_{ii} + \Gamma}{2\hbar\tau_{sp}}}. \tag{3.8}$$

Using the empty system as initial condition, the equations of motion are integrated numerically until a stationary solution is reached.

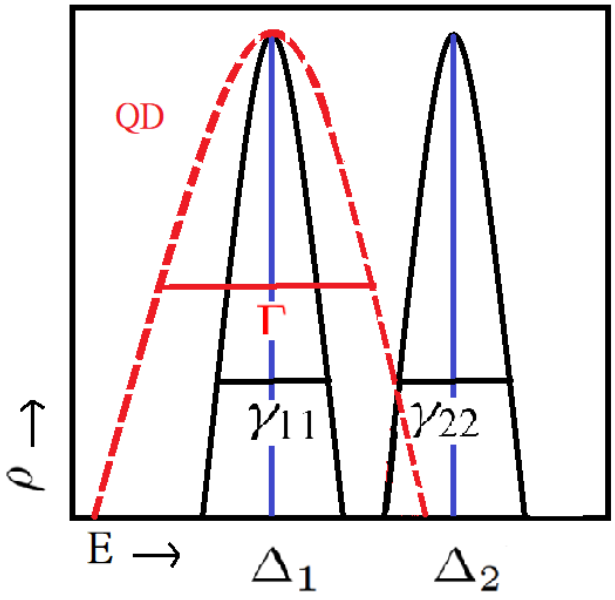

Figure 3.5: Schematic of the model for the density of states ρ of the QDs and two modes. The QDs have the inhomogeneous line broadening Γ that has an overlap with two modes with the loss rates γ_{11} and γ_{22} and the detuning of the modes to the QDs Δ_1 and Δ_2.

3.3.1 Results

The laser characteristics of two cavity modes are presented in Figure 3.6, which is analogous to the one discussed experimentally, see Figure 3.4, and theoretically in Ref. [Leymann et al., 2013b]. The modes are not directly coupled $\gamma_{12} = 0 = \gamma_{21}$ but interact indirectly via the QD-gain medium.

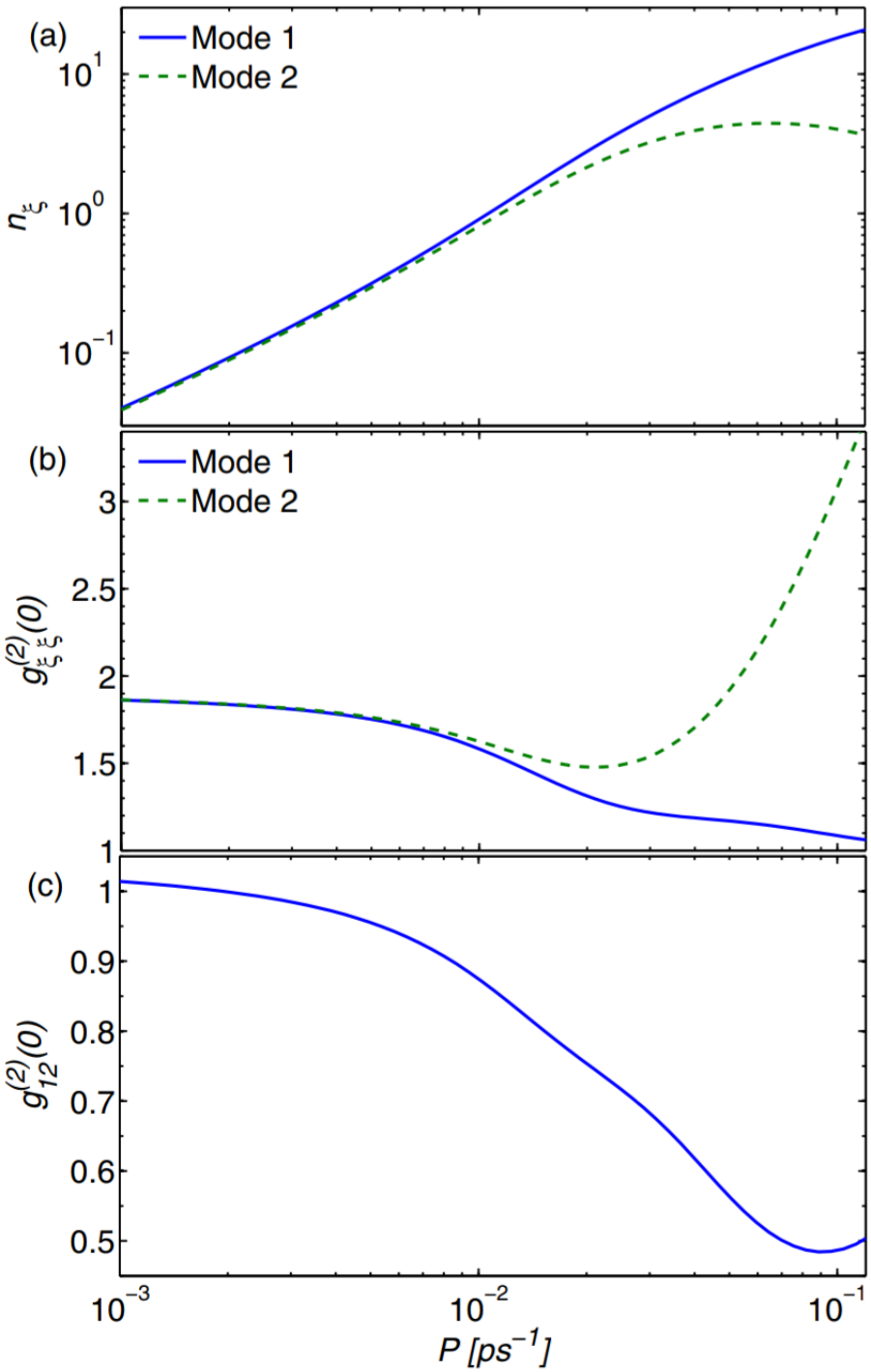

Figure 3.6: Laser characteristics calculated with the semiconductor model with zero off-diagonal elements of damping matrix γ. (a) Intensity of modes 1 and 2 as a function of the pump power in a log-log profile, (b) autocorrelation functions of the two modes, and (c) cross-correlation between modes. In these simulations, we assume $\gamma_{11} = 0.03\ ps^{-1}$, $\gamma_{22} = 0.0318\ ps^{-1}$ and the second mode is detuned by $\Delta_{12} = 0.2\ ps^{-1}$.

It can be seen in Figure 3.6(a) that, while the intensity $n_1 = \langle b_1^\dagger b_1 \rangle$ of mode 1 exhibits a typical S-shaped input-output curve, the intensity $n_2 = \langle a_2^\dagger a_2 \rangle$ of the second mode saturates and even declines with increasing the pump rate. The autocorrelation function of mode 1 at zero delay time $g_{11}^{(2)}(0)$ [see Figure 3.6(b)] reflects a laser transition similar to the standard result for the single-mode laser [Scully and Zubairy, 1997]. It drops from 2, corresponding to thermal light, to 1 indicating coherent light emission. The fact that for low pump rates the autocorrelation function is slightly below 2 is due to the finite number of QDs. In contrast, the autocorrelation function of the second mode $g_{22}^{(2)}(0)$ slightly decreases at first with increasing pump rate, before increasing again reaching superthermal values well above 2, indicating a strong bunching of photons in this mode. These results are in agreement with the experimental results depicted in Figure 3.4, though the autocorrelation function below the threshold could not be measured due to the limited temporal resolution of the HBT configuration [Ulrich et al., 2007]. Further Figure 3.6(c) shows that the cross-correlation function $g_{12}^{(2)}(0)$ for relatively low pump rates is 1 implying two statistically independent modes. With increasing the pump rate, the cross-correlation function decreases well below unity indicating anticorrelated modes which can be seen as a signature of gain competition [Redlich et al., 2016].

3.4 Laser characteristics with direct coupling

The developed microscopic semiconductor theory allows for inclusion of many-body effects and for detailed investigation of the emission characteristics in different interaction regimes. In contrast to previous studies which have only considered the coupling of two optical modes via the common gain medium, we investigate here additional direct mode coupling due to dissipative character of the laser resonator. This coupling is described by off-diagonal elements of the optical damping matrix γ in the Lindblad superoperator in Eq. (2.8).

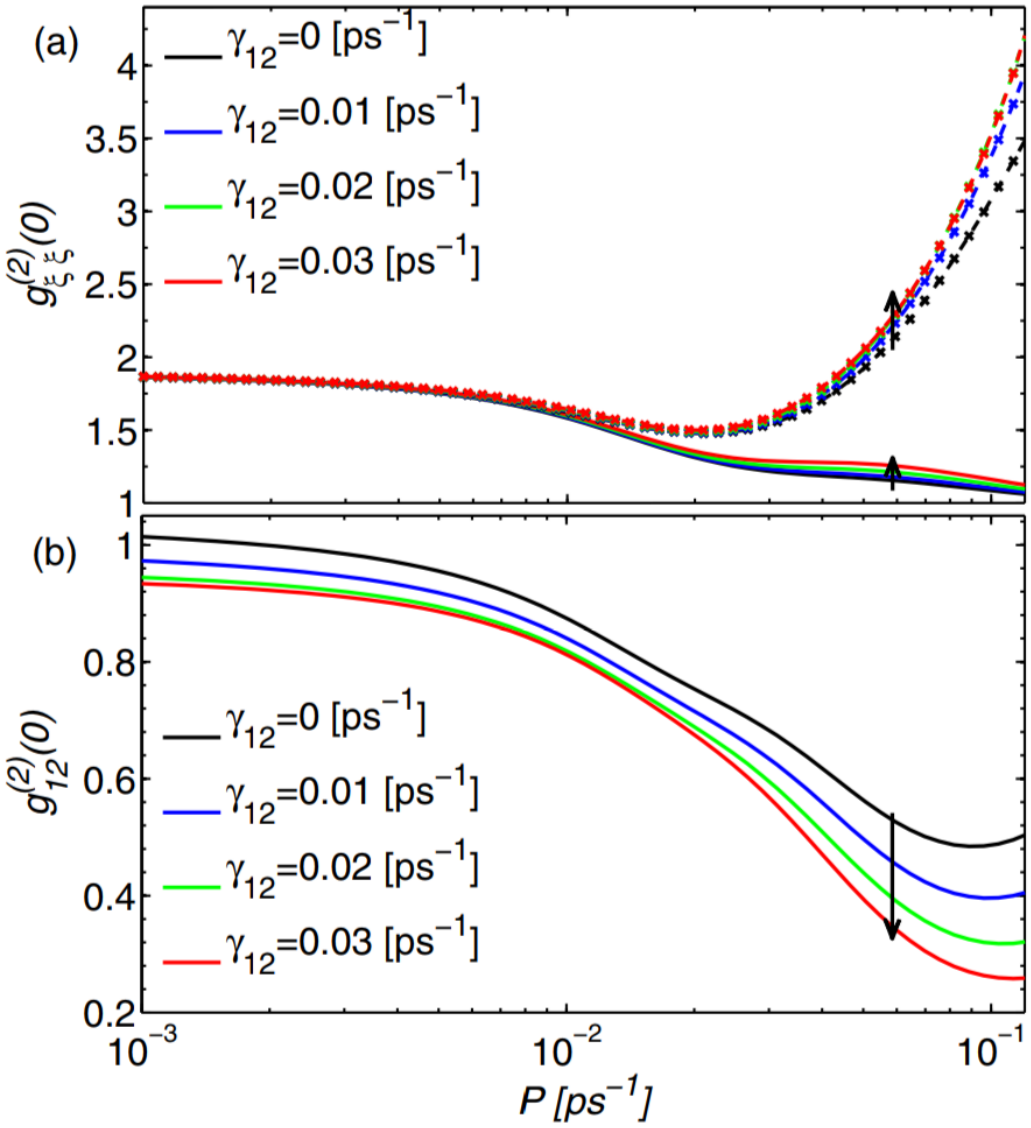

Figure 3.7: Laser characteristics calculated with the semiconductor model for various off-diagonal Lindblad terms γ_{12}. (a) Autocorrelation functions for modes 1 (solid curve) and 2 (dotted curve) as a function of the pump power. (b) Cross-correlation between modes 1 and 2 for the same values of parameters as in Fig. 3.6.

Figure 3.7 compares the behavior of the two modes for different values of γ_{12}. To this end we assume $\gamma_{12} = \gamma_{21}$ according to Refs. [Hackenbroich et al., 2002, Viviescas and Hackenbroich, 2003, 2004] and other parameters correspond to Figure 3.6. As illustrated in Figure 3.7(a) for large values of the pump rate, an increase in the off-diagonal Lindblad terms leads to stronger superthermal

photon bunching of mode 2, i.e., larger $g_{22}^{(2)}(0)$ compared to the case with zero γ_{12}. Furthermore, the direct coupling changes the behavior of the autocorrelation function $g_{11}^{(2)}(0)$ compared to the standard single-mode laser [Ulrich et al., 2007, Scully and Zubairy, 1997]. Above threshold $g_{11}^{(2)}(0)$ is slightly enhanced exhibiting a small "bulge". Figure 3.7(b) shows that the cross-correlation function $g_{12}^{(2)}(0)$ decreases with increasing γ_{12}. The anticorrelation of the two modes is therefore larger when the two modes are stronger coupled.

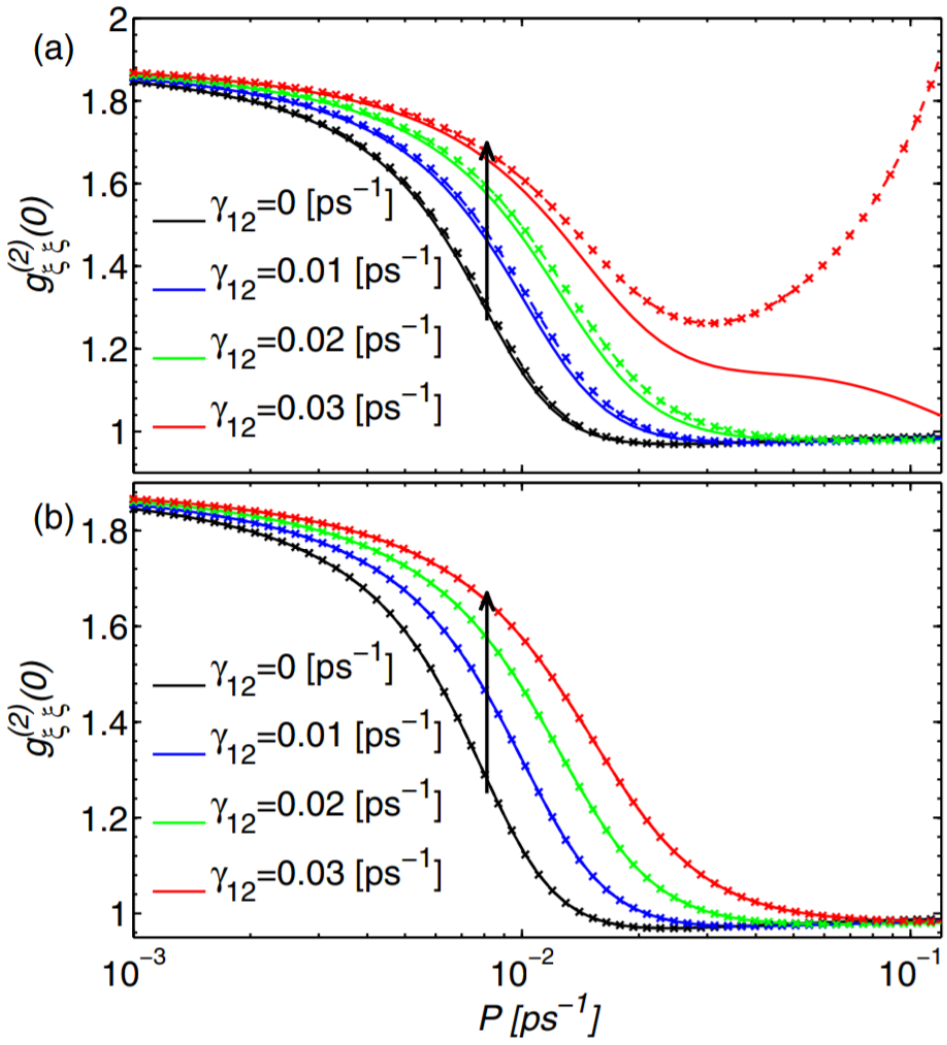

Figure 3.8: Autocorrelation function $g_{\xi\xi}^{(2)}(0)$ for mode 1 (solid curves) and mode 2 (dashed curves with crosses) vs pump rate P at zero detuning for various γ_{12}. (a) $\gamma_{11} = 0.03\ ps^{-1}$ and $\gamma_{22} = 0.0318\ ps^{-1}$. (b) $\gamma_{11} = \gamma_{22} = 0.03\ ps^{-1}$. The arrows indicate increasing γ_{12}. In (b) the curves for mode 1 and mode 2 are on top of each other.

For the specific case of $\omega_1 = \omega_2 = \omega$ in which both modes are in resonance with the QD transition, Figure 3.8(a) depicts the autocorrelation functions for asymmetric optical damping of the modes, $\gamma_{11} \neq \gamma_{22}$. It reveals that the signatures of gain competition are obvious only for large values of γ_{12}, whereas for small values the behavior of the two modes resembles that in a single-mode laser. Figure 3.8(b) shows the autocorrelation functions for the trivial case of zero detuning and symmetric optical damping, $\gamma_{11} = \gamma_{22}$. No signatures of gain competition are visible in the autocorrelation functions here. Both modes appear to behave as in a single-mode laser where the laser threshold increases on increasing the damping coefficient γ_{12}.

3.5 Dark and bright modes

To analyze the gain competition between the two modes, we study composite modes as in Refs. [Faghihi et al., 2014, Li et al., 2014, Eremeev et al., 2011, Majumdar et al., 2012]. We apply the unitary transformation [Svozil, 1990]

$$\begin{pmatrix} b_1 \\ b_2 \end{pmatrix} = \begin{pmatrix} \cos\theta & \sin\theta \\ -\sin\theta & \cos\theta \end{pmatrix} \begin{pmatrix} d \\ b \end{pmatrix} \tag{3.9}$$

with real-valued rotation angle θ. The so-defined operators b and d obey the commutation relations $[b, b^\dagger] = [d, d^\dagger] = 1$ and $[b, d^\dagger] = [d, d] = 0$, and the sum of the photon numbers is invariant, i.e., $\langle b_1^\dagger b_1 \rangle + \langle b_2^\dagger b_2 \rangle = \langle b^\dagger b \rangle + \langle d^\dagger d \rangle$. We define the occupations $n_b = \langle b^\dagger b \rangle$, $n_d = \langle d^\dagger d \rangle$ and the corresponding autocorrelation functions $g_{bb}^{(2)}(0)$ and $g_{dd}^{(2)}(0)$ in an analog way as in Eq. (3.1). Applying the unitary transformation to the whole Hamiltonian leads to

$$H = H_{carr}^0 + H_b + H_d + H_{bd}, \tag{3.10}$$

with (we set $\hbar = 1$ in the following)

$$H_b = (\omega_1 \sin^2\theta + \omega_2 \cos^2\theta) b^\dagger b - iN(g_1 \sin\theta + g_2 \cos\theta)(c_s^\dagger v_s b - v_s^\dagger c_s b^\dagger), \tag{3.11}$$

$$H_d = (\omega_1 \cos^2\theta + \omega_2 \sin^2\theta) d^\dagger d - iN(g_1 \cos\theta - g_2 \sin\theta)(c_s^\dagger v_s d - v_s^\dagger c_s d^\dagger), \tag{3.12}$$

and

$$H_{bd} = \frac{1}{2}(\omega_1 - \omega_2)(\sin 2\theta)(b^\dagger d + d^\dagger b). \tag{3.13}$$

The Lindblad superoperator transforms to

$$L = L_b + L_d + L_{bd}, \tag{3.14}$$

with

$$L_b\rho = (\gamma_{11}\sin^2\theta + \gamma_{22}\cos^2\theta + \gamma_{12}\sin 2\theta)(2b\rho b^\dagger - \rho b^\dagger b - b^\dagger b\rho), \tag{3.15}$$

$$L_d\rho = (\gamma_{11}\cos^2\theta + \gamma_{22}\sin^2\theta - \gamma_{12}\sin 2\theta)(2d\rho d^\dagger - \rho d^\dagger d - d^\dagger d\rho), \tag{3.16}$$

and

$$\begin{aligned} L_{bd}\rho =& (\frac{1}{2}(\gamma_{11} - \gamma_{22})\sin 2\theta + \gamma_{12}\cos 2\theta)[2(b\rho d^\dagger + d\rho b^\dagger) \\ & - (\rho b^\dagger d + \rho d^\dagger b) - (b^\dagger d\rho + d^\dagger b\rho)]. \end{aligned} \tag{3.17}$$

We choose θ such that the new mode d becomes a dark mode, which is decoupled from the QDs. To attain this, the gain term of the Hamiltonian H_d in the second term of Eq. (3.12) is zero for

$$\theta = \arctan\left(\frac{g_1}{g_2}\right). \tag{3.18}$$

Based on this choice, the bright mode b couples to the QDs with an effective coupling strength $\tilde{g} = \sqrt{g_1^2 + g_2^2}$ (see Eq. (3.11)). In the time evolution of the initially unexcited system, the dark mode cannot receive any photons directly from the interaction with the QDs. It therefore stays unpopulated unless it receives photons from the bright mode by the coupling terms H_{bd} and L_{bd} that depend on the detuning Δ_{12} and the elements of the damping matrix γ, respectively.

3.5.1 Case of zero detuning and equal light-matter coupling strength

Since we are mainly interested in the effects of L_{bd}, we focus on the situation of zero detuning. In this case $H_{bd} = 0$, i.e., the dark mode becomes populated only

via L_{bd}. Moreover, as for the used parameters we have $g_1 \approx g_2$ (see Eq. (3.8)); now we restrict the following discussion to $g_1 = g_2$, which implies $\cos 2\theta = 0$, $\sin 2\theta = 1$ and $\cos\theta = \sin\theta = 1/\sqrt{2}$. Equation (3.9) can then be written as

$$b_1 = \frac{1}{\sqrt{2}} b + \frac{1}{\sqrt{2}} d, \tag{3.19}$$

$$b_2 = \frac{1}{\sqrt{2}} b - \frac{1}{\sqrt{2}} d. \tag{3.20}$$

Hence the annihilation operator d and the corresponding creation operator $d^\dagger$ describe the transfer of photons between the original modes. In the following we use the occupation of the dark mode n_d as a signature of the gain competition between the original modes. To summarize, the operators b and d both have a clear physical meaning: b describes the coupling of the original modes to the QDs and d describes the transfer of photons between the original modes.

First, we consider the special case of two modes with symmetric losses, $\gamma_{11} = \gamma_{22}$. From Eq. (3.17) with $\cos 2\theta = 0$ follows $L_{bd} = 0$, i.e., the dark mode stays unpopulated. Therefore, we expect that there is no transfer of photons between the two original modes. As a consequence, the two modes recover the standard single-mode laser behavior. This finding can also be observed for the numerical results in Figure 3.8(b). Figure 3.9 confirms that the photon number (except the obvious factor 2) and the autocorrelation function of the original modes are equal to the bright mode b. This leads to the conclusion that these two modes build up a bright mode which exhibits all the lasing behavior of the single-mode laser. The off-diagonal element γ_{12} has influence on the lasing behavior because the overall decay rate of the bright mode depends on it as can be seen from Eq. (3.15). This finding has been previously observed for modes interacting with an ensemble of two-level atoms [Eremeev et al., 2011]. This is a special case because the dark mode is unpopulated and hence features that arise from the gain competition between the two lasing modes have not been discussed.

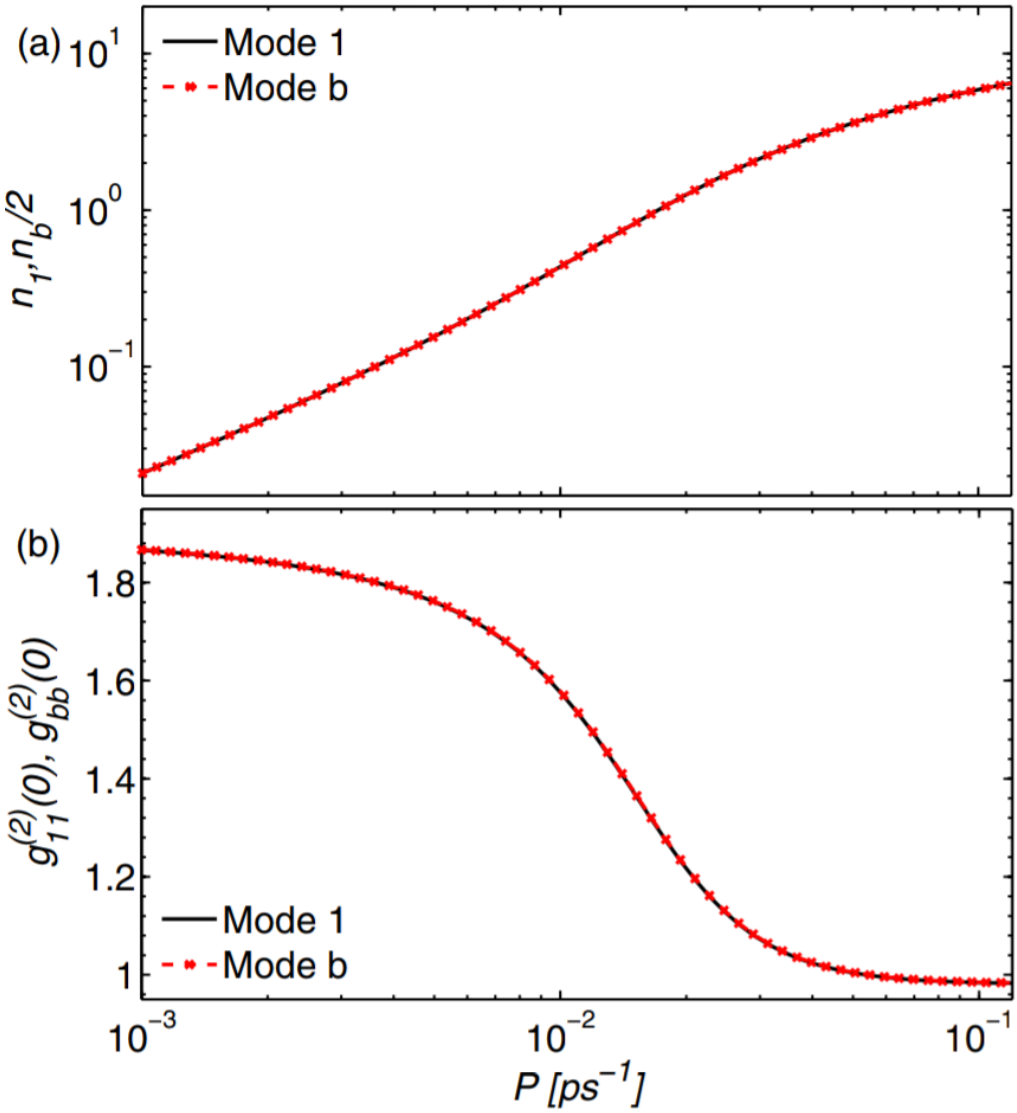

Figure 3.9: Comparison of (a) intensity and (b) autocorrelation function of the original mode 1 and the bright mode as a function of the pump rate calculated with the semiconductor theory for $\gamma_{11} = \gamma_{22} = 0.03\ ps^{-1}$,$\gamma_{12} = 0.03\ ps^{-1}$, and zero detuning. In both panels the two curves are on top of each other. Mode 2 gives the same curves as mode 1 (not shown).

By considering a system with asymmetric optical damping $\gamma_{11} \approx \gamma_{22}$ we go beyond the analysis of Ref. [Eremeev et al., 2011]. For this case the dark mode d can gain intensity because of a nonzero L_{bd} (see Eq. (3.17)) and hence there is a transfer of photons between the two original modes. For similar coupling strength $g_1 \approx g_2$, a further enhancement of the off-diagonal term γ_{12} leads to a decrease in the overall decay rate of the dark mode in Eq. (3.16). Therefore, the intensity of

the dark mode increases for increasing γ_{12} as depicted in Figure 3.10(a). Thus, for small values of γ_{12}, the dark mode has negligible contribution to the photon statistics of the original lasing mode, and the bright mode leads to a single-mode behavior for both original modes. On the other hand, at large values of γ_{12} the gain competition is enhanced due to significant transfer of photons between the two original modes. This is in agreement with different behaviors of the two original modes obtained from numerical results in Figure 3.8(a). Note that the intensity of the dark mode for zero off-diagonal elements in Figure 3.10(a) is not zero due to the asymmetric optical damping.

In order to predict which one of the original modes wins the gain competition, we analyze the contribution of the bright mode to the photon number of the original modes. As previously mentioned, only the bright mode b is directly coupled to the QDs. In the numerical results we observe that also for asymmetric optical damping the bright mode behaves always like a standard single-mode laser; see, e.g., the inset in Figure 3.10(b). The mode that has more contribution of mode b wins the gain competition. According to the photon number of the original modes in terms of the new modes, the contribution of bright and dark modes can be expressed as

$$n_1 = \frac{1}{2}\langle b^\dagger b\rangle + \frac{1}{2}\langle b^\dagger d + d^\dagger b\rangle + \frac{1}{2}\langle d^\dagger d\rangle, \tag{3.21}$$

and

$$n_2 = \frac{1}{2}\langle b^\dagger b\rangle - \frac{1}{2}\langle b^\dagger d + d^\dagger b\rangle + \frac{1}{2}\langle d^\dagger d\rangle. \tag{3.22}$$

Without loss of generality, we assume $\langle b^\dagger d + d^\dagger b\rangle \geqslant 0$. In the case of a non-positive value, the role of two original modes in the discussion is exchanged. We can conclude that destructive or constructive interference, depending on the sign in front of $\langle b^\dagger d + d^\dagger b\rangle$ in Eqs. (3.21) and (3.22), determines which mode wins the gain competition. Consequently, there is a destructive interference between the contributions of bright and dark modes in mode 2. In contrast, as can be found in Eq. (3.21), mode 1 is composed of the superposition of dark- and bright-mode contributions that interfere constructively. It therefore wins the gain competition and exhibits a coherent light emission similar to a single-mode laser. For low values of the pump rate, the dark mode has a small intensity relative to the bright mode (see Fig. 3.10(b)). Hence, there is no transfer of photons between the two original modes that therefore behave the same. Above the laser

threshold, the effect of the dark mode cannot be ignored and a further increase of its intensity leads to a saturation and even decrease in the intensity of mode 2 due to destructive interference, whereas the intensity of mode 1 continues to rise due to constructive interference.

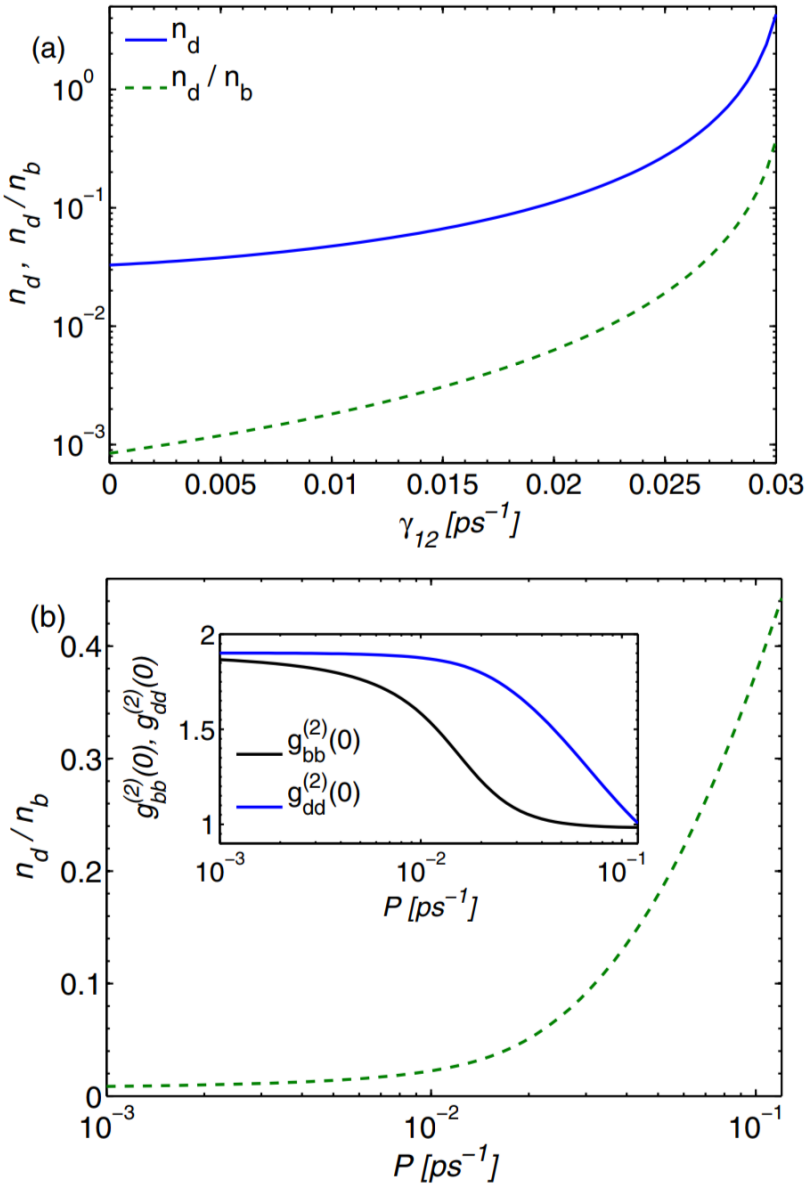

Figure 3.10: (a) Intensity of the dark mode n_d (solid curve) and ratio of intensity of the dark mode over the intensity of bright mode n_d/n_b (dashed curve) vs. off-diagonal coupling strength γ_{12} for asymmetric optical damping at zero detuning and pump rate $P = 0.1\ ps^{-1}$; (b) n_d/n_b pump rate for $\gamma_{12} = 0.03\ ps^{-1}$. The inset shows the corresponding intensity autocorrelation functions of the bright and the dark mode.

To estimate the behavior of the intensity autocorrelation functions of the original modes we define

$$R_{\xi\xi} = g^{(2)}_{\xi\xi}(0)/g^{(2)}_{bb}(0), \tag{3.23}$$

with $g^{(2)}_{bb}(0)$ being the autocorrelation function of the bright mode. The fact that for not too large pump rates the ratio of the photon number of mode d to the photon number of mode b is considerably smaller than unity (Fig. 3.10) motivates the following crude approximation. We assume that correlations with one or more d operators can be neglected. A straightforward calculation then shows that the behavior of R_{11} and R_{22} is determined by

$$R_{\xi\xi} \approx \frac{1}{4}\left(\frac{n_b}{n_\xi}\right)^2. \tag{3.24}$$

For small values of γ_{12} the photon number of the dark mode is small as already discussed earlier in the context of Figure 3.10(a). This implies $n_1 \approx n_2 \approx n_b/2$ and therefore $R_{11} \approx R_{22} \approx 1$. This explains why the autocorrelation function of both original modes behave as for a single-mode laser; see Figure 3.8(a) again.

In contrast, for $\gamma_{12} = 0.03$ the dark mode has considerable intensity. Correspondingly, transfer of photons from mode 1 and mode 2 leads to a distinct difference in R_{11} and R_{22} above threshold as can be seen in Figure 3.11(a). R_{22} approaches values well above unity because the intensity of mode 2 has values much smaller than the intensity of the bright mode. R_{11} behaves in the opposite way and decreases. This is due to the fact that mode 1 obtains a larger contribution from the bright mode.

Figure 3.11(b) shows the autocorrelation functions of the two original modes determined from the autocorrelation of the bright mode and the approximate expressions R_{11}, R_{22} using Eqs. (3.23) and (3.24). Below the laser threshold both autocorrelation functions are around 2 that indicates thermal bunching. When increasing the pump rate, $g^{(2)}_{11}(0)$ decreases and $g^{(2)}_{22}(0)$ first decreases and then increases again. Both observations are in qualitative agreement with the numerical results in Figure 3.8(a). However, quantitative differences for larger pump rates are obvious. Hence, the behavior of the autocorrelation functions of the original modes for low to medium pump rates can be understood in terms of the involved intensities and the autocorrelation function of the bright mode $g^{(2)}_{bb}(0)$.

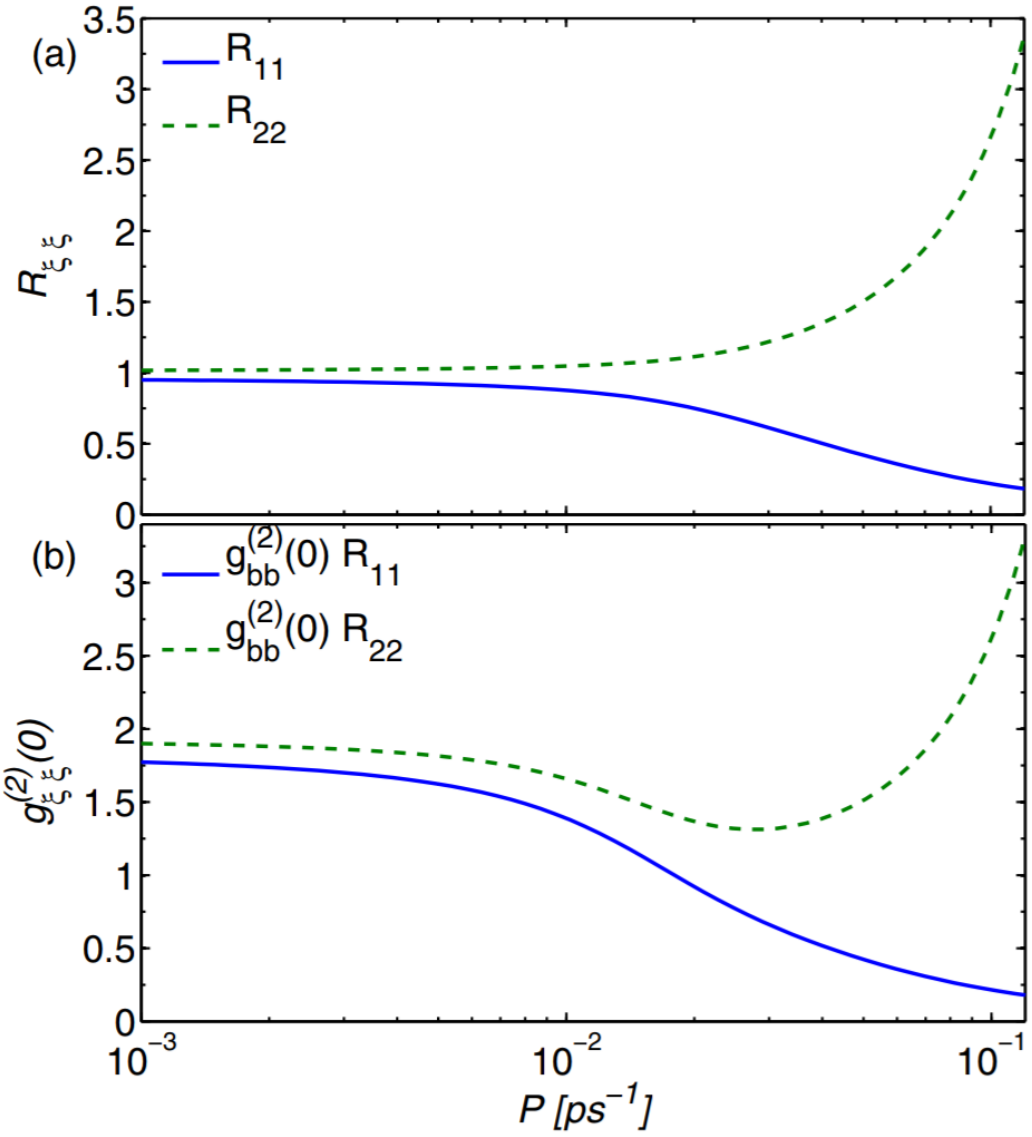

Figure 3.11: (a) R_{11} and R_{22} as a function of pump rate for asymmetric optical damping with $\gamma_{12} = 0.03\ ps^{-1}$ and zero detuning. (b) Autocorrelation function of the two original modes estimated from the autocorrelation function of the bright mode and Eqs. (3.23) and (3.24).

3.6 Chapter conclusion

In this chapter, we investigated a bimodal-microcavity laser with semiconductor quantum dots as gain material. Numerical results of a microscopic theory reveals that the two competing modes display completely different features. The typical behavior is that mode 1, which wins the gain competition, demonstrates statistical behavior of a conventional single-mode laser, whereas the losing mode 2 exhibits superthermal photon bunching for pump rates above the lasing threshold. The photon cross-correlation function reveals a strong anti-correlation between the modes, which has been also considered experimentally and theoretically in Ref. [Leymann et al., 2013b].

If the difference between the modes is adequately high, features like mode competition in the input-output characteristics, enhanced autocorrelation functions of the competition losing mode, and a pronounced anticorrelation become visible. In order to reproduce and explain the mode competition of bimodal microcavity lasers, we started from the microscopic semiconductor model of Gies et al. [2007] and derived the equation of motion that can reproduce experimental results qualitatively.

In contrast to previous studies which considered only the coupling of two optical modes via the common gain medium, we investigated here additional direct mode coupling due to the dissipative character of the laser resonator. This coupling is described by the off-diagonal elements of the optical damping matrix γ in the Lindblad superoperator. Our numerical results reveal that an increase in these off-diagonal elements leads to a stronger photon bunching for mode 2, whereas the autocorrelation function of mode 1 is only slightly enhanced. The cross-correlation function exhibits stronger anticorrelated behavior on increasing off-diagonal elements of γ.

In order to analyze the mode-coupling effects, a unitary transformation from the original modes to a new set of modes has been implemented. We studied the transformed system consisting of a bright mode coupled to the QDs and a decoupled dark mode that obtains photons only through the interaction with the bright mode. The occupation of the dark mode describes the transfer of photons between the two original modes. At zero detuning and symmetric optical damping, the dark mode is not populated. Hence there is no transfer between the two original modes. As a result, the two modes do not show the conventional signatures

of gain competition. The bright mode exhibits the features of single-mode lasing that depends on the off-diagonal elements.

For asymmetric optical damping of the modes, the gain competition behavior can be traced back to the increasing occupation of the dark mode. The intensity of the dark mode increases with the off-diagonal elements of γ. As a result, the off-diagonal elements of the damping matrix enhance the anticorrelated behavior of the modes in bimodal microcavities. Which one of the original modes becomes the lasing mode is related to the constructive and destructive interference of bright and dark mode contributions to the two original modes.

Chapter 4

Two-state lasing

4.1 Introduction

In the last decades the research efforts on QD microcavity lasers have attracted considerable attention due to their superior properties such as ultralow threshold currents, high temperature stability, high modulation bandwidth and efficiency as previously reported by [Grundmann et al., 2000, Park et al., 2000, Huang et al., 2000, Bhattacharya and Ghosh, 2002]. The three-dimensional confinement of electrons and holes in a QD leads to discrete levels that are here called ground (s-shell) or excited state (p-shell). Lasing occurs commonly by the recombination of electrons and holes in the ground state of the QD. However, the finite intraband relaxation time of QDs [Benisty et al., 1991], and a limited density of states have led to the recent demonstration of simultaneous excited-state (ES) and ground-state (GS) lasing, or the so-called two-state lasing [Kaptan et al., 2014, Markus et al., 2003, Gioannini, 2012, Röhm et al., 2015b,a, Grillot et al., 2011, Wang et al., 2014, Viktorov et al., 2005]. In this case, the lasing starts from the GS but with increasing the current injection, the lasing from the ES can be observed as well [Maximov et al., 2013, Asryan et al., 2001]. Appearance of the ES lasing extends the spectral range and can extend the field of application.

The possibility of two-state lasing is theoretically reported by Grundmann and Bimberg [1997] and Grundmann et al. [2000] in the framework of master-equation model of QD microstates, and then experimentally observed by Markus et al. [2003]. Experimental evidence of two wavelengths presence was previously reported in Refs. [Bhattacharya et al., 1999, Benisty et al., 1991]. However, due to large spectral overlap between two lasing peaks it was not mentioned

whether the lasing was related to two different states.

In this chapter we investigate two-state lasing in QD lasers through GS and ES transitions. In contrast to chapter 3 that is focused on the single-state dynamics of a QD lasers, we will study here the competing behavior of two-state lasers. The microscopic semiconductor theory of Leymann et al. [2013b], that was explained in detail in sec. 3.2 for single-state lasing, will be here developed to the case of two-state lasing. Numerical results reveal that GS lasing threshold is obtained and then saturates. While its occupation clamps, the carrier population of ES increases significantly. Consequently, at higher pump rates the carrier population of ES reaches its lasing threshold value and two-state lasing can be observable. The autocorrelation function of two modes illustrate the standard transition from spontaneous emission to stimulated emission but with different lasing thresholds. It indicates that there is no gain competition between modes which is also confirmed by the constant value of cross-correlation function. Moreover we will demonstrate that the GS laser is qualitatively uninfluenced by the beginning of lasing in the ES. However, the GS occupation probabilities is closely tied to the ES by the carrier relaxation into the GS and therefore the Q-factor of the ES mode leads to a quantitative effect on lasing operation of the GS mode.

4.2 Theoretical model

In this chapter the dynamical and statistical properties of QD lasers are numerically simulated, with special focus on two-state lasers. This type of semiconductor lasers can make simultaneous lasing at two well-separated wavelengths, owing to the discrete energy levels of the QD. The lasing states are labeled by GS and ES corresponding to the confined QD states. In order to describe and analyze this two-state lasing, we extend the microscopic semiconductor theory of section 3.2.1 by considering that the lasing occurs via GS and ES transitions.

The dynamics of the carrier population of the electrons in the GS and ES are given respectively by (for single-state lasing, see Eqs. (3.4) and (3.6))

$$\begin{aligned}\frac{d}{dt}\delta\langle c_G^\dagger c_G\rangle = &-\left(\sum_\xi g_{\xi G}\delta\langle c_G^\dagger v_G b_\xi\rangle + H.c.\right) + \delta\langle c_E^\dagger c_E\rangle(1-\delta\langle c_G^\dagger c_G\rangle)\tau_c^{-1} \\ &- \delta\langle c_G^\dagger c_G\rangle(1-\delta\langle v_G^\dagger v_G\rangle)\tau_{nl}^{-1},\end{aligned} \tag{4.1}$$

and

$$\frac{d}{dt}\delta\langle c_E^\dagger c_E\rangle = -\left(\sum_\xi g_{\xi E}\delta\langle c_E^\dagger v_E b_\xi\rangle + H.c.\right) + P\delta\langle v_E^\dagger v_E\rangle(1-\delta\langle c_E^\dagger c_E\rangle) - \delta\langle c_E^\dagger c_E\rangle(1-\delta\langle c_G^\dagger c_G\rangle)\tau_c^{-1} - \delta\langle c_E^\dagger c_E\rangle(1-\delta\langle v_E^\dagger v_E\rangle)\tau_{nl}^{-1}. \tag{4.2}$$

Also the EoMs of the carrier population of holes in GS and ES can be written as

$$\frac{d}{dt}\delta\langle v_G^\dagger v_G\rangle = \left(\sum_\xi g_{\xi G}\delta\langle c_G^\dagger v_G b_\xi\rangle + H.c.\right) - \delta\langle v_E^\dagger v_E\rangle(1-\delta\langle v_G^\dagger v_G\rangle)\tau_v^{-1} + \delta\langle c_G^\dagger c_G\rangle(1-\delta\langle v_G^\dagger v_G\rangle)\tau_{nl}^{-1}, \tag{4.3}$$

and

$$\frac{d}{dt}\delta\langle v_E^\dagger v_E\rangle = \left(\sum_\xi g_{\xi E}\delta\langle c_E^\dagger v_E b_\xi\rangle + H.c.\right) - P\delta\langle v_E^\dagger v_E\rangle(1-\delta\langle c_E^\dagger c_E\rangle) + \delta\langle v_E^\dagger v_E\rangle(1-\delta\langle v_G^\dagger v_G\rangle)\tau_v^{-1} + \delta\langle c_E^\dagger c_E\rangle(1-\delta\langle v_E^\dagger v_E\rangle)\tau_{nl}^{-1}, \tag{4.4}$$

respectively. Here the subscripts G and E denote the ground- and excited-state lasing, respectively. Moreover, the EoM for other quantities is similar to what mentioned in the appendix A.

In the experimental observations of two-state lasing by Markus et al. [2003], lasing characteristics were strongly influenced by the cavity length that depends on the total losses of the laser cavity. A stable two-state lasing could be thus achieved by the proper choice of parameters. In order to obtain two-state lasing, we use the following parameters: the loss rates $\gamma_{GG} = \gamma_{EE} = 0.02\ ps^{-1}$, $\beta = 0.2$, number of QDs $N = 40$, QD dephasing $\Gamma = 2.06\ ps^{-1}$, spontaneous emission time $\tau_{sp} = 50\ ps$ and time for relaxation of carriers from ES to GS in conduction and valence band $\tau_c = 10\ ps$ and $\tau_\nu = 5\ ps$, respectively. For the sake of simplicity of our discussion, we assume that two modes are not directly coupled $\gamma_{GE} = \gamma_{EG} = 0$ and are also in exact resonance with the corresponding QD transitions ($\Delta_{GG} = 0, \Delta_{EE} = 0$).

In the following we will first review the single-state lasing and then present the theoretical results obtained for a two-state microcavity laser by considering input-output characteristics, carrier population and correlation functions which allow one to study the gain competition behavior. Finally, we will analyze the

effects of ES mode on the operation of the GS lasing.

4.2.1 Standard GS laser

This section provides a short overview of the lasing characteristics of single ground-sate QD laser based on the microscopic semiconductor theory. To make only GS lasing occurs we set the coupling strength of ES $g_E = 0$ and the results are depicted in Figure 4.1.

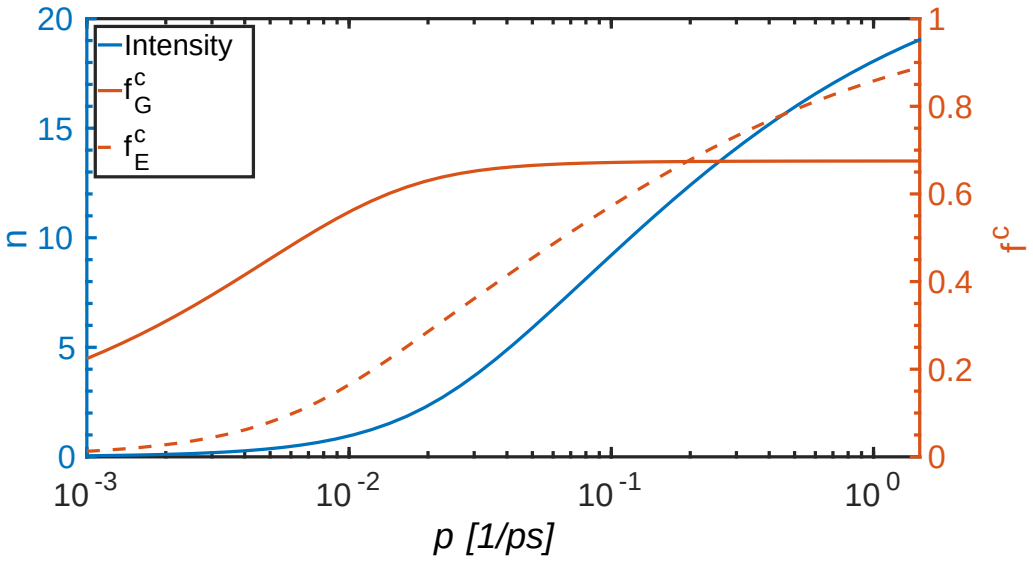

Figure 4.1: Intensity (blue line) and carrier occupation of conduction band (red lines) as a function of pump rate for single ground-state laser. The intensity starts lasing at about $P_{thr} \simeq 0.02\ ps^{-1}$. The carrier occupation of GS (solid line) saturates above $P_{sat} = 0.02\ ps^{-1}$, while the carrier occupation of ES (dashed line) increases.

In Figure 4.1 the blue solid line shows the GS intensity, $n = \langle a_G^\dagger a_G \rangle$, as a function of the pump rate. The resulting intensity exhibits a characteristic S-shaped input-output curve with a lasing threshold at about $P_{thr} \simeq 0.02\ ps^{-1}$. Additionally, the red lines show the occupations of conduction band $f^c = \langle c^\dagger c \rangle$ for GS and ES. First occupation of GS (solid line) is rising with increasing the pump rate. If enough carriers are injected into GS by relaxation from the ES, lasing threshold is reached and f_G^c saturates for values above the lasing threshold. This indicates that every carrier added to the GS, e.g., by raising the pump rate, is instantly interacted with a GS mode and is converted into the lasing

mode. It leads to saturation of carriers in f_G^c. This behavior is the well-known gain clamping effect [Markus et al., 2003] that has been known as a fundamental feature of lasing. On the other hand, f_E^c (dashed line) in Figure 4.1 shows a drastic increase of occupation in the excited state with increasing the pump rate, meaning that no gain clamping occurs for excited state. In the next section the laser characteristics of two-state lasing will be investigated.

4.3 Laser characteristic of two-state lasing

The most research efforts on microcavity lasers so far have focused on the single-state QD lasers. Generally, In(Ga)As-QDs can exhibit more than one confined state that can simultaneously obtain lasing on two separate wavelengths [Kaptan et al., 2014, Markus et al., 2003, Gioannini, 2012, Röhm et al., 2015b,a, Grillot et al., 2011, Wang et al., 2014, Viktorov et al., 2005] or even show three-state lasing [Zhang et al., 2010]. To study the competing mechanism between GS and ES lasing, we extended the microscopic semiconductor theory to the case of the lasing occurs via GS and ES transitions.

Figure 4.2 shows the simulation results for the intensity functions of two-state laser, the carrier occupation of states, and the auto- and cross-correlation as a function of the pump power with y-axis in logarithmic scale. In Figure 4.2(a), the photon number of the GS and ES mode demonstrate a standard S-shaped input-output characteristic but with different lasing thresholds. Above the lasing threshold of the ES mode, the intensity of the GS mode remains pinned while the intensity of the ES mode increases dramatically. The calculations further show the dependency of the carriers occupation for GS and ES on the pump power. As shown in Figure 4.2(b), the GS occupation is clamped after the onset of GS lasing. Here adding carriers to the GS leads to the carrier recombination through stimulated emission of a photon with the GS transition energy. To increase the stimulated emission rate from the GS, we need more carriers to relax into the GS from ES. As a result, the number of carriers of the ES starts to increase until ES reach sufficient levels to facilitate ES lasing. The population of ES clamps as well, but gain clamping does not occur for the ES once the GS has obtained threshold. The autocorrelation function of each mode at zero delay time can be seen in Figure 4.2(c) which shows the standard transition from the spontaneous emission to the stimulated emission [Ulrich et al., 2007, Scully and

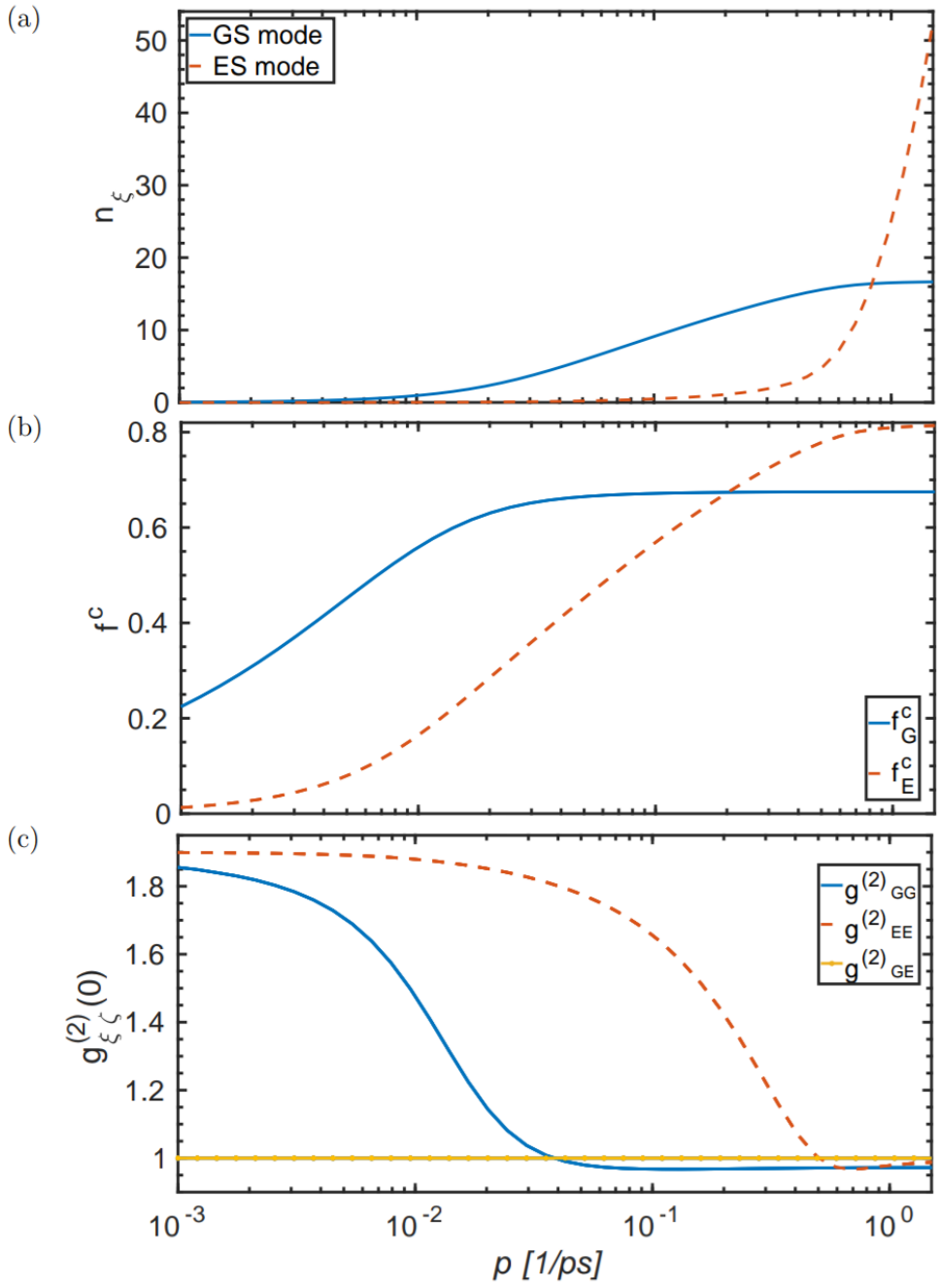

Figure 4.2: Laser characteristics calculated using the semiconductor theory for two-state lasing. (a) Intensity (as dimensionless photon number n_ξ, $\xi \in \{G, E\}$) for modes GS (solid curve) and ES (dashed curve) as a function of the pump rate P, (b) the carrier population of GS and ES for conduction band and (c) auto- and cross-correlation functions of two modes.

Zubairy, 1997]. They both drop from 2, corresponding to thermal light, to 1 corresponding to coherent light emission but with different threshold pumps of 0.01 ps^{-1} and 0.2 ps^{-1} for GS and ES mode, respectively. The cross-correlation function $g^{(2)}_{GE}(0)$ can be interpreted as a signature of gain competition as discussed in the previous chapter 3. Especially interesting is the competition behavior between GS and ES modes to catch carriers which can be found in Figure 4.2(c). It shows that the cross-correlation function is pinned to 1 for all pump rates. Thus, we may conclude that two modes do not show the conventional signatures of gain competition. In the following the influence of ES lasing on the GS mode will be studied numerically and analytically.

4.3.1 Effect of the ES on the GS lasing

The theoretical results of two-state lasing in section 4.3 showed that ES lasing surpasses the GS mode and for large values of the pump power ES can affect GS lasing efficiency. The competing behavior between GS and ES lasing for QD lasers has been the subject of some previous works [Cao et al., 2009, Markus et al., 2003], however only limited experiments have been done for the gain competition between two-state modes [Massé et al., 2006, Kaptan et al., 2014].

Since the signatures of gain competition has not been obvious in our numerical results, we measure the delay time between lasing of the GS and the ES around the lasing threshold of ES. The delay time can be approximated from the evaluated time for saturation of carriers in GS and ES, and can be seen in Figure 4.3. For two modes with equal Q-factors, the saturation state of carriers for ES mode occurs at about 600 ps, while the carries of the ground state saturates at 300 ps. The GS occupation reaches sufficient values to lase before the ES mode starts lasing and thus ES mode cannot qualitatively affect the GS lasing. We may postulate that two modes have not competed for the same carriers and therefore GS has a definite portion of carriers that relaxes from the excited state to the ground state. This portion is related to the relaxation rate of carriers in the conduction band $1/\tau_c$, and the carriers occupation of the excited state $\langle c^\dagger_E c_E \rangle$. This finding remains also valid for higher Q-factor ES-mode with lower cavity loss rate γ_{EE} as depicted in Figure 4.3.

Moreover, the distinct difference in the GS occupations for different values of γ_{EE} can be seen in the inset in Figure 4.3. The cavity loss rate of ES mode

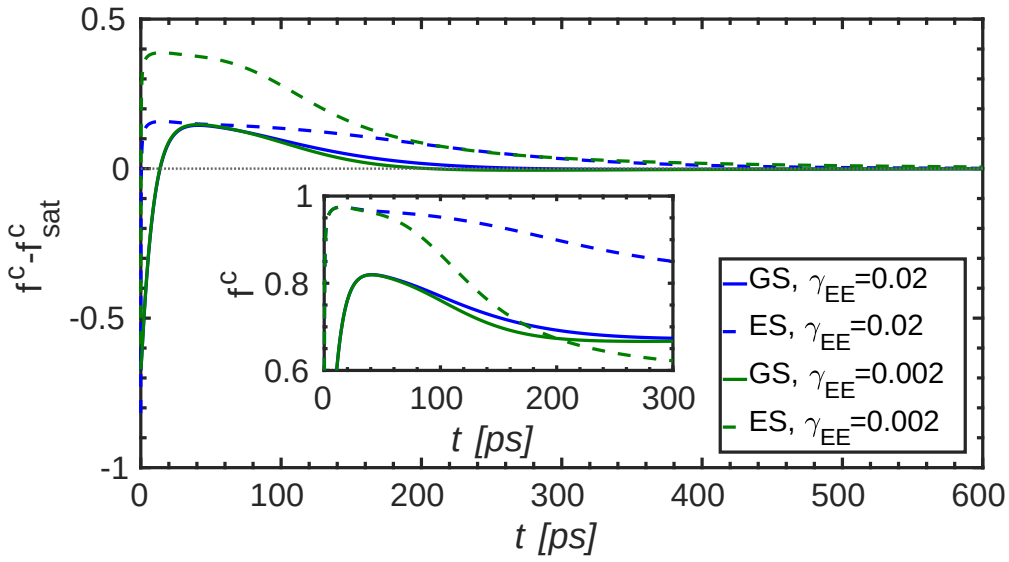

Figure 4.3: Evaluated time for saturation of carriers $f^c_{sat} =< c^\dagger c >_{sat}$ in GS (solid line) and ES (dashed line) modes at pump rate $P = 10\ ps^{-1}$. The blue lines correspond to two modes with the same quality $\gamma_{GG} = \gamma_{EE} = 0.02\ ps^{-1}$. On the other hand, the green lines are related to two different modes with $\gamma_{GG} = 0.02$ $ps^{-1}$and $\gamma_{EE} = 0.002\ ps^{-1}$. After the ground state reaches the saturation value of carriers, the ES occupation saturates. The inset shows more clearly the effect of γ_{EE} on the carriers occupation $f^c =< c^\dagger c >$ of GS and ES until the mode GS starts lasing ($t = 300\ ps$).

γ_{EE} has considerable effect on the time-dependence of ES occupations before GS lasing occurs. Therefore, the loss rate of mode ES can affect the number of carriers that relax into the ground state, even though ES lasing has not yet started.

Figure 4.4 illustrates the impact of γ_{EE} on the intensity of GS mode and carriers occupation of states as a function of pump rate. The γ_{EE} has effect on ES and GS populations and it therefore leads to the intensities of GS mode that exhibit significantly different value for various γ_{EE} at large values of the pump rate. Hence, the GS lasing is influenced solely by the injection carriers and it can be controlled only quantitatively by the ES mode.

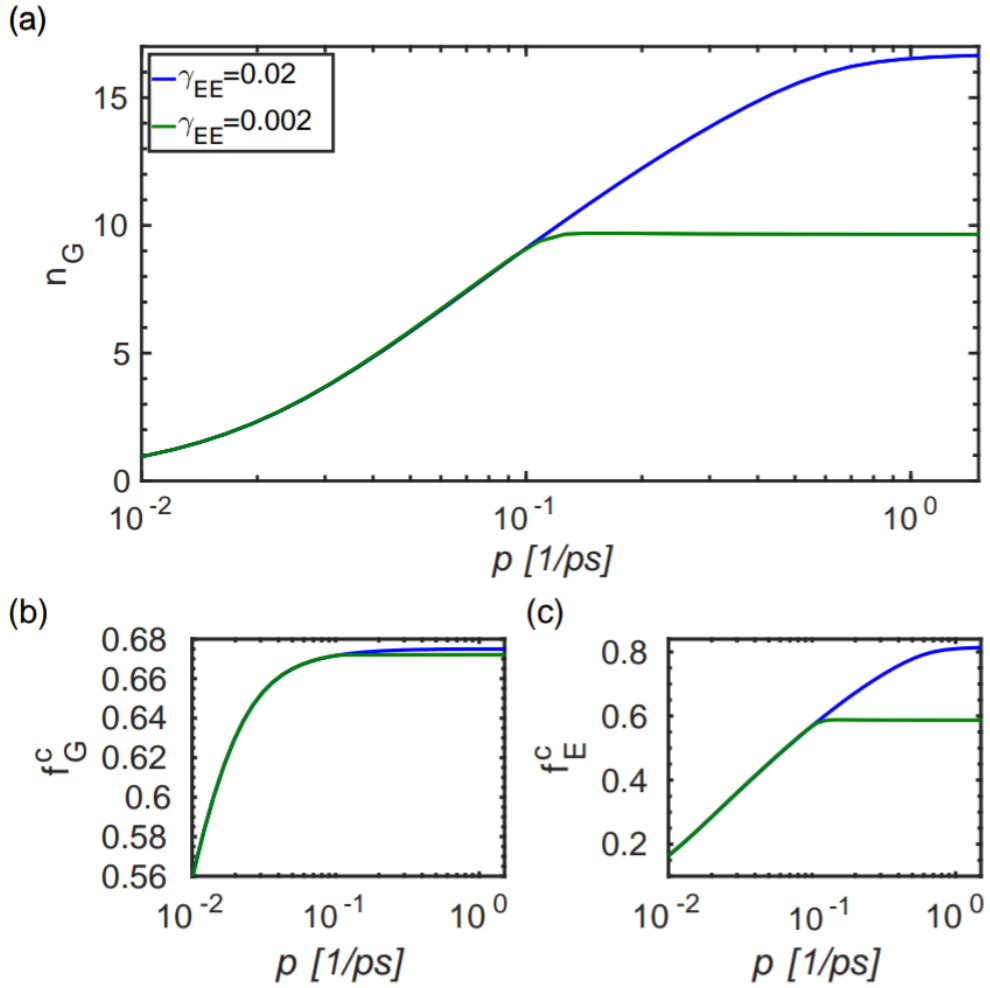

Figure 4.4: (a) Input-output characteristic of GS mode versus pump rates, and the carriers occupation of conduction band for (b) ground state and (c) excited state for various γ_{EE}.

4.4 Ground state quenching

With increasing the pump rate, some devices illustrate a decline and even quenching of the GS lasing intensity as shown in Figure 4.5 based on the numerical results of Röhm et al. [2015c]. The first observation of two-state lasing and GS quenching was reported in the experiments of Markus et al. [2003]; they observed a reduction of the GS emission for pump rates above ES threshold. However, they did not explain this phenomenon theoretically. GS quenching has been also the subject of several other researches such as those in Refs. [Korenev et al., 2013, Gioannini, 2012, Röhm et al., 2015c,b, Maximov et al., 2013] and its reason is

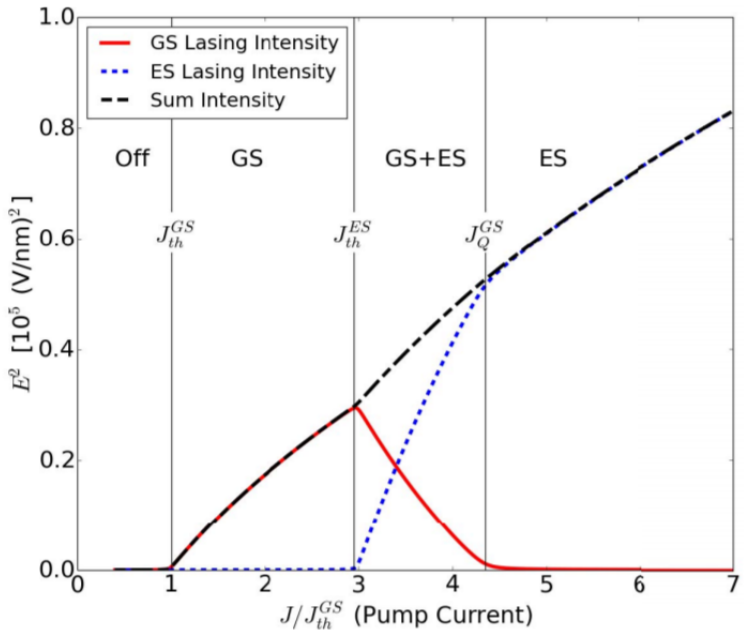

Figure 4.5: Lasing characteristics for GS (red), ES (dotted blue) and the sum of both intensities (dashed black). The picture is taken from [Röhm et al., 2015c].

still debated. Quenching of the GS lasing intensity is sometimes attributed to its temperature dependence [Lüdge and Schöll, 2011, Cao et al., 2009], electron–hole asymmetry [Viktorov et al., 2005], doping [Maximov et al., 2013], or specific gain [Röhm et al., 2015c] and cavity lengths [Markus et al., 2003].

Our numerical results, however, did not demonstrate such GS quenching event. Instead, we observed that the presence of ES mode has only quantitative effects on the GS lasing and not on its general trend and therefore the gain competition between two modes does not occur. It can be explained by following statements: First, GS quenching depends on various factors as mentioned previously. Figure 4.6 illustrates the influence of the length on GS quenching from Markus et al. [2003], where the need of short cavities have been found and examined. Röhm et al. [2015c] also found that the GS quenching is commonly occurred in p-doped, short cavity devices with low gain. Therefore, some of these factors must be directly included in a theoretical model for a direct comparison of experiment and simulation. Secondly, while two-state lasing has also been observed for InAs/InP QDs [Veselinov et al., 2007], GS quenching is to the best of our knowledge only detected in self-assembled InAs/InGaAs QDs. Also, the number of research papers published on this topic is limited. Hence, GS quenching might be limited

to some specific experimental circumstances and may completely disappear by the change of these conditions.

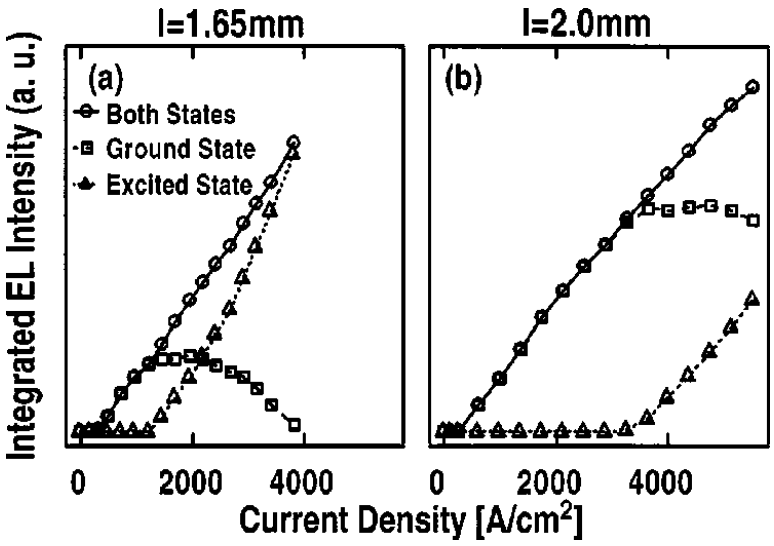

Figure 4.6: Illustration of GS quenching for different cavity lengths (a) 1650-μm and (b) 2000-μm. The picture is taken from [Markus et al., 2003]

4.5 Chapter conclusion

In this chapter the dynamical properties of two-state lasing in QD microcavity lasers were numerically simulated with a special emphasis on the effects induced by the presence of the ES mode on the GS efficiency. Numerical results of the microscopic semiconductor theory revealed that when GS lasing threshold is reached and its occupation clamps, the carrier population of ES tends to increase. Consequently, at high pump rates the carrier population of ES obtains sufficient carriers to lase and two-state lasing occurs. The autocorrelation function of two modes demonstrated the standard transition from spontaneous emission to stimulated emission but with different lasing thresholds. Moreover the cross-correlation functions were constant and equal to one implying two statistically independent modes. Accordingly, we have not considered the signature of the gain competition behavior between GS and ES modes.

The first experimental measurement of two-state lasing which has been done by Markus et al. [2003] exhibited that once the threshold of the ES transition is obtained, the GS mode saturates and then get quenched, whereas the intensity

of ES mode is significantly enhanced. However, in this work, we found that due to the delay time between carrier saturation of GS and ES modes, there is no gain competition between two modes. First, the GS received enough carriers to saturate and then the carriers increased in ES. Therefore, ES mode lased after GS mode and they could not compete with each other to catch the carriers. This implies that the laser operation of GS remained unaffected by the onset of lasing in the ES; the only effect of the ES mode on GS operation is related to the loss rate of ES mode. It has an effective role on the number of carriers which relax into the GS. We can therefore conclude that the presence of ES mode has only quantitative effects on the GS lasing and not qualitative effects.

Chapter 5

Final conclusions

Summary

In the scope of this work we explored and numerically simulated quantum-dot microcavity lasers with the focus on the interaction between two modes and the effect of the second mode on the lasing operation. The described QD contains two confined shells, a s- (ground state) and a p-shell (excited state) and thus the tasks of this thesis were divided into two main parts: two-mode microcavity lasers where both modes are coupled to the same QD transition (s-shell) and two-state lasing where two modes are coupled to different QD transitions.

To accomplish aforementioned tasks, we considered dynamics of an open quantum mechanical system based on a microscopic semiconductor QD theory for two-mode microcavity lasers. This approach allows to drive the equation of motion for desired quantities, including the average photon number of both modes and the average carriers population in the conduction and valence bands. However, this model leads to an infinite hierarchy of equations of motion for various expectation values for photon and carrier operators. One way to truncate this hierarchy is the cluster expansion model where the equations of motion for operator expectation values are substituted by equations of motion for correlation functions. In this regard, higher-order correlation functions are assumed to have minor contributions and are therefore neglected.

In the first part of this thesis, we investigated the lasing properties of two competing modes in a QD microcavity laser, where both modes were connected to the QD s-shell transition. Numerical results based on the microscopic semiconductor theory revealed different behaviors of two competing modes. Here,

mode 1 demonstrates the typical S-shaped behavior of the input-output curve in a double logarithmic plot, while the output intensity of mode 2 saturates and then decreases with increasing the pump rate above the threshold. Furthermore, the photon autocorrelation function $g^{(2)}(0)$ of the light emission reflects the onset of the lasing in the first mode; it drops from the value 2, corresponding to the thermal light, to 1 indicating coherent light emission. For the second mode, above the threshold, the autocorrelation function increases and reaches super-thermal values well above 2, indicating a strong bunching of photons in this mode. Distinct behaviors of two modes indicate the gain competition between two modes that is also confirmed by cross-correlation function. The decrease of cross-correlation function below unity exhibited stronger anticorrelated behavior of two modes. These results are in qualitative agreement with the experimental findings and the numerical results of Leymann et al. [2013b].

In contrast to previous works that considered only the indirect coupling between the modes induced by the interaction with the common gain medium, here we focused on the effects induced by additional direct mode coupling due to the dissipative character of the laser resonator. Here, the off-diagonal elements of the optical damping matrix γ in the Lindblad superoperator reflect the direct coupling between modes. Our numerical results based on the microscopic theory illustrated that photon bunching for the second mode becomes stronger with increasing the off-diagonal elements, whereas the autocorrelation function of the first mode is only slightly enhanced. Moreover, the cross-correlation function exhibited stronger anticorrelated behavior with increasing off-diagonal elements of γ.

To further analyze the mode-coupling effects, we applied a unitary transformation to a new set of modes. We studied the transformed system consisting of a bright mode coupled to the QDs and a decoupled dark mode that obtains photons only through the interaction with the bright mode. Thus, the transfer of photons between the two original modes was described by occupation of the dark mode. For example, at zero detuning and symmetric optical damping there was no transfer between the two original modes due to the unpopulated dark mode. As a result, the behavior of two modes did not reflect any signature of gain competition and the bright mode exhibited the features of single-mode laser depending on the off-diagonal elements. On the other hand, for asymmetric optical damping of the modes the gain competition behavior can be traced back

to the increasing occupation of the dark mode. The intensity of the dark mode increased with the off-diagonal elements of γ. As a result, the off-diagonal elements of the damping matrix enhanced the anticorrelated behavior of the modes in bimodal microcavities. We also showed that the contribution of the bright mode to the photon number of the original modes can predict the winner lasing mode. Since the first mode is composed of the superposition of dark- and bright-mode contributions that interferes constructively, it was found to be the winner mode in the competition.

The second part of this dissertation was concerned with the theoretical description of two-state microcavity lasers. The lasing states were labeled as ground state and excited state, referring to the confined QD energy states. In this case, the second mode was coupled to the excited-state transition of QD, while the first mode was coupled to the ground-state transition. Since QD microcavity lasers can simultaneously obtain lasing on two separate wavelengths, owing to the discrete energy levels of the QD, the effect of the ES mode on the efficiency of GS lasing is an interesting phenomenon. After reproducing the known results of the single-state lasing using the theoretical model, we investigated the dynamical properties of two-state lasing based on an extended microscopic semiconductor theory. It revealed that when GS lasing threshold was reached and its occupation clamped, the carrier population of ES tended to increase. As a result, at sufficiently high pump rates the ES occupation reached its threshold value and two-state lasing occurred. The autocorrelation function of two modes showed the standard transition from the spontaneous emission to the stimulated emission but with different thresholds pumping. The cross-correlation function reached constant value of one which indicated that no signature of gain competition was visible in the behavior of two modes. Both modes tended to behave independently as typical laser but with different lasing thresholds.

Based on our semiconductor model we showed that, the gain competition did not occur between GS and ES modes because of the delay time between carrier saturation of two modes. First, the ground state received enough carriers to saturate and then the carriers increased in excited state. Therefore, the lasing threshold of the ES mode occurred after GS lasing and therefore they did not compete with each other to catch the carriers. However, we found that the only effect of the ES mode on GS operation was related to the loss rate of ES mode. The loss rate influenced the number of carriers which relaxed into the GS. We

therefore concluded that the presence of ES mode affected only quantitatively the GS lasing and not qualitatively.

It was also found that the trend of GS lasing remained unaffected by the onset of lasing in the ES, whereas the first experimental measurements of two-state lasing of Markus et al. [2003] exhibited the GS quenching; namely, after reaching the threshold of the ES transition, the GS mode saturates and then get suddenly quenched, while the intensity of the ES mode significantly increases. Since the GS quenching depends on various factors and may also change by specific experiment circumstances, this issue needs consideration of specific experiment conditions and requires further investigation.

Outlook

In this work two-mode and two-state microcavity lasers have been numerically investigated. The principle theory has, however, the capability to be extended to a multi-mode theory that is of great practical importance. Multi-mode systems could be used efficiently in, for example, the multi-photon spectroscopy, that requires more than one photon at the same time to allow images to be taken with a higher resolution. The continuation of this work can be regarded as a fundamental research which can lay the groundwork for new laser devices and multi-photon spectroscopy.

Our developed microscopic semiconductor theory is applicable to the study of the emission characteristics in various interaction regimes depending on the spectral splitting between modes, decay rates or the many-body effects. Although we assumed the zero detuning situation in both parts of this thesis, detailed investigation of detuning effects can be the topic of future works.

In order to study the correlations between emission events from the two modes, the second order autocorrelation function has been investigated. However, higher-order coherence functions may anticipate interesting observations which have not been reported yet.

Understanding the GS quenching phenomenon in Ref. [Markus et al., 2003] can be helpful to get a deeper insight into the dynamical properties of QD lasers and has been a topic of debate among several researchers so far. Since the impact

of different parameters, such as cavity length, gain, doping, and electron-hole asymmetry, was not considered in the microscopic model of this work, it can be left for future research.

References

F. Albert, C. Hopfmann, S. Reitzenstein, C. Schneider, S. Höfling, L. Worschech, M. Kamp, W. Kinzel, A. Forchel, and I. Kanter. Observing chaos for quantum-dot microlasers with external feedback. *Nature Communications*, 2(1):366, 2011.

Z. Alferov. Electroluminescence of heavily-doped heterojunctions pAl_xGa_{1-x}As-n GaAs. *JOL*, 1:869 – 884, 1970.

S. Anders, C. S. Kim, B. Klein, M. W. Keller, R. P. Mirin, and A. G. Norman. Bimodal size distribution of self-assembled InGaAs quantum dots. *Phys. Rev. B*, 66(12):125309, 2002.

Y. Arakawa and H. Sakaki. Multidimensional quantum well laser and temperature dependence of its threshold current. *Appl. Phys. Lett.*, 40(11):939–941, 1982.

M. Asada, Y. Miyamoto, and Y. Suematsu. Gain and the threshold of three-dimensional quantum-box lasers. *IEEE Journal of Quantum Electronics*, 22(9):1915–1921, 1986.

R.C. Ashoori. Electrons in artificial atoms. *Nature*, 379(6564):413–419, 1996.

L. V. Asryan, M. Grundmann, N. N. Ledentsov, O. Stier, R. A. Suris, and D. Bimberg. Effect of excited-state transitions on the threshold characteristics of a quantum dot laser. *IEEE Journal of Quantum Electronics*, 37(3):418–425, 2001.

S. Ates, S.M. Ulrich, P. Michler, S. Reitzenstein, A. Löffler, and A. Forchel. Coherence properties of high-β elliptical semiconductor micropillar lasers. *Appl. Phys. Lett.*, 90(16):161111, 2007.

A. Badolato, K. Hennessy, M. Atatüre, J. Dreiser, E. Hu, P.M. Petroff, and A. Imamoğlu. Deterministic coupling of single quantum dots to single nanocavity modes. *Science*, 308(5725):1158–1161, 2005.

N. Baer, S. Schulz, S. Schumacher, P. Gartner, G. Czycholl, and F. Jahnke. Optical properties of self-organized wurtzite InN/GaN quantum dots: A combined atomistic tight-binding and full configuration interaction calculation. *Appl. Phys. Lett.*, 87(23):1–3, 2005.

N. Baer, C. Gies, J. Wiersig, and F. Jahnke. Luminescence of a semiconductor quantum dot system. *European Physical Journal B*, 50(3):411–418, 2006.

N. G. Basov, 0. N. Krokhin, and Yu. M. Popov. Use of indirect transitions in semiconductors for the determination of states with negative absorption coefficients. *Exp. Theo. Phys.*, 13:845–849, 1961.

H. Benisty, C. M. Sotomayor-Torre, and C. Weisbuch. Intrinsic mechanism for the poor luminescence properties of quantum-box systems. *Phys. Rev. B*, 44: 10945, 1991.

D. Bhattacharya, E. A. Avrutin, A. C. Bryce, J. H. Marsh, D. Bimberg, F. Heinrichsdorff, V. M. Ustinov, S. V. Zaitsev, N. N. Ledentsov, P. S. Kop'ev, Z. I. Alferov, A. I. Onischenko, and E. P. O'Reilly. Spectral and dynamic properties of InAs-GaAs self-organized quantum-dot lasers. *IEEE Journal of Selected Topics in Quantum Electronics*, 5(3):648–657, 1999.

P. Bhattacharya and S. Ghosh. Tunnel injection quantum dot lasers with 15 ghz modulation bandwidth at room temperature. *Appl. Phys. Lett.*, 80(19):3482, 2002.

D. Bimberg, M. Grundmann, and N. N. Ledentsov. *Quantum Dot Heterostructures*. John Wiley & Sons, 1999.

G. Björk, A. Karlsson, and Y. Yamamoto. Definition of a laser threshold. *Phys. Rev. A*, 50(2):1675–1680, 1994.

S. A. Blumenstein. *Classical ghost imaging with opto-electronic light sources: novel and highly incoherent concepts*. 2017. PhD Thesis.

H.-P. Breuer and F. Petruccione. *The Theory of Open Quantum Systems*. Oxford University Press, 2002.

Q. Cao, S.F. Yoon, C.Z. Tong, C.Y. Ngo, C.Y. Liu, R. Wang, and H.X. Zhao. Two-state competition in 1.3 μm multilayer InAs/InGaAs quantum dot lasers. *Appl. Phys. Lett.*, 95(19):191101, 2009.

A. Carmele, M. Richter, W.W. Chow, and A. Knorr. Antibunching of thermal radiation by a room-temperature phonon bath: A numerically solvable model for a strongly interacting light-matter-reservoir system. *Phys. Rev. Lett.*, 104 (15):156801, 2010.

P. H. J. Carmichael. *Dissipation in Quantum Mechanics: The Master Equation Approach*. Springer Berlin Heidelberg, 1999.

P. Chhantyal, S. Naskar, T. Birr, T. Fischer, F. Lübkemann, B.N. Chichkov, D. Dorfs, N.C. Bigall, and C. Reinhardt. Low threshold room temperature amplified spontaneous emission in 0d, 1d and 2d quantum confined systems. *Scientific Reports*, 8(1):3962, 2018.

W. W. Chow and F. Jahnke. On the physics of semiconductor quantum dots for applications in lasers and quantum optics. *Progress in Quantum Electronics*, 37:109–184, 2013.

F.W. Cummings. Stimulated emission of radiation in a single mode. *Phys. Rev.*, 140:A1051–A1056, 1965.

E. Del Valle, F.P. Laussy, and C. Tejedor. Luminescence spectra of quantum dots in microcavities. II. fermions. *Phys. Rev. B*, 79(23):235326, 2009.

R. Dingle and C. H. Henry. *Quantum effects in heterostructure lasers*. Patent, US 3982207, 1976.

P. A. M. Dirac. The quantum theory of the emission and absorption of radiation. *Proc. Roy. Soc.*, A114:243–265, 1927.

A. Einstein. Zur Quantentheorie der Strahlung. *Physik.Zeitschr.*, 18:121–128, 1917.

V. Eremeev, S.E. Skipetrov, and M. Orszag. Quantum theory of a two-mode open-cavity laser. *Phys. Rev. A*, 84(2):023816, 2011.

S. Fafard, Z.R. Wasilewski, C. Allen, D. Picard, M. Spanner, J.P. McCaffrey, and P.G. Piva. Manipulating the energy levels of semiconductor quantum dots. *Phys. Rev. B*, 59(23):15368–15373, 1999.

M.J. Faghihi, M.K. Tavassoly, and M. Hatami. Dynamics of entanglement of a three-level atom in motion interacting with two coupled modes including parametric down conversion. *Physica A: Statistical Mechanics and its Applications*, 407:100–109, 2014.

M. Fanaei, A. Foerster, H.A.M. Leymann, and J. Wiersig. Effect of direct dissipative coupling of two competing modes on intensity fluctuations in a quantum-dot-microcavity laser. *Phys. Rev. A*, 94(4):043814, 2016.

E. Fermi. Quantum theory of radiation. *Rev. Mod. Phys.*, 4:87–132, 1932.

A. Foerster. *Theory of Semiconductor Quantum-Dot Microcavity Lasers, Computational modeling and significance for experimental realization.* 2017. PhD Thesis.

J. Fricke. Transport equations including many-particle correlations for an arbitrary quantum system: A general formalism. *Annals of Physics*, 252(2):479–498, 1996.

J. Garrison and R. Chiao. *Quantum Optics.* Oxford University Press, 2014.

P. Gartner. Two-level laser: Analytical results and the laser transition. *Phys. Rev. A*, 84(5):053804, 2011.

C. Gies, J. Wiersig, M. Lorke, and F. Jahnke. Semiconductor model for quantum-dot-based microcavity lasers. *Phys. Rev. A*, 75(1):013803, 2007.

C. Gies, M. Florian, P. Gartner, and F. Jahnke. The single quantum dot-laser: Lasing and strong coupling in the high-excitation regime. *Optics Express*, 19 (15):14370–14388, 2011.

C. Gies, M. Florian, F. Jahnke, and P. Gartner. 3 - modeling single quantum dots in microcavities. *Quantum Optics with Semiconductor Nanostructures*, page 78 – 114, 2012.

M. Gioannini. Ground-state power quenching in two-state lasing quantum dot lasers. *Journal of Applied Physics*, 111(4):043108, 2012.

P. L. Gourley. *Nanolaser - Spektrum der Wissenschaft*. 1998.

F. Grillot, N.A. Naderi, J.B. Wright, R. Raghunathan, M.T. Crowley, and L.F. Lester. A dual-mode quantum dot laser operating in the excited state. *Appl. Phys. Lett.*, 99(23):231110, 2011.

M. Grundmann and D. Bimberg. Theory of random population for quantum dots. *Phys. Rev. B*, 55(15):9740–9745, 1997.

M. Grundmann, A. Weber, K. Goede, V.M. Ustinov, A.E. Zhukov, N.N. Ledentsov, P.S. Kop'ev, and Zh.I. Alferov. Midinfrared emission from near-infrared quantum-dot lasers. *Appl. Phys. Lett.*, 77(1):4–6, 2000.

G. Hackenbroich, C. Viviescas, and F. Haake. Field quantization for chaotic resonators with overlapping modes. *Phys. Rev. Lett.*, 89(8):083902, 2002.

H. Hakan. *Laser Light Dynamics*. North Holland, 1986.

R. N. Hall, G. E. Fenner, J. D. Kingsley, T. J. Soltys, and R. O. Carlson. Coherent light emission from GaAs junctions. *Phys. Rev. Lett.*, 9:366–368, 1962.

R. Hanbury Brown and R.Q. Twiss. A test of a new type of stellar interferometer on sirius. *Nature*, 178(4541):1046–1048, 1956.

H. Haug and S.W. Koch. *Quantum Theory of the Optical and Electronic Properties of Semiconductors*. World Scientific Publishing Co., 2009.

W.E. Hayenga and M Khajavikhan. Unveiling the physics of microcavity lasers. *Light: Science and Applications*, 6:e17091, 2017.

W. Hoyer, M. Kira, and S.W. Koch. Influence of coulomb and phonon interaction on the exciton formation dynamics in semiconductor heterostructures. *Phys. Rev. B*, 67(15):155113, 2003.

W. Hoyer, M. Kira, and S. W. Koch. Cluster expansion in semiconductor quantum optics. *Springer Berlin Heidelberg*, page 309–335, 2004.

Xi. Huang, A. Stintz, C. P. Hains, G. T. Liu, J. Cheng, and K. J. Malloy. Very low threshold current density room temperature continuous-wave lasing from a single-layer inas quantum-dot laser. *IEEE Photonics Technology Letters*, 12(3): 227–229, 2000.

K. Jacobi. Atomic structure of InAs quantum dots on GaAs. *Progress in Surface Science*, 71(5-8):185–215, 2003.

F. Jahnke, C. Gies, M. Aßmann, M. Bayer, H. A. M. Leymann, A. Foerster, J. Wiersig, C. Schneider, M. Kamp, and S. Höfling. Giant photon bunching, superradiant pulse emission and excitation trapping in quantum-dot nanolasers. *Nat. Commun. 7*, page 11540, 2016.

M.D. Kapetanakis and I.E. Perakis. Spin dynamics in (III,Mn)V ferromagnetic semiconductors: The role of correlations. *Phys. Rev. Lett.*, 101(9), 2008.

Y. Kaptan, A. Röhm, B. Herzog, B. Lingnau, H. Schmeckebier, D. Arsenijević, V. Mikhelashvili, O. Schöps, M. Kolarczik, G. Eisenstein, D. Bimberg, U. Woggon, N. Owschimikow, and K. Lüdge. Stability of quantum-dot excited-state laser emission under simultaneous ground-state perturbation. *Appl. Phys. Lett.*, 105(19):191105, 2014.

M. Khanbekyan. Three-dimensional cavity-assisted spontaneous emission as a single-photon source: Two cavity modes and rabi resonance. *Phys. Rev. A*, 97 (2):023809, 2018.

M. Khanbekyan, H.A.M. Leymann, C. Hopfmann, A. Foerster, C. Schneider, S. Höfling, M. Kamp, J. Wiersig, and S. Reitzenstein. Unconventional collective normal-mode coupling in quantum-dot-based bimodal microlasers. *Phys. Rev. A*, 91(4):043840, 2015.

M. Kira and S.W. Koch. Cluster-expansion representation in quantum optics. *Phys. Rev. A*, 78(2):022102, 2008.

M. Kira, F. Jahnke, and S.W. Koch. Microscopic theory of excitonic signatures in semiconductor photoluminescence. *Phys. Rev. Lett.*, 81(15):3263–3266, 1998.

D. Kleppner. Inhibited spontaneous emission. *Phys. Rev.Lett.*, 47:233–236, 1981.

V.V. Korenev, A.V. Savelyev, A.E. Zhukov, A.V. Omelchenko, and M.V. Maximov. Effect of carrier dynamics and temperature on two-state lasing in semiconductor quantum dot lasers. *Semiconductors*, 47(10):1397–1404, 2013.

H. Kroemer. A proposed class of hetero-junction injection lasers. *Proceedings of the IEEE*, 51:1782–1783, 1963.

K. Lüdge and E. Schöll. Temperature dependent two-state lasing in quantum dot lasers. *In Proc. 5th Rio De La Plata Workshop Laser Dyn. Nonlinear Photon*, pages 1–6, 2011.

B. Legrand, B. Grandidier, J.P. Nys, D. Stiévenard, J.M. Gérard, and V. Thierry-Mieg. Scanning tunneling microscopy and scanning tunneling spectroscopy of self-assembled inas quantum dots. *Appl. Phys. Lett.*, 73(1): 96–98, 1998.

H. A. M. Leymann, A. Foerster, F. Jahnke, J. Wiersig, and C. Gies. Sub- and superradiance in nanolasers. *Phys. Rev. Appl. 4*, page 044018, 2015.

H.A.M Leymann. *Theory of many-particle correlations and optical properties of semiconductor quantum dots*. 2016. PhD Thesis.

H.A.M. Leymann, A. Foerster, and J. Wiersig. Expectation value based cluster expansion. *Physica Status Solidi (C)*, 10(9):1242–1245, 2013a.

H.A.M. Leymann, C. Hopfmann, F. Albert, A. Foerster, M. Khanbekyan, C. Schneider, S. Höfling, A. Forchel, M. Kamp, J. Wiersig, and S. Reitzenstein. Intensity fluctuations in bimodal micropillar lasers enhanced by quantum-dot gain competition. *Phys. Rev. A*, 87(5):053819, 2013b.

H.A.M. Leymann, A. Foerster, and J. Wiersig. Expectation value based equation-of-motion approach for open quantum systems: A general formalism. *Phys. Rev. B*, 89:1242–1245, 2014.

J. Li, R. Yu, J. Ma, and Y. Wu. Proposal for efficient mode converter based on cavity quantum electrodynamics dark mode in a semiconductor quantum dot coupled to a bimodal microcavity. *Journal of Applied Physics*, 116(16):164306, 2014.

G. Lindblad. On the generators of quantum dynamical semigroups. *Commun. Math. Phys.*, 48(2):119–130, 1976.

P. Lodahl, A. Floris van Driel, I. S. Nikolaev, Overgaag K. Irman, A., D. Vanmaekelbergh, and W. L. Vos. Controlling the dynamics of spontaneous emission from quantum dots by photonic crystals. *Nature*, 430:654–657, 2004a.

P. Lodahl, A.F. Van Driel, I.S. Nikolaev, A. Irman, K. Overgaag, D. Vanmaekelbergh, and W.L. Vos. Controlling the dynamics of spontaneous emission from quantum dots by photonic crystals. *Nature*, 430(7000):654–657, 2004b.

G. D. Mahan. *Many-Particle Physics*. Springer US, 2000.

T. H. Maiman. Stimulated optical radiation in ruby. *Nature*, 187:493–494, 1960.

A. Majumdar, M. Bajcsy, A. Rundquist, and J. Vučković. Loss-enabled sub-poissonian light generation in a bimodal nanocavity. *Phys. Rev. Lett.*, 108(18):183601, 2012.

L. Mandel and E. Wolf. *Optical Coherence and Quantum Optics*. Cambridge University Press, 1995.

A. Markus, J.X. Chen, C. Paranthoen, A. Fiore, C. Platz, and O. Gauthier-Lafaye. Simultaneous two-state lasing in quantum-dot lasers. *Appl. Phys. Lett.*, 82(12): 1818–1820, 2003.

N. F. Massé, S. J. Sweeney, I. P. Marko, A. R. Adams, N. Hatori, and M. Sugawara. Temperature dependence of the gain in p-doped and intrinsic InAs-GaAs quantum dot lasers. *Appl. Phys. Lett.*, 89:191118, 2006.

M.V. Maximov, Yu.M. Shernyakov, F.I. Zubov, A.E. Zhukov, N.Yu. Gordeev, V.V. Korenev, A.V. Savelyev, and D.A. Livshits. The influence of p-doping on two-state lasing in InAs/InGaAs quantum dot lasers. *Semiconductor Science and Technology*, 28(10):105016, 2013.

P. Meystre and M. Sargent. Interaction between atoms and quantized fields. *Springer Berlin Heidelberg*, page 286–306, 1999.

P. Michler. *Single Quantum Dots: Fundamentals, Applications and New Concepts*. Springer Science and Business Media, 2003.

P. Michler, A. z, C. Becher, W.V. Schoenfeld, P.M. Petroff, L. Zhang, E. Hu, and A. Imamoğlu. A quantum dot single-photon turnstile device. *Science*, 290 (5500):2282–2285, 2000.

C.B. Murray, C.R. Kagan, and M.G. Bawendi. Synthesis and characterization of monodisperse nanocrystals and close-packed nanocrystal assemblies. *Annual Review of Materials Science*, 30:545–610, 2000.

M. I. Nathan, W. P. Dumke, G. Burns, F. H. Dill, and G. Lasher. Stimulated emission of radiation from GaAs p-n junctions. *Appl. Phys. Lett.*, 1:62–64, 1962.

S. Noda. Seeking the ultimate nanolaser. *Science*, 314(5797):260–261, 2006.

O. B. Park, G.and Shchek, D. L. Huffaker, and D. G. Deppe. Low-threshold oxide-confined 1.3-μm quantum-dot laser. *IEEE Photonics Technology Letters*, 12(3):230–232, 2000.

E. M. Purcell. Proceedings of the american physical society. *Phys. Rev.*, 69:681, 1946.

C. Redlich, B. Lingnau, S. Holzinger, E. Schlottmann, S. Kreinberg, C. Schneider, M. Kamp, S. Höfling, J. Wolters, S. Reitzenstein, and K. Lüdge. Mode-switching induced super-thermal bunching in quantum-dot microlasers. *New Journal of Physics*, 2016.

J.P. Reithmaier, G. Sek, A. Löffler, C. Hofmann, S. Kuhn, S. Reitzenstein, L.V. Keldysh, V.D. Kulakovskii, T.L. Reinecke, and A. Forchel. Strong coupling in a single quantum dot-semiconductor microcavity system. *Nature*, 432(7014): 197–200, 2004.

S. Reitzenstein and A. Forchel. Quantum dot micropillars. *Applied Physics*, 43 (3):033001, 2010.

S. Reitzenstein, C. Hofmann, A. Gorbunov, M. Strauß, S. H. Kwon, C. Schneider, A. Löffler, S. Höfling, M. Kamp, and A. Forchel. AlAs GaAs micropillar cavities with quality factors exceeding 150000. *Appl. Phys. Lett.*, (90(25)).

S. Reitzenstein, T. Heindel, C. Kistner, A. Rahimi-Iman, C. Schneider, S. Höfling, and A. Forchel. Low threshold electrically pumped quantum dot-micropillar lasers. *Appl. Phys. Lett.*, 93(6):061104, 2008.

A. Röhm, K. Lüdge, and E. Schöll. *Dynamic scenarios in two-state quantum dot lasers: Excited state lasing, ground state quenching, and dual-mode operation.* Springer Spektrum, 2015a.

A. Röhm, B. Lingnau, and K. Lüdge. Ground-state modulation-enhancement by two-state lasing in quantum-dot laser devices. *Appl. Phys. Lett.*, 106(19): 191102, 2015b.

A. Röhm, B. Lingnau, and K. Lüdge. Understanding ground-state quenching in quantum-dot lasers. *IEEE*, 51(1), 2015c.

P.R. Rice and H.J. Carmichael. Photon statistics of a cavity-qed laser: A comment on the laser phase-transition analogy. *Phys. Rev. A*, 50(5):4318–4329, 1994.

M. Richter, A. Carmele, A. Sitek, and A. Knorr. Few-photon model of the optical emission of semiconductor quantum dots. *Phys. Rev. Lett.*, 103(8):087407, 2009.

S. Ritter, P. Gartner, C. Gies, and F. Jahnke. Emission properties and photon statistics of a single quantum dot laser. *Opt. Express*, 18(10):9909–9921, 2010.

I. D. W. Samuel, E. B. Namdas, and G. A. Turnbull. How to recognize lasing. *Nat Photon*, 3:546–549, 2009.

A. L. Schawlow and C. H. Townes. Infrared and optical masers. *Phys. Rev.*, 112: 1940–1949, 1958.

A. Schliwa and M. Winkelnkemper. *Semiconductor Nanostructures*. Springer Berlin Heidelberg.

E. Schlottmann, M. Von Helversen, H.A.M. Leymann, T. Lettau, F. Krüger, M. Schmidt, C. Schneider, M. Kamp, S. Höfling, J. Beyer, J. Wiersig, and S. Reitzenstein. Exploring the photon-number distribution of bimodal microlasers with a transition edge sensor. *Phys. Rev. Appl.*, 9(6):064030, 2018.

S. Schulz and G. Czycholl. Tight-binding model for semiconductor nanostructures. *Phys. Rev. B, 72*, 16:165317, 2005.

M. Schwab, H. Kurtze, T. Auer, T. Berstermann, M. Bayer, J. Wiersig, N. Baer, C. Gies, F. Jahnke, J.P. Reithmaier, A. Forchel, M. Benyoucef, and P. Michler. Radiative emission dynamics of quantum dots in a single cavity micropillar. *Phys. Rev. B*, 74(4):045323, 2006.

F. Schwabl. *Quantenmechanik für Fortgeschrittene (QM II)*. Springer-Lehrbuch. Springer Berlin Heidelberg, 2008.

M. O. Scully and A. A. Svidzinsky. The super of superradiance. *Science*, 325(5947): 1510–1511, 2009.

M. O. Scully and M. S. Zubairy. *Quantum Optics*. Cambridge University Press, Cambridge, UK, 1997.

K. Sebald, C. Kruse, and J. Wiersig. Properties and prospects of blue–green emitting II–VI-based monolithic microcavities. *Phys. Status Solidi*, 246(2): 255–271, 2009.

W. Sheng, S.-J. Cheng, and P. Hawrylak. Multiband theory of multi-exciton complexes in self-assembled quantum dots. *Phys. Rev. B*, 71(3):035316, 2005.

S. Singh and L. Mandel. Mode competition in a homogeneously broadened ring laser. *Phys. Rev. A*, 20:2459–2463, 1979.

J. Singleton. *Band Theory and Electronic Properties of Solids*. Oxford, 2001.

S. Strauf, K. Hennessy, M.T. Rakher, Y.-S. Choi, A. Badolato, L.C. Andreani, E.L. Hu, P.M. Petroff, and D. Bouwmeester. Self-tuned quantum dot gain in photonic crystal lasers. *Phys. Rev. Lett.*, 96(12):127404, 2006.

K. Svozil. Squeezed fermion states. *Phys. Rev. Lett.*, 65(26):3341–3343, 1990.

V. V. Temnov and U. Woggon. Superradiance and subradiance in an inhomogeneously broadened ensemble of two-level systems coupled to a low-Q cavity. *Phys. Rev. Lett.*, 95(24):243602, 2005.

V. V. Temnov and U. Woggon. Photon statistics in the cooperative spontaneous emission. *Opt. Express*, 17(7):5774–5782, 2009.

H. Thyrrestrup, L. Sapienza, and P. Lodahl. Extraction of the β-factor for single quantum dots coupled to a photonic crystal waveguide. *Appl. Phys. Lett.*, 96: 231106, 2010.

S.M. Ulrich, C. Gies, S. Ates, J. Wiersig, S. Reitzenstein, C. Hofmann, A. Löffler, A. Forchel, F. Jahnke, and P. Michler. Photon statistics of semiconductor microcavity lasers. *Phys. Rev. Lett.*, 98(4):043906, 2007.

K.J. Vahala. Optical microcavities. *Nature*, 424(6950):839–846, 2003.

K. Veselinov, F. Grillot, C. Cornet, J. Even, A. Bekiarski, M. Gioannini, and S. Loualiche. Analysis of the double laser emission occurring in 1.55 InAs - InP (113)b quantum-dot lasers. *IEEE*, 43(9):810–816, 2007.

E.A. Viktorov, P. Mandel, Y. Tanguy, J. Houlihan, and G. Huyet. Electron-hole asymmetry and two-state lasing in quantum dot lasers. *Appl. Phys. Lett.*, 87 (5):053113, 2005.

M. Virte, K. Panajotov, H. Thienpont, and M. Sciamanna. Deterministic polarization chaos from a laser diode. *Nature Photonics*, 7(1):60–65, 2013.

C. Viviescas and G. Hackenbroich. Field quantization for open optical cavities. *Phys. Rev. A*, 67(1):16, 2003.

C. Viviescas and G. Hackenbroich. Quantum theory of multimode fields: Applications to optical resonators. *Journal of Optics B: Quantum and Semiclassical Optics*, 6(4):211–223, 2004.

C. Wang, B. Lingnau, K. Lüdge, J. Even, and F. Grillot. Enhanced dynamic performance of quantum dot semiconductor lasers operating on the excited state. *IEEE Journal of Quantum Electronics*, 50(9):723–731, 2014.

J. Wiersig. *Light-Matter Interaction and Quantum Chaos in Semiconductor Nanostructures and Optical Microcavities*. Habilitation Treatise, Bremen, 2007.

J. Wiersig, C. Gies, F. Jahnke, M. Aßmann, T. Berstermann, M. Bayer, C. Kistner, S. Reitzenstein, C. Schneider, S. Höfling, A. Forchel, C. Kruse, J. Kalden, and D. Hommel. Direct observation of correlations between individual photon emission events of a microcavity laser. *Nature*, 460(7252):245–249, 2009.

D. Witthaut, F. Trimborn, H. Hennig, G. Kordas, T. Geisel, and S. Wimberger. Beyond mean-field dynamics in open bose-hubbard chains. *Phys. Rev. A*, 83 (6):063608, 2011.

A. Wojs, P. Hawrylak, S. Fafard, and L. Jacak. Electronic structure and magneto-optics of self-assembled quantum dots. *Phys. Rev. B*, 54(8):5604–5608, 1996.

Y. Wu and X. Yang. Strong-coupling theory of periodically driven two-level systems. *Phys. Rev. Lett.*, 98(1):013601, 2007.

Z.G. Xie, S. Götzinger, W. Fang, H. Cao, and G.S. Solomon. Influence of a single quantum dot state on the characteristics of a microdisk laser. *Phys. Rev. Lett.*, 98(11):117401, 2007.

T. Yoshle, A. Scherer, J. Hendrickson, G. Khitrova, H.M. Gibbs, G. Rupper, C. Ell, O.B. Shchekin, and D.G. Deppe. Vacuum rabi splitting with a single quantum dot in a photonic crystal nanocavity. *Nature*, 432(7014):200–203, 2004.

Z. Y. Zhang, Q. Jiang, and R. A. Hogg. Simultaneous three-state lasing in quantum dot laser at room temperature. *Electronics Letters*, 46(16):1155–1157, 2010.

Appendix A

Equations of motion for the microscopic bimodal laser model

In this appendix we provide supplementary material to chapter 3. We introduce the other equations of motion for one-time correlation functions on the quadruplet level of the cluster expansion:

$$\begin{aligned}\frac{d}{dt}\delta\langle c_j^\dagger v_j b_\xi\rangle =& i(\Delta_{\xi j}+i\gamma_{\xi\xi}+i\Gamma)\delta\langle c_j^\dagger v_j b_\xi\rangle + g_{\xi j}\delta\langle c_j^\dagger c_j\rangle(1-\delta\langle v_j^\dagger v_j\rangle)\\ &+\sum_{\xi\neq\xi'}\gamma_{\xi\xi'}\delta\langle c_j^\dagger v_j b_{\xi'}\rangle + \sum_\zeta [g_{\zeta j}\delta\langle b_\zeta^\dagger b_\xi\rangle(\delta\langle c_j^\dagger c_j\rangle-\delta\langle v_j^\dagger v_j\rangle)\\ &+ g_{\zeta j}\delta\langle c_j^\dagger c_j b_\zeta^\dagger b_\xi\rangle - g_{\zeta j}\delta\langle v_j^\dagger v_j b_\zeta^\dagger b_\xi\rangle],\end{aligned} \tag{A.1}$$

$$\begin{aligned}\frac{d}{dt}\delta\langle v_s^\dagger v_s\rangle =& \left(\sum_\xi g_{\xi j}\delta\langle c_s^\dagger v_s b_\xi\rangle + H.c.\right) - \delta\langle v_p^\dagger v_p\rangle(1-\delta\langle v_s^\dagger v_s\rangle)\tau_v^{-1}\\ &+\delta\langle c_p^\dagger c_p\rangle(1-\delta\langle v_p^\dagger v_p\rangle)\tau_{sp}^{-1},\end{aligned} \tag{A.2}$$

$$\begin{aligned}\frac{d}{dt}\delta\langle v_p^\dagger v_p\rangle =& -P(\delta\langle v_p^\dagger v_p\rangle-\delta\langle c_p^\dagger c_p\rangle)+\delta\langle v_p^\dagger v_p\rangle(1-\delta\langle v_s^\dagger v_s\rangle)\tau_v^{-1}\\ &+\delta\langle c_p^\dagger c_p\rangle(1-\delta\langle v_p^\dagger v_p\rangle)\tau_{sp}^{-1},\end{aligned} \tag{A.3}$$

$$\frac{d}{dt}\delta\langle c_j^\dagger c_j b_\xi^\dagger b_\zeta\rangle = -(\gamma_{\xi\xi}+\gamma_{\zeta\zeta})\delta\langle c_j^\dagger c_j b_\xi^\dagger b_\zeta\rangle + \sum_{\xi\neq\xi',\zeta\neq\zeta'}(\gamma_{\xi\xi'}\delta\langle c_j^\dagger c_j b_\xi^\dagger b_{\zeta'}\rangle + \gamma_{\zeta'\zeta}\delta\langle c_j^\dagger c_j b_{\xi'}^\dagger b_\zeta\rangle)$$
$$- g_{\xi j}\delta\langle c_j^\dagger c_j\rangle\delta\langle c_j^\dagger v_j b_\zeta\rangle - g_{\zeta j}\delta\langle c_j^\dagger c_j\rangle\delta\langle v_j^\dagger c_j b_\xi\rangle - \sum_{\xi'}[g_{\xi' j}\delta\langle c_j^\dagger v_j b_\xi^\dagger b_{\xi'} b_\zeta\rangle$$
$$- g_{\xi' j}\delta\langle c_j^\dagger v_j b_\zeta\rangle\delta\langle b_\xi^\dagger b_{\xi'}\rangle - g_{\xi' j}\delta\langle v_j^\dagger c_j b_{\xi'}^\dagger b_\xi b_\zeta\rangle - g_{\xi' j}\delta\langle v_j^\dagger c_j b_\xi^\dagger\rangle\delta\langle b_{\xi'}^\dagger b_\zeta\rangle], \tag{A.4}$$

$$\frac{d}{dt}\delta\langle v_j^\dagger v_j b_\xi^\dagger b_\zeta\rangle = -(\gamma_{\xi\xi}+\gamma_{\zeta\zeta})\delta\langle v_j^\dagger v_j b_\xi^\dagger b_\zeta\rangle + \sum_{\xi\neq\xi',\zeta\neq\zeta'}(\gamma_{\xi\xi'}\delta\langle c_j^\dagger c_j b_\xi^\dagger b_{\zeta'}\rangle + \gamma_{\zeta'\zeta}\delta\langle c_j^\dagger c_j b_{\xi'}^\dagger b_\zeta\rangle)$$
$$+ \sum_{\xi'}[g_{\xi' j}\delta\langle c_j^\dagger v_j b_\xi^\dagger b_{\xi'} b_\zeta\rangle + g_{\xi' j}\delta\langle c_j^\dagger v_j b_\zeta\rangle(1-\delta\langle v_j^\dagger v_j\rangle + \delta\langle b_\xi^\dagger b_{\xi'}\rangle)$$
$$+ g_{\xi' j}\delta\langle v_j^\dagger c_j b_{\xi'}^\dagger b_\xi b_\zeta\rangle + g_{\xi' j}\delta\langle v_j^\dagger c_j b_\xi\rangle(1-\delta\langle v_j^\dagger v_j\rangle + \delta\langle b_{\xi'}^\dagger b_\zeta\rangle)], \tag{A.5}$$

$$\frac{d}{dt}\delta\langle c_j^\dagger v_j b_\xi^\dagger b_\zeta b_{\xi'}\rangle = i[\Delta_{\xi' j} + \Delta_{\zeta j} - \Delta_{\xi j} + i(\gamma_{\xi\xi}+\gamma_{\zeta\zeta}\gamma_{\xi'\xi'}) + i\Gamma]\delta\langle c_j^\dagger v_j b_\xi^\dagger b_\zeta b_{\xi'}\rangle$$
$$\sum_{\xi\neq\xi'',\zeta\neq\zeta',\xi'\neq\xi'''}(\gamma_{\xi''\xi}\delta\langle c_j^\dagger v_j b_{\xi''}^\dagger b_\zeta b_{\xi'}\rangle + \gamma_{\zeta\zeta'}\delta\langle c_j^\dagger v_j b_\xi^\dagger b_{\zeta'} b_{\xi'}\rangle) + \gamma_{\xi'\xi'''}\delta\langle c_j^\dagger v_j b_\xi^\dagger b_\zeta b_{\xi'''}\rangle$$
$$- g_{\xi' j}\delta\langle c_j^\dagger c_j\rangle(\delta\langle v_j^\dagger v_j b_\xi^\dagger b_\zeta\rangle - \delta\langle v_j^\dagger v_j b_\xi^\dagger b_{\xi'}\rangle + \delta\langle b_{\zeta'}^\dagger b_\xi^\dagger b_\zeta b_{\xi'}^\dagger\rangle)$$
$$+ \sum_{\zeta'}[g_{\zeta' j}\delta\langle c_j^\dagger c_j b_\xi^\dagger b_\zeta\rangle(1-\delta\langle v_j^\dagger v_j\rangle + \delta\langle b_{\zeta'}^\dagger b_{\xi'}\rangle) + g_{\zeta' j}\delta\langle c_j^\dagger c_j b_\xi^\dagger b_{\xi'}\rangle(1-\delta\langle v_j^\dagger v_j\rangle$$
$$+ \delta\langle b_{\zeta'}^\dagger b_\zeta\rangle) - 2g_{\zeta' j}\delta\langle c_j^\dagger v_j b_\zeta\rangle\delta\langle c_j^\dagger v_j b_{\xi'}\rangle - g_{\zeta' j}\delta\langle v_j^\dagger v_j\rangle\delta\langle b_{\zeta'}^\dagger b_\xi^\dagger b_\zeta b_{\xi'}\rangle$$
$$- g_{\zeta' j}\delta\langle v_j^\dagger v_j b_\xi^\dagger b_\xi\rangle\delta\langle b_{\zeta'}^\dagger b_{\xi'}\rangle - g_{\zeta' j}\delta\langle v_j^\dagger v_j b_\xi^\dagger b_{\xi'}\rangle\delta\langle b_{\zeta'}^\dagger b_\zeta\rangle], \tag{A.6}$$

$$\frac{d}{dt}\delta\langle v_j^\dagger c_j b_\xi^\dagger b_\zeta b_{\xi'}\rangle = i[-\Delta_{\xi j} - \Delta_{\zeta j} + \Delta_{\xi' j} + i(\gamma_{\xi\xi} + \gamma_{\zeta\zeta} + \gamma_{\xi'\xi'}) + i\Gamma]\delta\langle v_j^\dagger c_j b_\xi^\dagger b_\zeta b_{\xi'}\rangle$$
$$\sum_{\xi\neq\xi'',\zeta\neq\zeta',\xi'\neq\xi'''} (\gamma_{\xi\xi''}\delta\langle v_j^\dagger c_j b_{\xi''}^\dagger b_\zeta b_{\xi'}\rangle + \gamma_{\zeta'\zeta}\delta\langle v_j^\dagger c_j b_\xi^\dagger b_{\zeta'} b_{\xi'}\rangle + \gamma_{\xi'''\xi'}\delta\langle v_j^\dagger c_j b_\xi^\dagger b_\zeta b_{\xi'''}\rangle)$$
$$- g_{\xi' j}\delta\langle c_j^\dagger c_j\rangle(\delta\langle v_j^\dagger v_j b_\xi^\dagger b_{\zeta'}\rangle - \delta\langle v_j^\dagger v_j b_\zeta^\dagger b_{\xi'}\rangle + \delta\langle b_\xi^\dagger b_\zeta^\dagger b_{\zeta'} b_{\xi'}^\dagger\rangle)$$
$$+ \sum_{\zeta'}[g_{\zeta' j}\delta\langle c_j^\dagger c_j b_\xi^\dagger b_{\xi'}\rangle(1 - \delta\langle v_j^\dagger v_j\rangle + \delta\langle b_\zeta^\dagger b_{\zeta'}\rangle) + g_{\zeta' j}\delta\langle c_j^\dagger c_j b_\zeta^\dagger b_{\xi'}\rangle(1 - \delta\langle v_j^\dagger v_j\rangle$$
$$+ \delta\langle b_\xi^\dagger b_{\zeta'}\rangle) - 2g_{\zeta' j}\delta\langle v_j^\dagger c_j b_\xi\rangle\delta\langle v_j^\dagger c_j b_\zeta\rangle - g_{\zeta' j}\delta\langle v_j^\dagger v_j\rangle\delta\langle b_\xi^\dagger b_\zeta^\dagger b_{\zeta'} b_{\xi'}\rangle$$
$$- g_{\zeta' j}\delta\langle v_j^\dagger v_j b_\xi^\dagger b_{\xi'}\rangle\delta\langle b_\zeta^\dagger b_{\zeta'}\rangle - g_{\zeta' j}\delta\langle v_j^\dagger v_j b_\zeta^\dagger b_{\xi'}\rangle\delta\langle b_\xi^\dagger b_{\zeta'}\rangle]. \tag{A.7}$$

List of Publications

- **M. Fanaei**, A. Foerster, H. A. M. Leymann, and J. Wiersig, *The effect of direct dissipative coupling of two competing modes on intensity fluctuations in a quantum-dot-microcavity laser.* Phys. Rev. A., 98(4): 043814, 2016.